THE ROLE OF RESERVOIR FLOW REGULATION AND EVAPORATION IN WATER RESOURCES MANAGEMENT

A Dissertation

by

GANG ZHAO

Submitted to the Office of Graduate and Professional Studies of
Texas A&M University
in partial fulfillment of the requirements for the degree of

DOCTOR OF PHILOSOPHY

Chair of Committee,	Huilin Gao
Committee Members,	Francisco Olivera
	Ralph Wurbs
	John Nielsen-Gammon
Head of Department,	Robin Autenrieth

December 2018

Major Subject: Civil Engineering

ABSTRACT

Surface water reservoirs have been used for supporting many water resources applications such as flood control, water supply, and hydropower generation. Modeling of reservoir systems and observations of the key water budget terms are essential for providing precise information for modern water resources management. In this dissertation, a series of modeling and remote sensing approaches were established to improve our understanding about reservoir systems under a changing environment. These approaches are presented in three step-by-step studies:

1. In the first study, a reservoir module was incorporated into a physically-based distributed hydrological model to fill in the gap between rainfall-runoff models and river/watershed management models. The new modeling framework was calibrated and validated over Lake Whitney. The simulated results were found robust at daily, weekly, and monthly levels. The new model provides the capability of simulating reservoir flow regulation in a changing environment.
2. The integrated modeling framework was then applied to the Dallas metropolitan area to evaluate the impacts of potential droughts and population growth on future water supply reliability. Results suggested that reservoir storage and water supply reliability during the second half of the 21st century (2050–2099) are projected to decline by 16.1% and 14.2% when compared to the first half (2000–2049). The uncertainty associated with future climate projection is larger than that associated with urbanization.
3. In the last study, an algorithm was developed by combining the remotely sensed reservoir surface area with the modeled evaporation rate to quantify the evaporation amount for 209

major reservoirs in the United States. The evaporation rate shows a positive trend (due to the current brightening trend) while the total surface area shows a negative trend (due to reduced precipitation in the western US). Consequently, the total evaporation amount shows no significant trend from 1985 to 2014.

ACKNOWLEDGEMENTS

I would like to express the deepest appreciation to my committee chair, Professor Huilin Gao. My Ph.D. study has been an amazing experience, and I thank Dr. Gao wholeheartedly—not only for her tremendous academic support, but also for giving me so much other guidance and advice during the past five years. Without her optimism, enthusiasm, encouragement, and persistent help; this dissertation would not have been possible.

I also want to thank my committee members, Dr. Francisco Olivera, Dr. Ralph Wurbs, and Dr. John Nielsen-Gammon for their valuable support throughout this research endeavor. My sincere gratitude also goes to our lab members: Shuai Zhang, Kyungtae Lee, Xiao Shen, Yuhang Wei, Yao Li, Manqing Shao, and Cheryl Holmes for all the help they provided in my Ph.D. period. I also want to thank the co-authors of the publications: Dr. Lan Cuo, Dr. Shih-Chieh Kao, Dr. Bibi S. Naz, and Dr. Nathalie Voisin for their help during the publication process.

I thank Dr. Yulong Zhang, as well as other faculty and staff, for making my time here at Texas A&M University a great experience. This research has also benefitted from the use of the Google Earth Engine platform (https://earthengine.google.com), the Texas A&M Supercomputing Facility (http://sc.tamu.edu), and the Oak Ridge Leadership Computing Facility (https://www.olcf.ornl.gov/).

Finally, I am deeply grateful to my mother and father for their encouragement, and for their patience and love.

CONTRIBUTORS AND FUNDING SOURCES

This work was supported by a dissertation committee consisting of Dr. Huilin Gao [advisor], Dr. Francisco Olivera, and Dr. Ralph Wurbs of the Department of Civil Engineering; and Dr. John Nielsen-Gammon of the Department of Atmospheric Sciences. All work for the dissertation was completed independently by the student.

My graduate study was supported by TAMU-CONACYT Collaborative Research Grant Program 2014-028; U.S. National Science Foundation Grant CBET-1454297; the NASA Science of Terra, Aqua, and Suomi NPP (TASNPP) Program (80NSSC18K0939); and the Earth and Space Science Fellowship (NESSF) Program (17-EARTH17F-0297). I was also partially supported by the W. G. Mills Scholarship (02-650509) and the USGS Graduate Student Research Program (G16AP00085) provided by the Texas Water Research Institute.

TABLE OF CONTENTS

Page

LIST OF FIGURES

Page

LIST OF TABLES

Page

CHAPTER I

INTRODUCTION AND LITERATURE REVIEW

To increase the flexibility of water resources management, global artificial impoundment increased dramatically during the last century (Chao et al., 2008). According to Lehner et al. (2011), there are about 16.7 million reservoirs worldwide that are larger than 100 m^2— providing a total storage capacity of 8070 km^3. With the help of reservoirs, water managers are able to redistribute surface water more efficiently and deliver benefits to human society such as flood damage reduction, drought mitigation, hydropower generation, etc (Hsu and Wei, 2007). At the same time, however, reservoirs have also substantially altered our natural hydrological processes. Graf (2006) showed that annual peak discharges have decreased by 67% (on average), and daily discharges have been reduced by 64%, due to the construction of many large dams on North American rivers. In the continental United States (CONUS), the amount of water that can be stored by its 75,000 dams is as much as one year's mean runoff (Graf, 1999). In addition, owing to the dam-induced expanded surface water area, the increased surface water losses through evaporation from reservoirs are considerably large (Gallego-Elvira et al., 2010; Gökbulak and Özhan, 2006). These alterations increase the challenge of understanding the hydrological cycle.

Most reservoirs have the capability to supply water and/or generate energy for sustaining human societies. Of the 600 largest global reservoirs (with an integrated capacity of 5,268 km3), irrigation or municipal use is the main/secondary purpose for 274 reservoirs, and hydropower is the main/secondary purpose for 447 reservoirs (statistics based on Lehner et al. (2011)). Compared to extracting water directly from streams, reservoir water-supply systems increase supply reliability in most regions (Moy et al., 1986). However, global

environmental/anthropogenic changes—such as climate change, land-cover/land-use change (LCLUC), and population growth—pose great challenges to the reservoir systems (Vörösmarty et al., 2000). More variable precipitation, increasing evaporation, and more frequent floods and droughts are all threatening the sustainability of our water resource management (Conway, 1996; Zhao et al., 2016a).

Therefore, the overarching objective of this proposal is to evaluate how reservoir systems are affected by the ever-changing environment. To achieve this goal, three scientific questions will be answered specifically:

1) How to accurately simulate the coupling between watershed hydrological processes and reservoir flow regulation?

Although watershed hydrology and flow regulation are closely coupled, addressing them in an interactive fashion is challenging. In many cases, flow regulation models only handle flows and withdrawals within river networks, using exogenously defined hydrological inputs. Consequently, the coupling effects (e.g., return flows from irrigation) are not represented. While a few water management models contain a hydrologic component, they are usually rather simple. Similarly, most of the reservoir modules embedded in hydrological models are overly simplified. To address this issue, we have developed a modeling framework by integrating a reservoir flow regulation scheme into a physically-based and fully-distributed hydrological model. The new model is tested over Lake Whitney to demonstrate its capabilities and robustness.

2) How can we leverage modeling techniques to achieve more accurate reservoir information to support local water resources management under global environmental changes?

Throughout the world, many reservoirs were constructed to provide a supply of water to human society. These reservoirs are usually located close to urban areas, and thus they are

affected by—not only the changing climate—but also the ongoing process of urbanization (i.e., impervious coverage expansion and population growth). These changing environments make the simulation of reservoir systems in urban areas more challenging. Thus, determining the best way to account for all of these factors and provide useful suggestions to the policymakers is a pressing task for the scientific community. Using our integrated modeling framework, we can simulate urbanization (because of the fully-distributed feature), changing climate (physically-based), and flow regulation (reservoir scheme) simultaneously. Specifically, we use a case study in the Dallas metropolitan area to demonstrate how changing climate and population growth can affect water supply resilience.

3) What is the role of evaporation in reservoir systems and how can accurate evaporation information help with water resources management?

Accurate knowledge of evaporation amount is very important to modern precise water resources management. However, even though evaporation accounts for a large amount of water loss from reservoirs, accurate evaporation information is still rarely incorporated into current operational water management practices. This gap is caused by the unavailability of both high-quality reservoir surface area data and high-quality evaporation rate data. To answer this question, we have developed an algorithm to estimate the evaporation amount from reservoirs. This algorithm was carefully validated, and was then applied to major reservoirs in the United States to support current water resources management.

1.1 Integrating a reservoir module into a distributed hydrological model

Two types of models are generally used to represent reservoir flow regulation effects. They are the rainfall-runoff models and river/watershed management models. Rainfall-runoff

models focus on representing natural hydrological processes, while river/watershed management models concentrate more on Best Management Practices (BMPs) for water uses. Many rainfall-runoff models, such as the Distributed Large Basin Runoff Model (DLBRM; Croley and He, 2005) and Regional Hydroclimate Model (RegHCM; Karvvas et al., 1998), do not have a reservoir component. Some hydrologic models with reservoir simulation capabilities include the Soil and Water Assessment Tool (SWAT; Arnold and Fohrer, 2005), Variable Infiltration Capacity (VIC; Haddeland et al., 2006), and the global water resources model H08 (Hanasaki et al., 2006). The reservoir operating schemes employed by these models are generally based on monthly generic operating rules, which are simplified such that representations of inter-annual variability are limited. In addition, these models are not designed to reproduce the timing-sensitive sub-monthly operational flood control activities, so their results have limited simulation agreement with historical sequence (Voisin et al., 2013a).

River/watershed management models typically adopt operational node-based reservoir functions. Examples of these models are the Water Evaluation and Planning System (WEAP; Yates et al., 2005), the Hydrologic River Operations Study System (HYDROSS; USBR, 1991), RiverWare (Zagona et al., 2001), OASIS software (HydroLogics, 2007), and MODSIM (Labadie and Larson, 2007). These models each have an embedded optimization algorithm to optimize the releases based on specified rules, and they require perfect knowledge of demand and inflow at current and future time steps. Yet because the corresponding hydrologic simulations—either coupled with the reservoir functions, or conducted offline—are usually lumped and parametric, they are limited in representing LCLUC effects on watershed processes. This significantly inhibits the models' ability to make predictions and perform scenario analysis in a changing environment. Although some commercial models, such as the MIKE SHE model (DHI, 2003),

can also support a variety of applications (including hydrologic simulation and water resources management), the unavailability of their source codes greatly limits their use for public scientific research.

To fill the gap between the two types of models discussed above, a model that combines accurate hydrological simulations with explicit reservoir simulations is desired. In parallel to present efforts toward modeling in a non-stationary environment (Milly et al., 2008; Wood et al., 2011), the new model needs a physical basis (towards climate change simulations), fully distributed characteristics (towards land cover change—especially urbanization simulations), and a flow regulation scheme (towards anthropogenic water resources management simulations).

1.2 Reservoir modeling under environmental changes

The future resilience of water supply systems is unprecedentedly challenged by non-stationary processes, such as fast population growth and a changing climate (Milly et al., 2008). Subsequently, the sustainability of our water resources management is at unprecedented risk (Dovers & Handmer, 1992; Hirsch, 2011). To manage a water supply system sustainably, the key is to make water availability meet demand. Yet both availability and demand are susceptible to non-stationarity. On the availability side, there are multiple non-stationary factors such as climate change, flow regulation, LULC change, and increasing groundwater withdrawals (Kundzewicz et al., 2008; Zhang et al., 2015; McDonald et al., 2014; Barlow & Leake, 2012). Among these, climate change induced precipitation alteration is expected to result in the largest impact on water availability (Milly et al., 2005; Schewe et al., 2014). In the past several decades, both observations and model simulations have shown increasing aridity trends across the globe due to the changing climate (Dai, 2013). Moreover, with enhanced evapotranspiration loss due to

increasing global temperatures, droughts are likely to be more severe with longer duration (Parry, 2007). On the demand side, the net growth and the migration of population both challenge the assumption of stationarity. Global freshwater consumption has increased about six-fold from 1900 to 1995 as a result of population growth (Shiklomanov, 1999). Specifically, regional water demand has surged due to urbanization (population redistribution) for many regions in the world. Thus, a thorough understanding of how these non-stationarities impact water supply resilience is vital to supporting sustainable decision making, particularly for large cities in arid and/or semi-arid regions.

However, evaluating future water supply resilience in a non-stationary fashion is exceptionally difficult, primarily due to three challenges. First, the current modeling tools are inadequate to represent the dynamic feedback between hydrologic variabilities and water management decisions. Second, droughts are intrinsically difficult to predict—especially in the long-term future (given the large uncertainties). Third, both availability and demand estimates involve large uncertainties, which add another layer of complexity to the water supply resilience evaluation. To our knowledge, there have been very few studies that focus on water supply resilience under an assumption of non-stationarity using distributed fully integrated models (Amarasinghe et al., 2016; Watts et al., 2012; Collet et al., 2015). Most of these studies mainly test the system resilience based on historical or artificially designed droughts—not on the expected future droughts derived from state-of-the-art climate models.

1.3 Reservoir evaporation quantification

To quantify reservoir evaporation, two pieces of information are necessary: evaporation rate and surface area. However, most studies have focused on the former and neglected the latter.

Instead, fixed surface area is widely used. Yet this can introduce significant biases for reservoirs that have considerable surface area changes.

The evaporation rate of open water has been studied for decades (Friedrich et al., 2017; Wurbs and Ayala, 2014). The pan evaporation method is employed by the National Weather Service (NWS) for estimating the point evaporation rate operationally (Texas Water Development Board, 2017). Although there are about 950 pan evaporation stations across the CONUS, only a very small portion are located close enough to dams to represent reservoir evaporation. Furthermore, because of the extra heat taken through a pan's sides and the lack of a heat storage effect, pan evaporation cannot accurately represent reservoir evaporation. In addition to the pan evaporation method, eddy covariance, mass balance, energy budget, and combination equation methods are frequently used. In general, eddy covariance is considered the most accurate approach, but it is primarily used for evapotranspiration related research and is constrained by the expensive cost and the sensitivity to upwind direction. Mass balance and energy budget methods are data intensive, and they can introduce considerable errors because of the complex interactions between the reservoir and its surrounding environment. Therefore, the most practical approach for estimating the evaporation rate at a large scale is to use physically based combination equations such as the Penman-Monteith method (Monteith, 1965). These physically based models are proven to be reliable for applications over shallow water reservoirs where heat storage is insignificant (Abtew, 2001; Linacre, 1993; Zhao et al., 2016b). However, the thermodynamics of a deep reservoir may affect the water temperature and the consequential surface water evaporation notably. For instance, Lake Tahoe (California, US) has its highest air temperature in July, but the largest evaporation rate usually occurs in September (Tahoe Environmental Research Center, 2015).

Reservoir surface area cannot be measured directly. Instead, it is usually inferred from in-situ measurements, or estimated from remote sensing images. By applying the reservoir rating curve to the measured water height, the surface area can be estimated. However, the rating curve information is generally difficult to collect and can be biased due to long-term sedimentation. Compared to in-situ measurement, remote sensing has the advantage of estimating water surface area at low cost (McFeeters, 1996; Sawaya et al., 2003; Gao, 2015). Even though there is a compromise between spatial and temporal resolution with remote sensing technologies, high-quality images with acceptable time intervals can be obtained. Compared with other remote sensing data, Landsat has the advantages of long temporal coverage (with a 16-day revisit time) and high spatial resolution (30 m), which make it suitable for water surface area change studies (Pekel et al., 2016).

Leveraging the legacy of the Landsat mission, Pekel et al. (2016) provided a global water mapping dataset (GWMD), which used an expert system classifier to consistently map the global water coverage. GWMD contains monthly water coverage data from 1984 to 2015. Using this dataset, monthly time series of water surface area for any individual reservoir can be generated. However, the resultant time series is usually not reliable because of contaminations from cloud, cloud shadow, terrain shadow, and the recent Scan Line Corrector (SLC) failure (for Landsat 7). Because all of the contaminated pixels were removed from the GWMD monthly water coverage dataset, the water areas for contaminated images can be significantly underestimated. To obtain more reliable time series values, most studies discarded the images with contaminated areas and only kept the uncontaminated ones (Vicente-Serrano et al., 2008; Huang et al., 2010). This approach is valid in regions with less frequent cloud cover for Landsat images other than those from Landsat 7. With respect to the regions with high-frequency cloud cover (or regions whose

images were obtained with Landsat 7), it is possible that most of the images in the time series will be discarded. For instance, using 5% as the removal threshold of contaminated images (i.e., images with contaminated pixels covering more than 5% of the target area), 70% of the images from 1984 to 2015 for the Danjiangkou Reservoir, China, have to be discarded (Pekel et al., 2016).

Even though contaminated images lead to underestimation of water surface area, they contain valuable information about the water body (such as portions of the water body boundaries). By removing these images, this information is discarded. Several studies used a digital elevation model (DEM) to correct contaminated pixels (Khandelwal et al., 2015; Klein et al., 2015). However, DEMs cannot reveal the bathymetry of most global reservoirs. Instead of explicit bathymetry, water bodies in DEMs generally have a flat area, which shows the water surface elevation during the DEM acquisition period (Gesch et al., 2002; Jarvis et al., 2008). As a result, the DEM based contamination correction method cannot be applied to a situation where the water level is lower than the DEM water surface. Thus, how to take advantage of the contaminated images and apply an automatic correction to get full water coverage is an important scientific problem that needs to be addressed.

CHAPTER II

INTEGRATING A RESERVOIR REGULATION SCHEME INTO A SPATIALLY DISTRIBUTED HYDROLOGICAL MODEL[*]

2.1 Introduction

To maximize the benefits from limited freshwater resources, and to mitigate flood risks, numerous reservoirs have been constructed during the past several decades throughout the world. According to Chao et al. (2008), the volume of global accumulative water impounded by reservoirs on land has risen from about 1,000 km^3 in 1950 to 11,000 km^3 in 2007, which is equivalent to an extra 30 mm of global sea level. Throughout the world, there are about 16.7 million reservoirs that have surface areas of 100 m^2 or greater (Liu et al., 2016). These reservoirs expand the global terrestrial water surface by about 305,000 km^2 (Lehner et al., 2011). Different types of reservoirs can serve a variety of applications such as flood control, agricultural/municipal/industrial water supply, and hydropower (World Commission on Dams, 2000). Of the most importance, reservoirs reduce the uneven temporal distribution in river runoff (Shiklomanov, 2000). Serving as a buffer against natural water disasters, reservoirs provide us with great convenience and flexibility in water resources management.

While reservoirs redistribute large amounts of surface water, they also dramatically alter the natural hydrological processes. Results from Graf (2006) show annual peak discharges that are decreased by 67% (on average), and daily discharge ranges that are reduced by 64% due to

---

[*] *Reprinted from Advances in Water Resources, Volume 98, Gang Zhao, Huilin Gao, Bibi S. Naz, Shih-Chieh Kao, Nathalie Voisin, "Integrating a reservoir regulation scheme into a spatially distributed hydrological model", Pages 16-31, Copyright (2016), with permission from Elsevier*

the construction of many large dams on North American rivers. In the continental United States (CONUS), the total amount of water that can be stored by its 75,000 dams is as much as one year's mean runoff (Graf, 1999). In addition, because of dam-induced expanded surface water area, the increased water loss through evaporation from reservoirs is considerably large (Gallego-Elvira et al., 2010; Gökbulak and Özhan, 2006). These alterations increase the complexity involved with understanding the hydrological cycle.

Most reservoirs have the capability of storing water for supply purposes, mitigating floods, and/or generating energy for sustaining human societies. Of the 600 largest global reservoirs (with an integrated capacity of 5,268 km^3), irrigation and/or municipal use is the main or secondary purpose for 274 reservoirs, and hydropower is the main or secondary purpose for 447 reservoirs (statistics based on Lehner et al. (2011)). Compared with extracting water directly from streams, a reservoir based water-supply system increases the supply reliability in most regions (Moy et al., 1986). However, global environmental/anthropogenic changes—such as climate change, land-cover/land-use change (LCLUC), and population growth—pose great challenges to the reservoir systems (Vörösmarty et al., 2000). More variable precipitation, constantly increasing temperatures, and more frequent floods and droughts are all threatening the sustainability of water resource management (Conway, 1996; Zhao et al., 2016a). Meanwhile, water demands are increasing drastically driven by a fast-growing population (Oki and Kanae, 2006).

River/watershed management models have been widely used for simulating reservoir flow regulations. They usually adopt operational node-based reservoir functions. Examples of these models are the Water Evaluation and Planning System (WEAP; Yates et al., 2005), the Hydrologic River Operations Study System (HYDROSS; U.S. Bureau of Reclamation 1991),

RiverWare (Zagona et al., 2001), OASIS software (HydroLogics Inc, 2007), MODSIM (Labadie and Larson, 2007), and the Water Rights Analysis Package (WRAP; Wurbs, 2012). Some management models use embedded optimization algorithms to identify operating rules (e.g., WRAP), while others use predefined rules to dictate reservoir operations (e.g., RiverWare and WEAP). The river routing is either coupled with the reservoir functions (e.g., WEAP) or is conducted offline (e.g., WRAP). Because the hydrological simulations are usually lumped and parametric, these models are limited in representing LCLUC effects on watershed processes.

To accurately simulate the impacts of LCLUC on the hydrological processes, physically-based and fully-distributed models are needed. Compared to lumped models, fully distributed models have the capability to represent sophisticated surface routing process, and thus can better capture the saturation-excess and infiltration-excess runoff (Reed et al., 2004; Smith et al., 2004). In addition, distributed models are designed to simulate the spatial heterogeneity of the land cover. Because most LCLUC are not uniformly distributed in the watershed, different spatial pattern can generate significantly different streamflow amount. For instance, Yang et al. (2011) examined 7 different urban sprawl scenarios and found flood peak can be enhanced if the urban development occurs closer to the river channel.

With the increase of computational capability, a number of distributed model has emerged (Reed et al., 2004). For example, the widely used distributed hydrology soil vegetation model (DHSVM) has been successfully applied in Puget Sound basin to evaluate the impacts of urbanization and climate change on streamflow (Cuo et al., 2008; Cuo et al., 2009). With the increasing impacts of anthropogenic activities on the hydrological cycle, the needs for incorporating flow regulation components into distributed models are also increasing. Additionally, how the current flow regulation facilities perform and how the operation rules of

these facilities should be updated in the light of global environmental changes are of great concern for the water managers (Matthews et al., 2011; Hirsch, 2011). In parallel with present efforts toward hyper-resolution (e.g. less than 500m) hydrologic modeling (Bader et al., 2014, Wood et al., 2011), in this study we explore ways to incorporate reservoir operations at fine spatial and temporal scales—which will support hyper-resolution hydrologic modeling and decision-making for local policy makers at the scale of a specific utility, reservoir(s), or watershed.

In this Chapter, a reservoir simulation module that uses conditional rules based on observed operational and more complex operating rules are presented. The reservoir module is similar to the reservoir operations schemes of ColSim over the Columbia River Basin (Hamlet and Lettenmaier, 1999), the Central Valley Model (CVMod) (VanRheenen et al., 2004) over California, and the Colorado River Reservoir Model (Christensen et al., 2004)—each of which are simplifications of applied complex offline reservoir operations management models. We integrate the reservoir module with a physically based distributed hydrologic model. More specifically, the new reservoir module is applicable to multiple reservoirs with multi-purpose flow regulations (such as hydropower water release and municipal/industrial/agricultural water supply). Although the model does not consider incoming flows over a future period, it is structured so that reservoirs share their status (storage) and conditional releases can be optimized. This new model builds upon the node-based reservoir models with complex operating rules, and adds flexibility in exploring new demand, new hydro-plants, and/or new operation rules. It also builds upon generic operating rules by being fully integrated with the hydrologic cycle. Together, the new model brings the application and decision-making capabilities from the monthly regional scale to the sub-monthly and sub-regional scales. These capabilities are crucial

for understanding flow regulations in an environment that is changing in response to fine spatial and temporal resolution conditions, such as extreme climate events and LCLUC.

While the focus of this Chapter is mainly on the technical implementation of the integrated model, its application in a sub-basin of the Brazos River Basin is also presented. The integrated modeling framework and development of the reservoir module is first described in Section 2. A case study using the model to simulate the effects of multi-purpose reservoirs is presented in Section 3. Furthermore, sensitivity analyses (as described in Section 4) are conducted to evaluate how different designs of reservoir and input climate forcings will affect water storage and release.

2.2 Modeling Approach

2.2.1 The Distributed Hydrology Soil and Vegetation Model (DHSVM)

The DHSVM is an open source hydrological model that has the capability of simulating various land surface processes (Figure 2.1a, 2.1b) (Wigmosta et al., 1994). It is physically based and supports high spatial and temporal resolution simulations. This model employs full water-energy balance to calculate the water partitioning within each grid cell. Specifically, the Penman-Monteith equation is used to calculate evapotranspiration (ET) from both over-story and under-story vegetation. Surface runoff and baseflow from each grid cell are first accumulated to the streams, and then routed downstream according to a Digital Elevation Model (DEM)-based river network using the linear reservoir method. DHSVM has been successfully applied in many research areas, including climate change (Battin et al., 2007), urbanization (Cuo et al., 2008; Cuo et al., 2009), sediment transportation (Doten et al., 2006), glacier dynamics (Naz et al., 2014), stream temperature, and water quality simulations (Sun et al., 2015).

As a hyper-resolution model, DHSVM has the capability of simulating fast hydrologic responses (e.g., flash flood), especially over domains which are highly spatially heterogeneous. Additionally, this spatially distributed and physically-based model can be used for investigating hydrologic impacts from changing environmental conditions such as climate change and LCLUC. It should be noted that DHSVM can explicitly simulate the effects of urbanization on the hydrological regime because of its capability to represent impervious land cover and detention ponds (Cuo et al., 2008).

However, because existing versions of DHSVM can only simulate naturalized flow, the advantages of DHSVM have been greatly hindered when applied in regions where flow regulation is significant. To overcome this model limitation and leverage the model's strengths, a reservoir module was developed and fully integrated into DHSVM in this study. We expect the DHSVM-reservoir model to be used for predicting water availability over regions with notable environmental changes, and/or over regions with flood control operations which require a dynamic response.

2.2.2 Reservoir Module

To maximize the functionality of reservoirs, most water management agencies divide their reservoirs into several pools. This approach has been well adopted worldwide, such as by the United States Army Corps of Engineers (USACE) (Wurbs, 1996), the China Ministry of Water Resources (http://www.mwr.gov.cn/), and the Central Water Commission of India (http://www.cwc.gov.in/). As illustrated in Figure 2.1c, each pool is designated with a specific service objective. The surcharge pool is the part of the reservoir that is above the spillway crest. The flood control pool is right below the surcharge pool, and is regulated to reduce the regional flood risk. Regular water supply—such as that for agricultural, municipal, and industrial use—is

provided from the conservation pool, which is below the flood control pool. If hydropower facilities are connected to the reservoir, the conservation pool will also be responsible for providing water to the turbines. Because inflow varies by season, it is a common practice that the top of the conservation pool is adjusted accordingly by the reservoir managers. The inactive pool (i.e., “dead storage”) is the bottom portion of a reservoir that is retained to support several functionalities, such as sediment containment and ecosystem protection. In general, the top of the conservation pool is considered the optimal water level. If the current storage is maintained at this optimal level, the reservoir will have enough space to store possible incoming floodwater from upstream—and will also be able to release enough water (from the conservation pool) for various water uses.

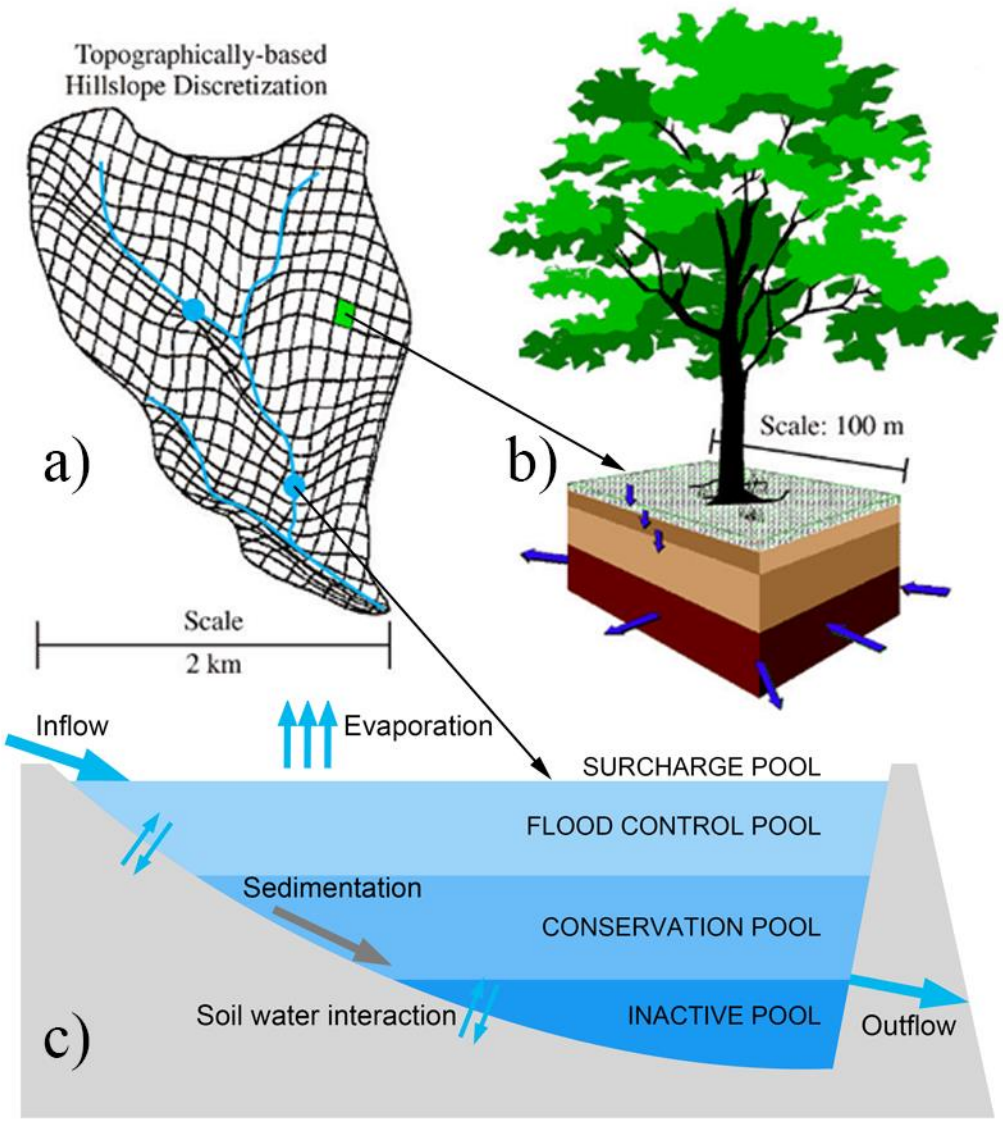

Figure 2.1 Conceptual representation of DHSVM and the newly integrated multi-purpose reservoir module, which includes: (a) topographically based basin discretization in DHSVM; (b) water movement for each grid cell; and (c) the newly integrated, multi-purpose reservoir with a flood control pool, a conservation pool, and an inactive pool. Panels (a) and (b) are modified according to Wigmosta et al. (1994). Blue points in (a) represent the point reservoirs that can be simulated in the integrated model. (Reprinted with permission from Zhao et al., 2016b)

Reservoir bathymetric information is important for assigning the pools. Generally, the storage-area and storage-elevation relationships can be depicted by tabular data, linear equations,

or some non-linear equations that can better fit the observations. In this module, we defined the default option for these relationships using two exponential functions (Equations 2.1 and 2.2).

$$A = \alpha_A \cdot S^{\beta_A} + \gamma_A \quad (2.1)$$

$$H = \alpha_H \cdot S^{\beta_H} + \gamma_H \quad (2.2)$$

where $A, H,$ and S are the reservoir surface area (m^2), the water elevation (m), and the storage (m^3) values, respectively; and $\alpha_A, \beta_A, \gamma_A$ and $\alpha_H, \beta_H, \gamma_H$ are the coefficients for the storage-area and storage-elevation relationships. These coefficients can be obtained by regression. The two equations can represent a wide range of relationships including convex ($\beta > 1$), concave ($\beta < 1$), or linear ($\beta = 1$) relationships. Furthermore, users have the option to characterize the bathymetry use other equations (e.g. quadratic). This is a user-defined parameterization which is specifically included for hyper-resolution modeling (and differs from large scale integrated hydrology-reservoir models, which usually provide a default shape (Fekete et al., 2010; Liu et al., 2016)).

Using the reservoir characteristics described above, a point reservoir module was developed and coupled to DHSVM. While the reservoir evaporation loss is calculated based on water surface area, the use of a point reservoir implies that the storage is not distributed over multiple grid cells but is to be managed for releases. Point reservoirs are assigned to their actual dam locations, and are jointly managed throughout the basin using conditional operating rules. There can be only one point reservoir per grid cell, and—in the case of DHSVM—one reservoir per river segment. Given the hyper-fine spatiotemporal resolution of DHSVM, the river routing was constructed using river segments that can encompass multiple grid cells for computational stability (Wigmosta et al., 1994). Forced by upstream inflow and local precipitation, outflow and storage values at each reservoir in the basin are calculated based on the release scheme and the

mass balance. Figure 2.2 shows the schematic of the reservoir module and its integration into DHSVM. At each DHSVM time step, the reservoir simulation involves three components: the reservoir storage evaporation scheme, the release scheme, and the reservoir storage balance calculation.

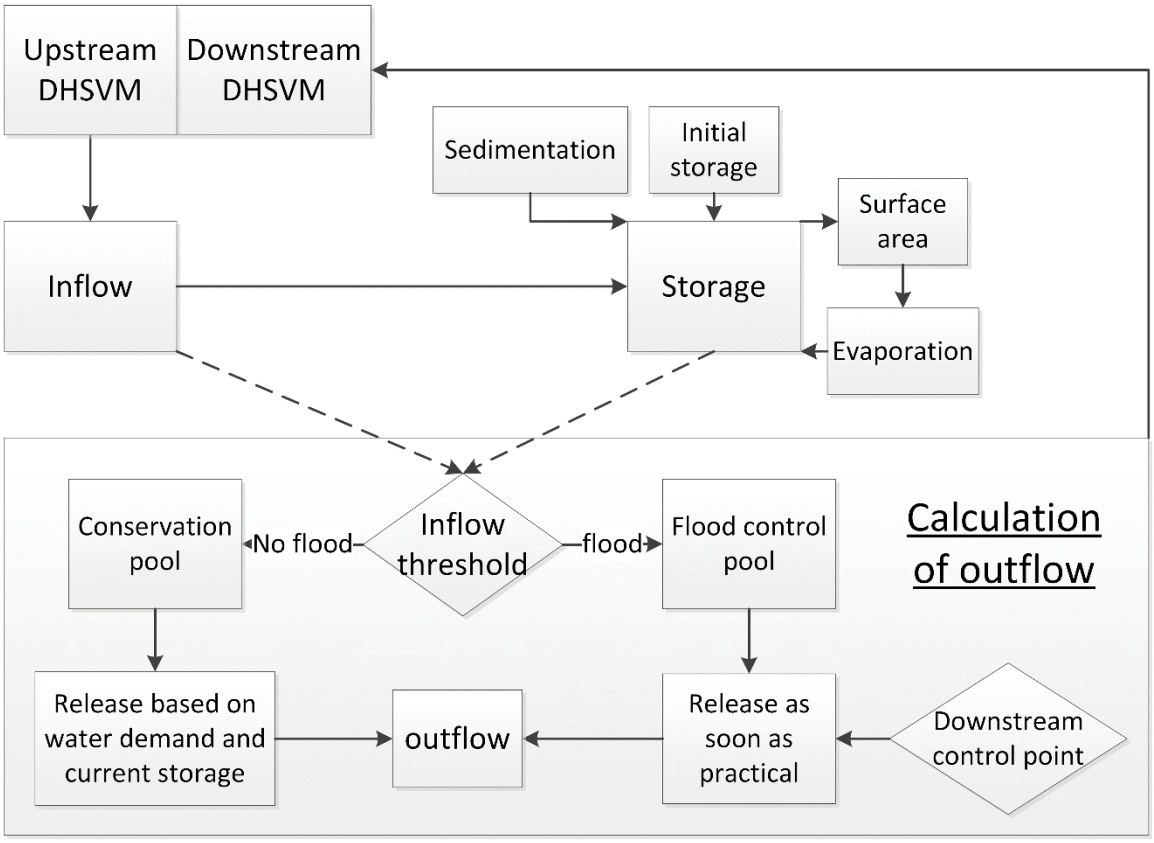

Figure 2.2 Schematic of the reservoir module and its integration into DHSVM. (Reprinted with permission from Zhao et al., 2016b)

2.2.2.1 Evaporation Scheme

Evaporation losses from open water can be considerably large, especially in arid and semi-arid regions. In this study, we used Penman's Equation (Equation 2.3; Penman, 1948) to estimate the open water evaporation from a given reservoir:

$$E_t^o = \frac{mR_n + \rho_a c_p (\delta e) g_a}{\lambda_v (m + \gamma)} \tag{2.3}$$

where E_t^o is the open water evaporation rate (kg/m^2/s) at time *t*; m is the slope of the saturation vapor pressure curve (Pa/K); R_n is the net radiation (W/m^2); ρ_a is the air density (kg/m^3); c_p is the heat capacity of air (J/kg/K); δe is the vapor pressure deficit (Pa); g_a is the surface aerodynamic conductance (m/s); λ_v is the latent heat of vaporization (J/kg); and γ is a psychometric constant (Pa/K). Although $\boldsymbol{\lambda_v}$ depends on water temperature, we used air temperature as a substitute by assuming that surface water and surface air are in a state of temperature equilibrium, without considering the thermal stratification within the water. All of the inputs are readily available from DHSVM forcings, or are computed by DHSVM. The calculated reservoir evaporation, E_t^o, is then used in the reservoir storage water balance computations (as discussed below in the Section 2.2.2).

2.2.2.2 Release Scheme

In the reservoir module, the water released at time *t*, Q_t^{out} (m^3/time step), is calculated as a function of several factors (such as upstream flow conditions, current storage values, downstream flow conditions, and water demand) using Equation 2.4:

$$Q_t^{out} = \begin{cases} 0 & (H_t \le H_I) \\ U_w & (H_I < H_t \le H_C) \\ \alpha \cdot r \cdot (H_t - H_C) & (H_C < H_t \le H_F \; and \; Q_d \le Q_{d\_max}) \\ 0 & (H_C < H_t \le H_F \; and \; Q_d > Q_{d\_max}) \\ (S_t - S_F)/\Delta t & (H_F < H_t) \end{cases} \quad (2.4)$$

where $H_I, H_C, H_F, S_I, S_C,$ and S_F are the elevation and corresponding storage values at the top of the inactive, conservation, and flood control pools, respectively (m and m^3). H_t and S_t are the real-time elevation and storage values (m and m^3). U_w is the water demand (m^3/time step), which includes multi-sectoral demand and environmental flow, and α is the flooding condition multiplier (which is equal to 1 when the inflow is not flood inflow, and is greater than 1 when the inflow is flood inflow). The threshold for determining flood inflow is a user-defined parameter, Q_f^{in}. r is the discharge coefficient (m^2/time step), which is an empirical parameter associated with the dam structure. Q_{d_max} and Q_d are the maximum acceptable streamflow and the current streamflow at downstream control points (m^3/time step), and Δt is the modeling time step (e.g., 24 hours).

As described in Equation 2.4, if the real time water level in the reservoir is less than that of the inactive pool ($H_t \le H_I$), water release will not be allowed. If the water level is greater than that of the inactive pool—but less than that of the conservation pool ($H_I < H_t \le H_C$)—water release will be allocated based on the water demand (U_w). Water demand defined in the current module includes both consumptive and non-consumptive uses, including municipal, industrial, agricultural, environmental flow, and hydropower. If a reservoir is used to simultaneously meet both the hydropower generation purposes and any of the other three water supply needs, water

first goes through the turbines to generate electricity as long as the release does not exceed turbine capacity. Otherwise, the excess water is released through the spillway.

In this reservoir module, water demand (U_w) can be either prescribed or calibrated, depending on data availability. If water demand information of a specific reservoir is well documented and accessible at the modeled time step (e.g., daily), the time series data can be used directly as the reservoir module input. However, this does not apply to most of the reservoirs. To solve this problem, we provided an empirical monthly water-demand option in this module. The monthly water demand data can be either acquired from existing sources (e.g., technical reports, water-use surveys, and/or limited observations) or estimated through calibration (when information is unavailable or only partially available). The monthly data is then partitioned evenly into water demand for each modeling time step. At a global or continental scale, water demand information for each reservoir is typically derived by associating spatially distributed estimates of demand with the nearest reservoirs. This is based on a grid cell's location with respect to the reservoir (elevation, distance from downstream impounded channel) and the reservoir's capacity (Haddeland et al., 2006; Hanasaki et al., 2006). However, the derivation of the demand can be a source of significant uncertainty in reservoir operations (Biemans et al., 2011; Voisin et al., 2013a; Voisin et al., 2013b).

When the water level in the reservoir is greater than that of the conservation pool—but less than that of the flood control pool ($H_C < H_t \leq H_F$)—water is evacuated as soon as practical to protect the dam. However, this release cannot exceed the maximum flow capacity of the downstream river channels (Q_{d_max}). If the downstream flow is less than the channel capacity ($Q_d \leq Q_{d\_max}$), the water release rate is calculated based on the difference in elevation between the current water level and that of the conservation pool (Equation 2.4). When the upstream river

basin is flooded, the flood control pool is evacuated and the flooding condition multiplier α is assigned a value greater than 1. The parameter α was first introduced by Lund and Ferreira (1996) to prevent the dam from being overtopped by floods. If α is not provided for a given reservoir, users can either assign it based on experience or calibrate it against downstream flows. According to Equation 2.4, if a flood event is detected downstream ($Q_d > Q_{d\_max}$), all of the reservoir gates are closed immediately—and they will remain closed until the downstream flow is under the channel capacity. Finally, in this reservoir module, when a severe flood event causes the flood control pool to be overtopped ($H_F < H_t$), the reservoir will release all of the water that exceeds its flood control capacity.

For a multi-reservoir system, water needs to be held in upstream reservoirs as much as possible to increase the flexibility of supplying water to downstream users. To implement this, our reservoir module is designed as follows: For each reservoir in the system, its water supply is first used to meet the demands (i.e., hydropower, municipal, agricultural) located in the immediate downstream river reach (but not downstream of any other reservoirs). If extra water is still available after meeting such demands, then the extra water can be allocated to reservoirs further downstream which cannot meet their own local demands (i.e., the demands from their immediate downstream river reaches). Similarly, if a given reservoir does not have enough water to meet local demands, then water will be extracted from upstream reservoirs. Thus, in this model there are multiple options for satisfying the demands of a multi-reservoir system. This process is consistent with other approaches used in coupled hydrology-routing-reservoir models (Hanasaki et al., 2006), which also use generic operating rules. In this case study, parameters associated with reservoir operating rules were calibrated (see Section 4.1) by adjusting the releases to provide downstream reservoirs with the supplies they need to satisfy their own local

demands. For a complicated system, optimization is an option to achieve specific objectives (e.g., highest economic outcome). The rule of holding water in upstream reservoirs is also applicable to flood conditions. The release from an upstream reservoir needs to be stopped if its adjacent downstream reservoir is crested. However, if the upstream reservoir water level is above the flood control pool, water will be released. Both cases are described in Equation 2.5,

$$Q_t^{out} = \begin{cases} 0 & (H_t^{DR} > H_F^{DR} \; and \; H_t \leq H_F) \\ Q_t^{out} & (H_t^{DR} \leq H_F^{DR}) \end{cases} \tag{2.5}$$

where H_t^{DR} and H_F^{DR} are the downstream reservoir real-time elevation and flood control pool elevation values, respectively.

In large-scale integrated hydrologic modeling, the caveat for generic reservoir operating rules is that they do not allow for joint management among reservoirs (Hanasaki et al., 2006). However, basin-specific case studies, which provide more information about joint management practices, allow for simulations of joint operating rules among reservoirs (e.g., for flood control) (Mateo et al., 2014). Offline optimization of reservoir operations is also possible in large-scale modeling, although it increases the computational burden—and still results in a simplified regulation system in which only major reservoirs are represented (Haddeland et al., 2006; Zhou et al., 2016). In operational basin-scale reservoir management, multiple sets of optimized seasonal to inter-annual operating rule curves are available—and the selection of the optimum set is based on a projection of seasonal inflow into the reservoir. This insight is usually available when the reservoir model is run offline of the hydrology model, with a time series of naturalized inflow into the upstream reservoir (and the contributing segments) provided. Because those reservoir models are offline, 2-way coupling and the representation of interdependencies

(between the hydrology model and the river routing and reservoir models) are limited. In this study, we chose to better represent the above mentioned interdependencies (by implementing a reservoir module into the DHSVM hydrologic model), while using a compromised choice with regard to the optimum set of operating rules (e.g., the release decision has no insight on the future inflow). The implementation of this reservoir module within DHSVM (with fully coupled hydrology, river routing, and reservoir processes) is compatible with future applications involving the coordination of reservoirs through the optimization of the empiric release rules. However, the computational burden of the hydrology part remains, and therefore the future optimization of DHSVM reservoir operations will need to be accompanied by computational changes such as parallel processing.

2.2.2.3 Reservoir Storage calculation

Considering the mass balance, Equation 2.6 is used to represent the change in reservoir storage:

$$S_t = S_{t-1} + \Delta t \cdot (Q_t^{in} - E_t^o \cdot A_t - Q_t^{out} - \Delta_{sed}) \quad (2.6)$$

where Q_t^{in} and Q_t^{out} are the inflow and release values (m^3/time step); E_t^o is the open water evaporation (which is calculated in Equation 2.3, m^3/time step); Δ_{sed} is the sedimentation rate (m^3/time step); and Δt is the time step.

Sedimentation, which is caused by the trap efficiency (TE) of the dams (Brune, 1953), is an important process within a given reservoir. It reduces the reservoir storage capacity by gradually accumulating the sediment from upstream inflows and from the surrounding areas. According to Mahmood (1987), one percent of the total storage capacity in global reservoirs is filled by sediment every year. In this module, we introduced a sedimentation parameter to

account for this impact (Δ_{sed}). Even though our reservoir module can also be integrated into other simpler and coarser (or even statistical) watershed models, the implementation is customized to the hyper-resolution hydrology model DHSVM for two reasons. First, although the difference between a simpler/coarser model and a fully distributed physically based model (e.g., DHSVM) may be very small for a relatively homogeneous large watershed at a low temporal resolution (e.g., monthly), a simpler model is unlikely to accurately represent highly spatially heterogeneous land cover and/or to accurately simulate flows at fine time steps. Second, DHSVM can provide a full set of input data to the reservoir module, which allows the module to accurately represent all of the attributes involved in the operations (e.g., flood control, evaporation from reservoir, sedimentation, and (future) water temperature).

2.2.3 Model Integration

The point reservoir module is integrated into the DHSVM routing scheme to represent reservoirs at their real locations (instead of lumping them together at basin/subbasin outlets). Meanwhile, multiple reservoirs can be simulated simultaneously as part of the channel routing process. In the latest version of DHSVM, the river channels are represented by connected river segments, and the routing is executed according to the order of the segments. However, by adding the point reservoirs, the connected segments (where the dams are located) are divided into upstream and downstream sections. To represent the reservoir regulation effects, DHSVM was modified as follows: (1) If the routed flow reaches a segment where a point reservoir is located, the reservoir receives inflow from the upstream section. (2) Reservoir storage and release at the current time step is then determined according to the operation rules, previous storage values, evaporation, release amounts, and sedimentation rates (Figure 2.2, Equation 2.6). In addition, the reservoir module examines the streamflow from the downstream controlled river

segments and then modifies the release scheme accordingly. (3) Released water enters the routing network at the downstream section. After computing the reservoir release amounts, downstream water users can extract water from specified downstream river segments. This is implemented by specifying the locations (i.e., the given river segments) and amounts of extracted water in the module. Similar to the reservoir water demand data, water extraction data can also be input as time-series or empirical monthly values at the segments of interest. Extracted water can be used for multiple purposes including agricultural, municipal, industrial, and others. In the current module version, non-point return flow is not accounted for, and only consumptive use is extracted. However, point return flow may enter the river network at any location (either the same as the extraction location, or somewhere else). For instance, a drinking water treatment plant (water user) and a wastewater treatment plant (water contributor) could both be simulated in the module. In this application, the water demand is prescribed and it has combined the information such as consumptive use, irrigation technologies, and delivery efficiencies. Return flow, and groundwater dynamics associated with pumping, will need to be developed during future work. Implicit return flow and groundwater components are currently being developed within certain existing water management (WM) models (Voisin et al., 2015). A future 2-way coupling between the WM and hydrology models would explicitly address i) the redistribution of withdrawn water onto crop covered grid cells as an additional forcing, and ii) groundwater dynamics when WM is coupled to models (like DHSVM) with water table dynamics and lateral flow.

The integrated model can be executed on any Linux/Unix system with a C language compiler. Due to the high spatiotemporal resolution of DHSVM, significant computational capability is needed to run this integrated model (even though the reservoir module only adds to

the running time slightly). However, users can reduce the modeling time by dividing the study sites into multiple parts. Thus, even though the integrated model is better when used at a watershed scale (due to computational expense), it can also be employed at a basin scale by dividing the basin into multiple watersheds (sub-basins) which can be simulated simultaneously using high performance computing capabilities (Zhao et al., 2016a).

2.3 Integrated Model Application: Case Study over the Lake Whitney Watershed

2.3.1 Study Area

The Lake Whitney watershed (Figure 2.3) is located in the middle of the Brazos River Basin, which is the second largest river basin in Texas. The total area of the Lake Whitney watershed is 5,290 km^2, and its elevation ranges from 125 to 454 m. Besides Lake Whitney (a USACE reservoir with a capacity of 2.59×10^9 m^3), there are three other lakes/reservoirs in this watershed —Squaw Creek reservoir, Lake Pat Cleburne, and Aquilla Lake. The main purpose of the Squaw Creek reservoir (with a capacity of 1.87×10^8 m^3, about 7% the size of Lake Whitney) is to provide cooling water for the Comanche Peak Nuclear Power Plant. Lake Pat Cleburne (with a capacity of 3.21×10^7 m^3, which is about 1% the size of Lake Whitney) is owned and managed by the City of Cleburne (population 29,377 in 2010) to provide water for municipal uses. Aquilla Lake (with a capacity of 2.64×10^8 m^3, about 10% the size of Lake Whitney) is also managed by the USACE as a part of the Brazos River Basin flood control project. Compared to Lake Whitney, storage variations over the Squaw Creek reservoir and Lake Pat Cleburne are so small that their alteration of the streamflow can be ignored. Therefore in this study, we chose to focus on modeling Lake Whitney and Aquilla Lake.

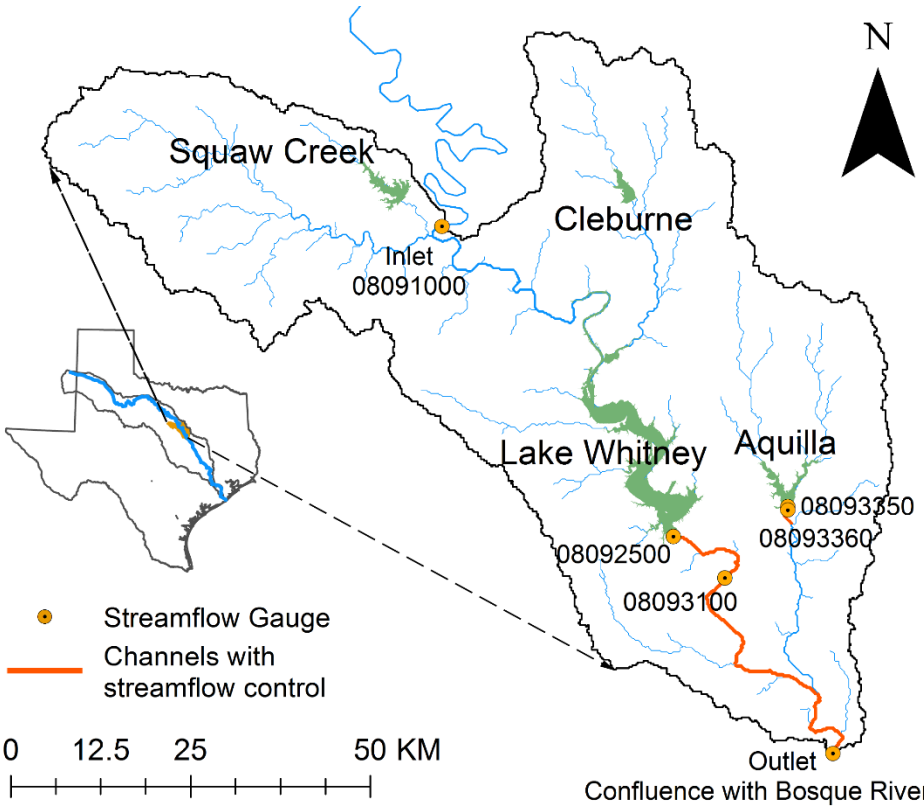

Figure 2.3 The Lake Whitney watershed in the Brazos River Basin, Texas. The confluence of the Brazos River with the Bosque River was chosen as the outlet, and U.S. Geological Survey (USGS) Gauge 08091000 was chosen as the inlet. The streamflow from Lake Whitney to the outlet is restricted to under 708 m^3/s, and to under 85 m^3/s for Aquilla Lake. (Reprinted with permission from Zhao et al., 2016b)

As the largest of all 28 reservoirs (by storage capacity) in the Brazos River Basin, Lake Whitney (Figure 2.3) plays an essential role in water resources management in central Texas. Whitney Dam was constructed during the period from May 1947 to April 1951, followed by deliberate impoundment. The main purpose of this reservoir is to prevent the flooding of downstream areas. It is also used for hydropower generation, municipal and industrial water supply, and recreation.

Since the construction of the Lake Whitney Dam, the natural streamflow in the downstream areas of the Brazos River has been altered significantly (Figure 2.4). After the impoundment, downstream averaged monthly maximum flow decreased from 213.79 m^3/s (USGS Gauge 08093100, from October 1938 to November 1951) to 108.74 m^3/s (from January 1954 to December 2014). The presence of Lake Whitney has significantly reduced the downstream flood risk. The only exception occurred in May 1957, when southern and central Texas experienced catastrophic floods. And even though Lake Whitney was forced to release more water because its flood pool was full, it prevented the downstream area from suffering more severe flood damage. Figure 2.4 also shows that—even on a monthly scale—the precipitation variability is still quite large, which adds to the necessity of efficient reservoir operations. Meanwhile, the annual evaporation of Lake Whitney is about 2.47×10^8 m^3, which is about one-third of the conservation pool volume.

Aquilla Lake is a relatively smaller lake in the Lake Whitney watershed. It was impounded deliberately in April 1983, shortly after the construction of the Aquilla Lake Dam (from March 1982 to January 1983). It is part of the flood control project in the Brazos River Basin. Besides flood control, other purposes of Aquilla Lake include water supply and recreation.

Historically, Lake Whitney and Aquilla Lake have significantly contributed to water resources management in this region. However, under the impacts of future climate change (such as extreme events), there is an increasing concern about the resilience of these lakes in terms of flood control, water supply, and hydropower generation. In addition, the operation rules--which were made based on an assumption of historical stationarity —need more quantitative evaluation and are subject to change (Milly et al., 2008). The investigation of non-stationarity (of a non-

linear nature) in integrated natural and human systems to support adaptations was the overall motivation for the development of this integrated model. Therefore, we use the modeling results and analysis over Lake Whitney to answer some important water management questions, such as: 1) How will climate change induced extreme events affect the current water management practices and hydropower generation? 2) Is there a need for adapting current operation rules to a changing climate, and (if so) how to go about this? Furthermore, an integrated model such as this will help us to better evaluate the need for constructing more reservoirs in a given river basin (for increasing water availability)—or, conversely, for removing outdated reservoirs in an attempt to restore the natural ecosystem.

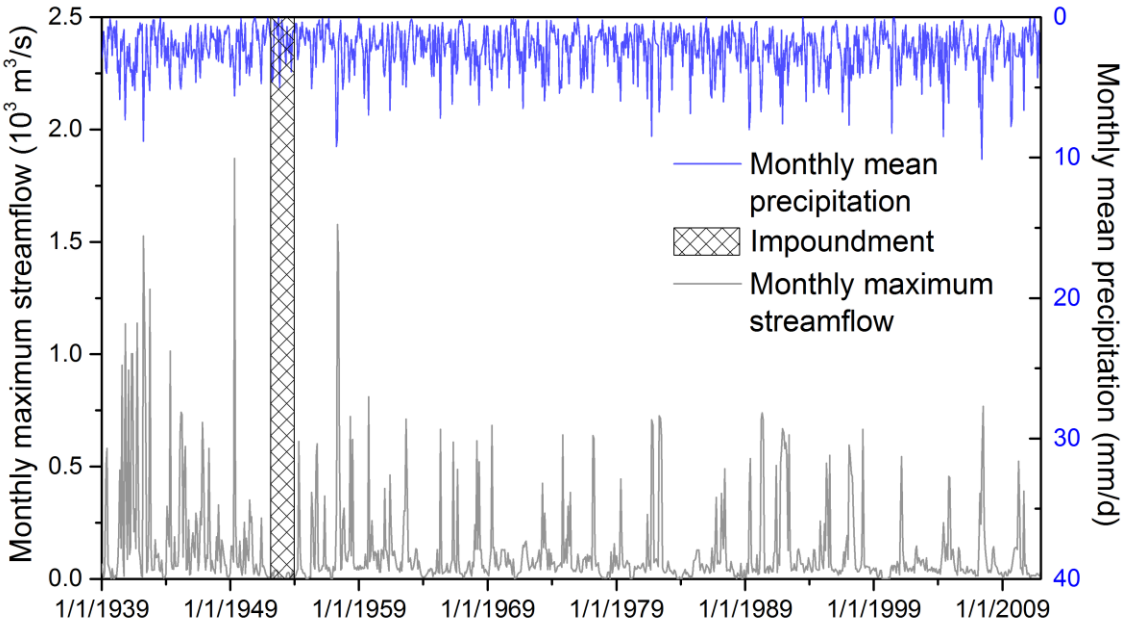

Figure 2.4 Monthly maximum streamflow observations (USGS Gauge 08093100) at the downstream channel of Lake Whitney. The blue line shows the monthly mean precipitation in the Lake Whitney watershed. (Reprinted with permission from Zhao et al., 2016b)

2.3.2 Model Input Data

Inputs for the integrated model include three categories—hydrologic parameters, reservoir configurations, and meteorological forcings—as described below.

2.3.2.1 Hydrologic Parameters

Hydrologic parameters include elevation, soil, and vegetation characteristics. The DEM was obtained from the Shuttle Radar Topography Mission (SRTM) (Jarvis et al., 2008) and was resampled to 200 m (i.e. to the DHSVM model resolution). Flow directions, basin mask, soil depth, and stream network were generated from the DEM using Arcinfo Workstation tools. The land-cover map was downloaded from the National Land Cover Database (NLCD) Multi-Resolution Land Characteristics Consortium (MRLC) website (http://www.mrlc.gov/). Because there was little LCLUC in the Lake Whitney watershed during the past several decades, NLCD 2001 (Homer et al., 2007) was used for the entire simulation period. In the Lake Whitney watershed, the main land-cover type is native grass, which accounts for 55% of the entire area. The rest of the watershed is covered by conifer forest (15%), mixed/deciduous forest (10%), urban area (8%), and other land cover types (12%). Soil texture information was acquired from the STATSGO2 database (Soil Survey Staff, 2016). The dominant soil type is clay loam (47%), followed by clay (25%), and sandy loam (19%).

2.3.2.2 Reservoir Configurations

Reservoir storage, elevation, and surface area data were obtained from the Texas Water Development Board (TWDB) to derive the rating curves for Lake Whitney and Aquilla Lake. The coefficients in Equation 2.1 and Equation 2.2 were estimated through regression. For Lake Whitney, the coefficients of determination (R^2) for these two relationships are 0.999 and 0.995,

respectively (Figure 2.5a). The corresponding R^2 values for Aquilla Lake are 0.998 and 0.996, respectively (Figure 2.5b).

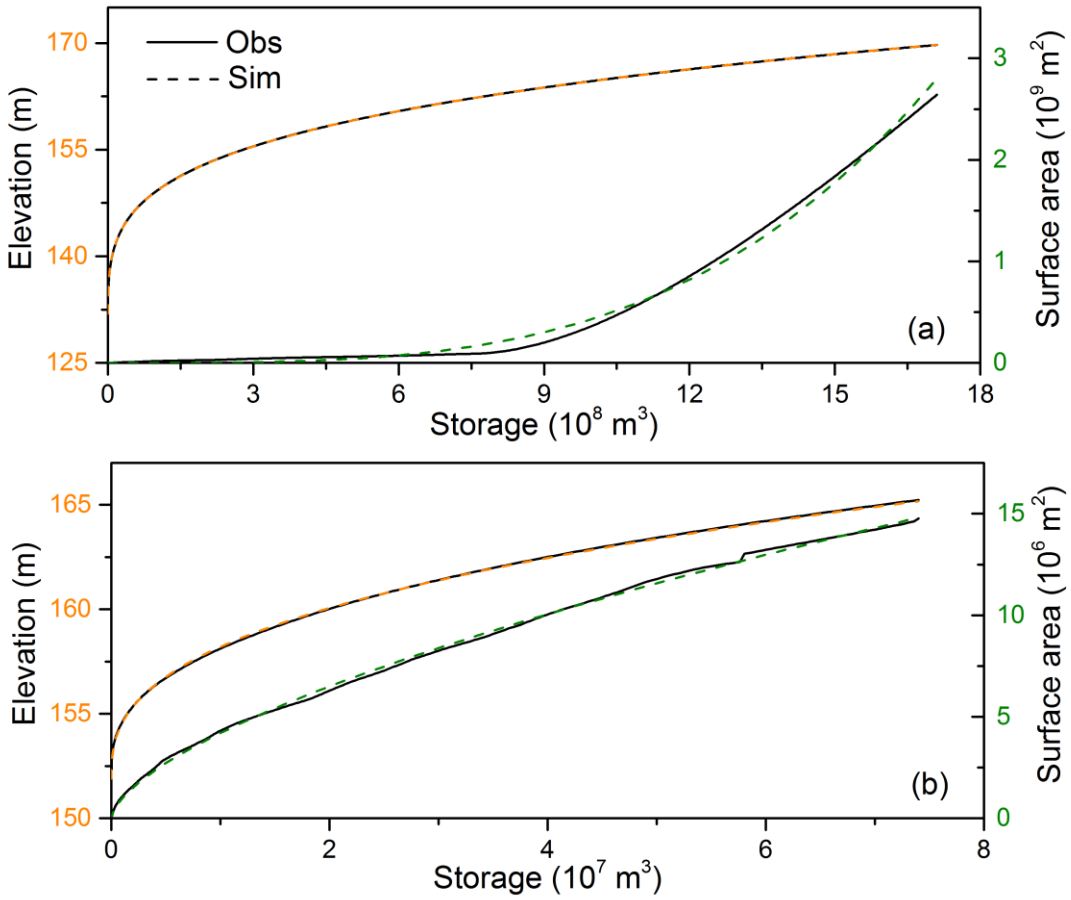

Figure 2.5 Fitted storage-area and storage-elevation relationships according to observations at a) Lake Whitney; and b) Aquilla Lake. (Reprinted with permission from Zhao et al., 2016b)

For both reservoirs, the pertinent operational data were acquired from the USACE. The Lake Whitney storage capacity (2.59×10^9 m^3) was divided into the surcharge pool (1.11×10^6 m^3), the flood control pool (1.69×10^9 m^3), the conservation pool (7.68×10^8 m^3), and the inactive pool (5.27×10^6 m^3) (Table 2.1). The lake surface area is 95.34 km^2 when its water level

is at the top of the conservation pool. The dam has a power generation rate of 30,000 KW/hr at capacity, and its average annual power production (from 1953 to 2005) is 73 million kilowatt-hours (TWDB, 2006).

In addition to reservoir water level, flows at downstream control points are examined at each time step to decide whether water should be released (after Equation 2.4). For Lake Whitney, two downstream control points are designated by the USACE. Among these two, Control Point 1 (located at the confluence of the Brazos River and the Bosque River, as shown in Figure 2.3) is closest to the reservoir and has the minimum capacity of channel streamflow (amongst the two) of 708 m^3/s. Control Point 2, National Weather Service (NWS) Gauge WBAT2, is located 64 km downstream of the reservoir and has a minimum channel streamflow capacity of 1,700 m^3/s. Control Point 1 was selected as our outlet to represent downstream flow-control operations. This is based on the historical experience that a full load at Control Point 1 (708 m^3/s) tends to occur more often, in which case the release from Lake Whitney will shut down long before Control Point 2 reaches its capacity. In fact, the flows at Control Point 2 have always been much less than its capacity threshold over the past 50 years (with a maximum value of 1,215.60 m^3/s occurring on May 17, 1965). With respect to sedimentation, the survey conducted by the TWDB in June 2005 suggests that the conservation volume of Lake Whitney has decreased by 11.6% during the past 50 years (with the sedimentation rate being about 1.91×10^6 m^3/yr) (TWDB, 2006).

Aquilla Lake has a capacity of 2.64×10^8 m^3, including the surcharge pool (8.35×10^7 m^3), the flood control pool (1.15×10^8 m^3), the conservation pool (6.35×10^7 m^3), and the inactive pool (1.15×10^6 m^3) (Table 2.1). To reduce the downstream flood risk, outflow from

Aquilla Lake is controlled to under 85 m^3/s. The sedimentation rate of Aquilla Lake is approximately 1.91×10^5 m^3/yr (TWDB, 2009).

Table 2.1 Reservoir configuration of Lake Whitney and Aquilla Lake (Reprinted with permission from Zhao et al., 2016b)

Reservoir	Lake Whitney		Aquilla Lake	
Impoundment Date	December 10, 1951		April 29, 1983	
Downstream control point	Confluence of Brazos River and Bosque River		Discharge gate of Aquilla Lake	
Downstream controlled streamflow (m^3/s)	708		85	
Sedimentation rate (m^3/year)	1.91×10^6		1.91×10^5	
	Storage (accumulative, m^3)	Elevation* (m)	Storage (accumulative, m^3)	Elevation (m)
Inactive pool	5.27×10^6	136.79	1.15×10^6	155.45
Conservation pool	7.73×10^8	162.46	6.46×10^7	163.83
Flood control pool	2.47×10^9	174.04	1.80×10^8	169.47

* Elevation is measured at the top of each pool.

2.3.2.3 Meteorological forcings.

The Long-Term Hydrologically Based Dataset (1915–2011) (Livneh et al., 2013; Livneh et al., 2015) was used to drive the integrated model. This data set covers the CONUS at 1/16° spatial resolution. The daily data set contains four meteorological variables: precipitation, maximum temperature, minimum temperature, and wind speed. The same approach from Livneh

et al., (2013) was employed to obtain the other meteorological inputs for DHSVM (i.e., relative humidity, incoming shortwave radiation, and incoming longwave radiation). Specifically, the 1/16° resolution forcings were downscaled to the modeling resolution (i.e., 200 m) using the Cressman interpolation method in DHSVM (Cressman, 1959; Wigmosta et al., 1994).

2.4 Results and Discussion

2.4.1 Calibration and Validation Results

Two sets of parameters need to be calibrated: soil and vegetation parameters associated with the original DHSVM model, and reservoir parameters for the reservoir module. Because inflows into the two reservoirs are not regulated, the soil and vegetation parameters for the watershed were calibrated against inflow observations made by the USACE at Fort Worth District (http://www.swf-wc.usace.army.mil/). The calibrated soil parameters include hydraulic conductivity, maximum infiltration rate, and porosity. Vegetation parameters include the Leaf Area Index, the canopy attenuation coefficient, and the maximum/minimum stomatal resistance. The reservoir module parameters are the discharge coefficient and the flood inflow threshold. Because water-demand data by category (e.g., municipal, hydropower) are not completely available for both reservoirs, the empirical monthly water demand for each reservoir was calibrated and then evenly partitioned into daily demand in this case study. The relative bias, R^2, and the NSE between the daily observations and the modeled results were used as the objective functions. These statistical variables were also used to validate the model performance.

Table 2.2 Simulation error statistics (calculated on a daily, weekly, and monthly basis) for Lake Whitney and Aquilla Lake (Reprinted with permission from Zhao et al., 2016b)

Lake	Variable	Time Step	Obs. Mean	Sim. Mean	Relative bias	R^2	NSE
Lake Whitney[a]	Storage[1] (10^8 m^3)	Daily	5.94	6.23	4.9%	0.87	0.72
		Weekly	5.94	6.23	4.9%	0.87	0.73
		Monthly	5.94	6.23	4.8%	0.88	0.77
	Release[2] (m^3/s)	Daily	41.26	37.94	-8.0%	0.75	0.74
		Weekly	41.26	37.94	-8.0%	0.82	0.81
		Monthly	41.20	37.89	-8.0%	0.93	0.92
	Hydropower (MWh)	Monthly	4494	3951	-12.0%	0.80	0.68
Aquilla Lake[b]	Storage[3] (10^8 m^3)	Daily	0.52	0.50	-3.3%	0.83	0.77
		Weekly	0.52	0.50	-3.3%	0.83	0.77
		Monthly	0.52	0.50	-4.2%	0.85	0.79
	Release[4] (m^3/s)	Daily	2.38	2.69	13.1%	0.54	0.51
		Weekly	2.38	2.69	13.1%	0.70	0.51
		Monthly	2.38	2.72	14.3%	0.70	0.63

[a] Error statistics were calculated from 1950 to 2011.

[b] Error statistics were calculated from 1983 to 2011.

[1,2,3,4] Observation data from USGS Gauges 08092500, 08093100, 08093350, 08093360, respectively.

For Lake Whitney, the model was calibrated from January 1, 2001 to December 31, 2011 and validated from December 10, 1951 (impoundment) to December 31, 2000. Figure 2.6 suggests that the integrated model was able to reconstruct observed flow and storage variations reasonably well, including the impoundment in the 1950s and the change of conservation level in the 1960s. Both the R^2 and NSE values in Table 2.2 indicate that the model performed robustly at the multi-decadal scale. For reservoir elevation and release at Lake Whitney, the weekly R^2 values were 0.87 and 0.82, while the weekly NSE values were 0.73 and 0.81. With regard to

downstream flows, the respective weekly R^2 and NSE values for USGS Gauge 08093100 were 0.82 and 0.81.

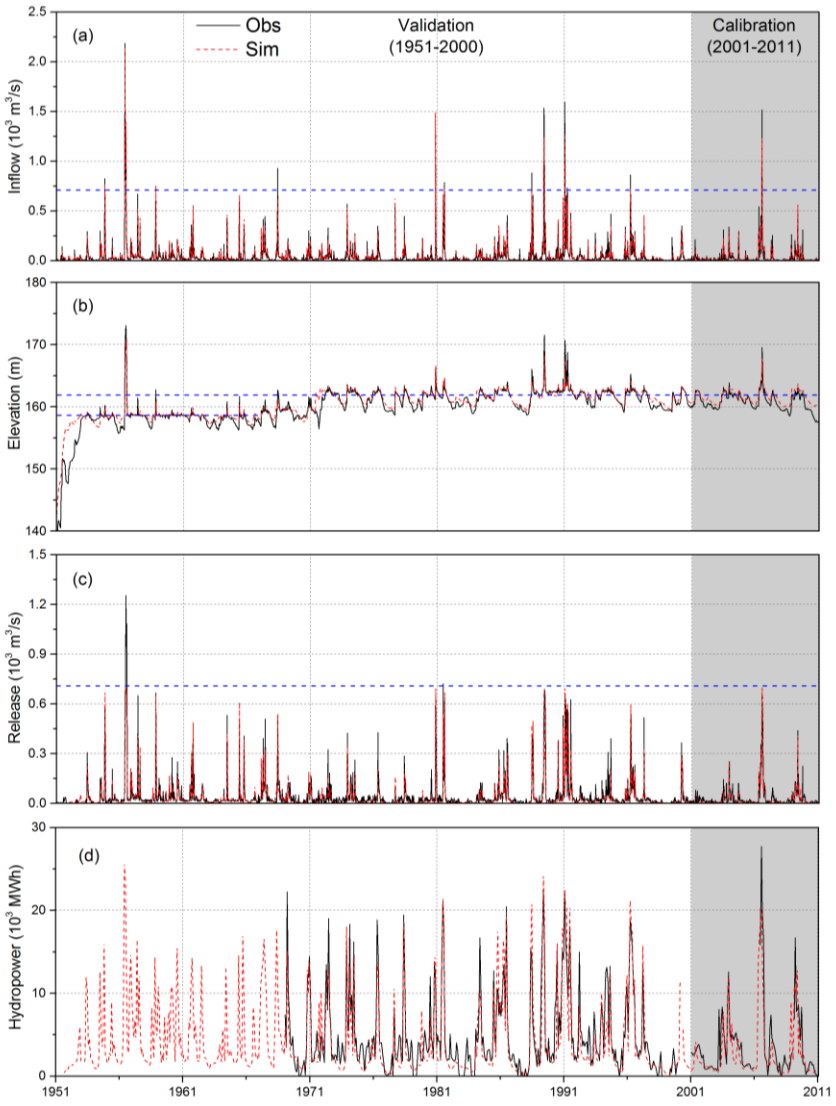

Figure 2.6 Calibration and validation results for Lake Whitney: (a) inflow (weekly); (b) elevation (weekly); (c) release (weekly); and (d) hydropower generation (monthly). Blue dashed lines represent the downstream channel capacity in (a) and (c), and the top of the conservation pool in (b). (Reprinted with permission from Zhao et al., 2016b)

According to USACE records, the conservation pool of Lake Whitney has been adjusted three times in history. In March 1968, its elevation (blue dashed line in Figure 2.6b) was raised from 158.50 m to 159.11 m, which later increased to 159.41 m in March 1969. In May 1972, it was raised to its current level (i.e., 162.46 m). The effects of this conservation pool adjustment on reservoir water level can be clearly observed in Figure 2.6b.

Simulated hydropower generation results (for Lake Whitney) were also validated by comparing them with US Energy Information Administration (EIA) hydropower net generation data (http://www.eia.gov/electricity/; Figure 2.6d). The R^2 value, which is equal to 0.80, shows good correlation. The disparity is partially due to the adoption of monthly averaged hydropower water releases in the case study, when in reality this varies on a daily basis. This can be improved by considering the sub-daily, daily, and weekly hydropower demand and scheduling in the future study (which would require further sub-daily hydropower generation data, and a more in-depth hydropower module). Nevertheless, long-term generation characteristics can be captured through the current integrated modeling approach.

Because the Aquilla Lake Dam was built in 1983, the calibration and validation were conducted from 2008 to 2011 and from 1983 to 2007, respectively (Figure 2.7). The R^2 values for storage and release were 0.83 and 0.70, and the weekly NSE values were 0.77 and 0.51. The daily R^2 and NSE values were lower than the weekly and monthly values because water supply data for calibrating the monthly demand was not available for this reservoir.

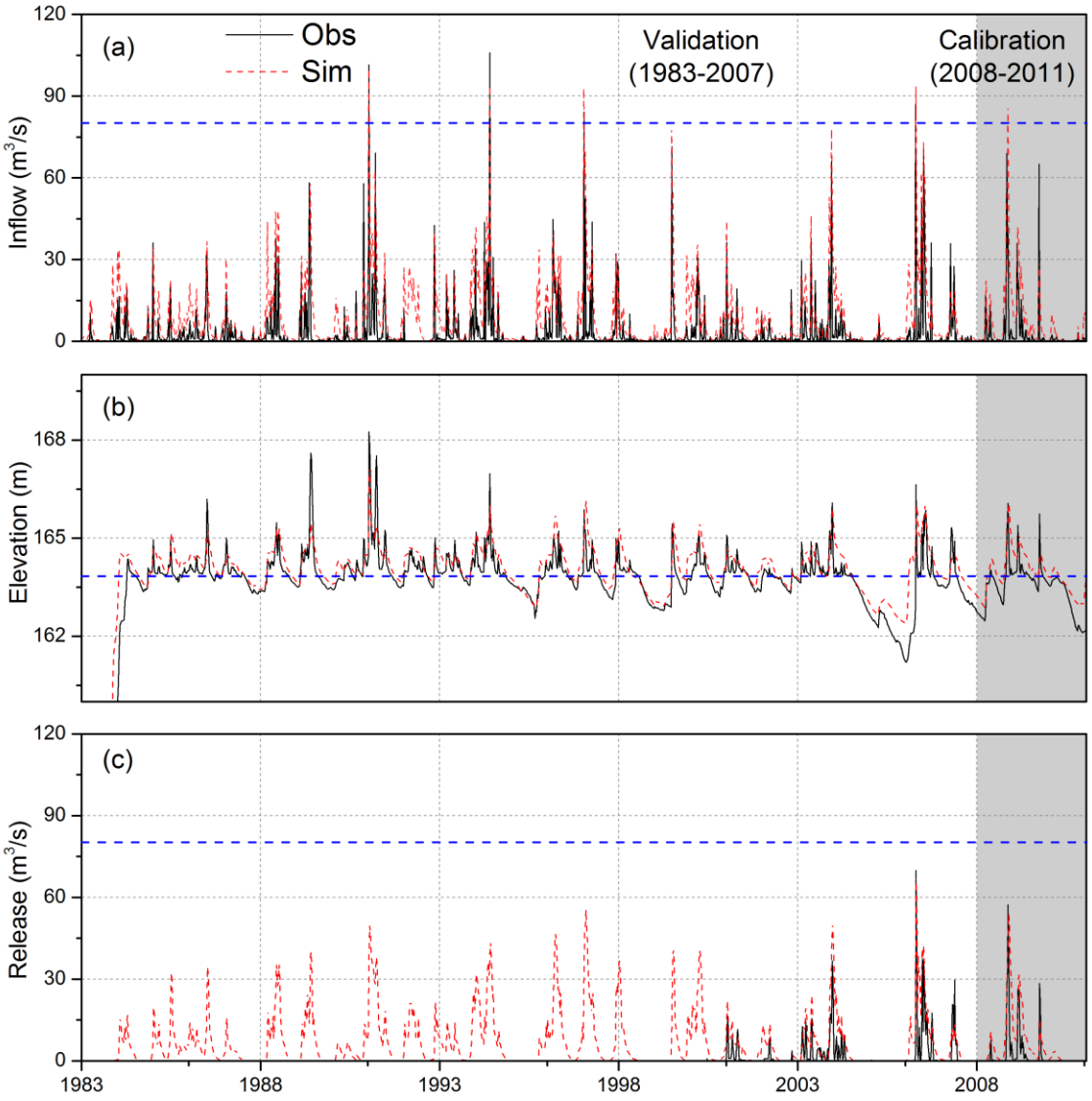

Figure 2.7 Weekly calibration and validation results for Aquilla Lake (a) inflow; (b) storage; and (c) release. Blue dashed lines represent the downstream channel capacity in (a) and (c), and the top of the conservation pool in (b). (Reprinted with permission from Zhao et al., 2016b)

2.4.2 Effects of Lake Whitney on Peak and Low Flows

The effect of reservoirs in mitigating flood peaks was also explored by comparing the simulated inflows and releases for Lake Whitney. Because point reservoirs were used in the

integrated model, the inflow to a given reservoir can be roughly regarded as the unregulated/naturalized outflow without the reservoir. Thus, differences between inflows (Figure 2.6a) and releases (Figure 2.6c) reflect the influence of Lake Whitney on flow regulation. Here we use statistical analysis of the simulated peak flows and low flows during the period of 1953 to 2011 to explain the impact of reservoir regulation. The averaged monthly maximum streamflow is 76 m^3/s with Lake Whitney regulation, while the value of natural flow is two times larger (235 m^3/s). In contrast, the low flows – represented by the lowest 7-day average flow that occurs on average once every 10 years (7Q10) – is 0.45 m^3/s with reservoir and 0.37 m^3/s without reservoir. These results clearly show the capability of Lake Whitney in mitigating both floods and droughts.

In this study, we chose the flow from 1980 to 1985 as a representative to illustrate the reservoir impacts (Figure 2.8). Using the flood event in October 1981 as an example (Figure 2.8b), maximum inflow was 1,471 m^3/s in the week of October 14. If this streamflow had been directly routed downstream with no reservoir, a huge flood event would have occurred because the downstream channel capacity would have been exceeded by about 700 m^3/s. With flood control at Lake Whitney, the release was reduced to 708 m^3/s.

As compared to peak flows--which are mainly affected by dam operations--low flows are primarily driven by downstream water users. As explained in Section 2.2.2, model users have several options for incorporating information about water demand. In the case of Lake Whitney, hydropower water use is dominant. Thus, the released low flow mainly depends on hydropower water demand. We selected the low flow event that occurred from 1982 to 1984 as an example to show the impacts of reservoir operation on low flows (Figure 2.8c). Compared with naturalized

flow (inflow), the release shows significantly improved stability which increases that the water supply reliability in the study site.

Thus, with the new module, the major added value is the reservoir storage simulation, which incorporates water use and reservoir operations. Without the reservoir module, it can be very difficult to assess water availability and flood risks. Along with better simulated streamflow, the integrated DHSVM can now be used in watersheds that have flow regulation activities. In addition, the integrated model provides the important capability of simulating detailed hydrology and water management practices simultaneously. This characteristic can be used for further exploration of the interdependence of these two systems.

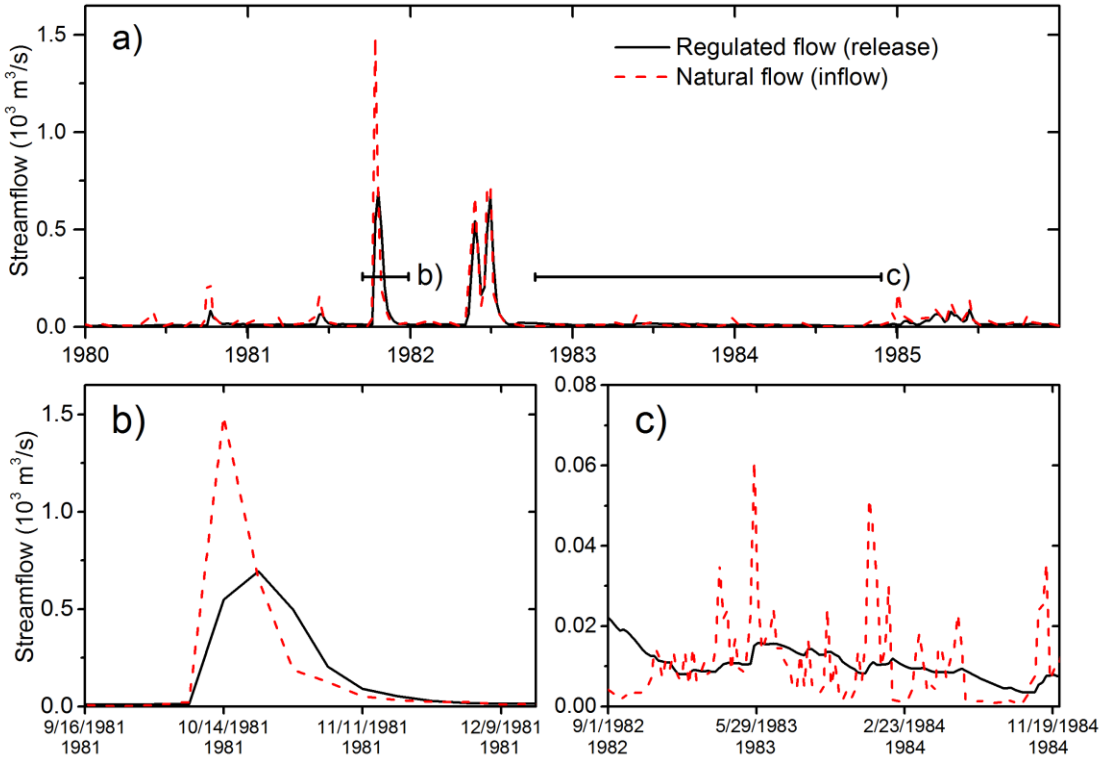

Figure 2.8 Impacts of reservoir operations on streamflow. Particularly, a peak flow event in 1981 (panel b) and a low flow event from 1982 to 1984 (panel c) were selected out for better illustration. (Reprinted with permission from Zhao et al., 2016b)

2.4.3 Model Parameter Sensitivity Analysis

The integrated modeling framework provides a unique benefit for conducting comprehensive sensitivity tests of the reservoir parameters (which present the operation rules). Given the same hydrologic conditions, the effects of flow regulation depend on the selection of the reservoir parameters. Insufficient water storage will plague the reservoir ecosystem, hydropower, and recreation, while excessive amounts of water in a reservoir will increase the risk of dam fracturing and downstream flooding. Thus, in this study, a series of parameter sensitivity analyses were conducted for reservoir storage and downstream flows. In addition, the sensitivity analyses also help to quantify the uncertainties associated with the module parameters. We demonstrate the results from Lake Whitney, which has a much larger socio-economic and environmental impact than Aquilla Lake. Among all reservoir parameters, reservoir storage and release are the most sensitive to the following four inputs in our current model configuration: monthly hydropower water demand (MHWD; the amount of water that needs to be released to the turbines in order to provide hydropower), flood inflow threshold (FIT; Q_f^{in} in Section 2.2.2) to determine if inflow is a flood inflow), conservation pool storage (CPS; S_C in Equation 2.4), and a discharge coefficient related to the dam structure (DC; r in Equation 2.4). Figure 2.9 shows the sensitivity test results of storage and release (peak, mean, and low) to these parameters. Analysis of the sensitivity of reservoir storage and release was performed by changing the calibrated value of these parameters by ±10%, ±20%,and ±50%— except in the case of CPS, which was changed by the order of +20% to -20%.

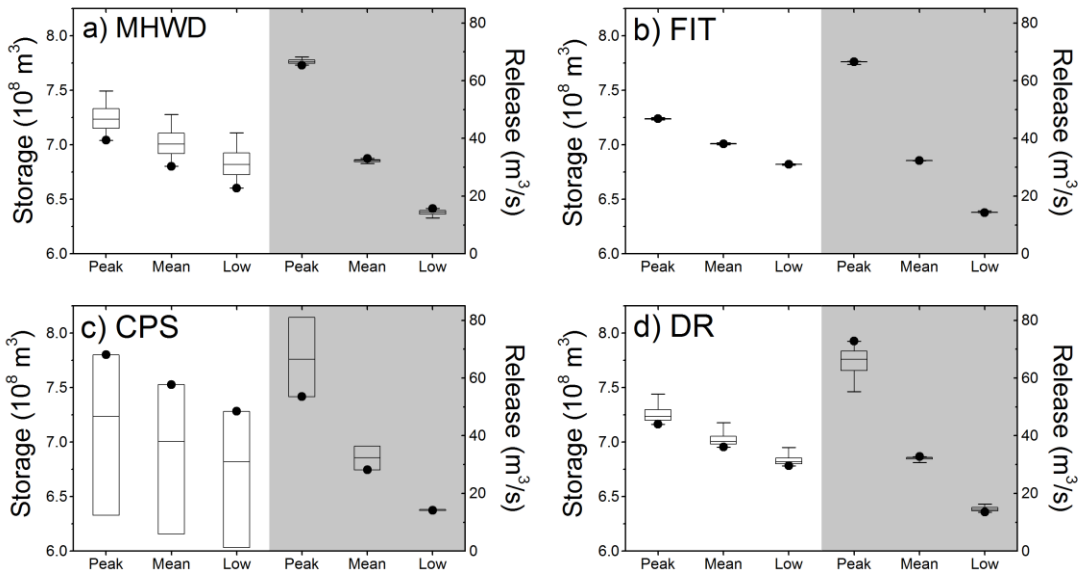

Figure 2.9 Sensitivities of reservoir storage (non-shaded area) and release (shaded area) to (a) monthly hydropower water demand; (b) flood inflow threshold; (c) conservation pool storage (with -20% to +20% variability); and (d) discharge coefficient. The middle bar is the result using the calibrated parameter value. The box represents the results using the parameter when perturbed from -20% to +20%. The whisker represents the results using the parameter perturbed from -50 (without dots) to +50% (with dots). Peak/Low storage was calculated by averaging the monthly maximum/minimum storage. Low release flow was defined as the minimum 3-day streamflow, while peak release was calculated by averaging the monthly maximum release. (Reprinted with permission from Zhao et al., 2016b)

Results indicate that MHWD has a significant inverse correlation with storage. If MHWD is reduced by 50%, average storage will correspondingly increase by 3.9% (Figure 2.9a, non-shaded area). However, because peak release is mostly affected by flood events while low release is influenced by environmental control flow, the impact of MHWD on release was insignificant in this study (Figure 2.9a, shading area). FIT has a very small effect on both storage and release (a -50% change produces a 0.2% storage increase and a 0.3% release decrease, and a 50% change yields a 0.1% storage decrease and a 0.3% release increase; Figure 2.9b). This is because in the integrated model—even though the use of the flood control pool depends on

whether the inflow is greater than the FIT—real-time release values are only based on the current storage conditions. For instance, if the current water level is above the top of the conservation pool but—at the same time—the simulated inflow is less than the IT, the reservoir will still need to release water quickly in order to drop the water level. Our analyses suggest that CPS is the parameter that both the storage and release are most sensitive to (Figure 2.9c). A reduction of 20% CPS results in a 12.2% decrease in storage volume and a 12.6% increase in release. In contrast to the small effect on storage, the release is more sensitive to changes in model parameter values (as reflected by large variations of peak, mean, and low outflows). Peak release turned out to be most sensitive to CPS; a 20% decrement of CPS resulted in a 14.44 m^3/s (21.7%) increase of peak release. In contrast, a 20% decrement of CPS only reduced the low release by 0.37 m^3/s (2.5%). This is because when CPS is reduced, more water is released during flood events. For DC, clear nonlinearity can be observed (Figure 2.9d). In the -20% to 50% range, there is little change in storage and release values. But when DC was decreased by -50%, reservoir storage volume dramatically increased and release volume dramatically decreased.

2.4.4 Sensitivity to Precipitation and Temperature Changes

In addition to their sensitivity to model parameters (determined by operation rules), storage and release values are also sensitive to the meteorological forcings. Precipitation intensity can vary greatly over different spatial/temporal domains. Moreover, because of the impact of climate change and decadal oscillations such as the El Niño Southern Oscillation (ENSO), variability of precipitation is very likely to increase (Seager et al., 2005). Such increased variability clearly aggravates the complexity of water resources management in reservoir systems (Christensen et al., 2004; Gutierrez and Dracup, 2001; Milly et al., 2008). According to the Intergovernmental Panel on Climate Change (IPCC) Fifth Assessment Report

(Stocker et al., 2013), global temperature is projected to be 3.7 °C higher at the end of the 21st century globally than the 1986–2005 average under Representative Concentration Pathways 8.5. This increase of temperature will result in a higher evapotranspiration rate, which will subsequently affect other water budget terms. Therefore, it is necessary to evaluate how reservoir systems will respond to changes in precipitation and temperature.

In this study, storage and release were examined for each season in terms of precipitation elasticity and temperature sensitivity. Precipitation elasticity of release ($\varepsilon_P(P,Q)$), as defined in Equation 2.7, is commonly used to estimate how the streamflow will change based on changes of precipitation (Sankarasubramanian et al., 2001; Schaake, 1990). To evaluate the effect of precipitation on storage, we defined the precipitation elasticity of storage, $\varepsilon_P(P,S)$ (Equation 2.8). Similarly, temperature sensitivity of release (Nash and Gleick, 1991), $S_T(P,Q)$, and temperature sensitivity of storage, $S_T(P,S)$, were defined in Equations 2.9 and 2.10, respectively. Here, the unit for Q and P is m^3/s and mm/day, while the unit for T is °C.

$$\varepsilon_P(P,Q) = \frac{\Delta Q/Q}{\Delta P/P} \tag{2.7}$$

$$\varepsilon_P(P,S) = \frac{\Delta S/S}{\Delta P/P} \tag{2.8}$$

$$S_T(P,Q) = \frac{\Delta Q/Q}{\Delta T/T} \tag{2.9}$$

$$S_T(P,S) = \frac{\Delta S/S}{\Delta T/T} \tag{2.10}$$

Results from Figure 2.10a-b indicate that both $\varepsilon_P(P,Q)$ and $\varepsilon_P(P,S)$ will increase as precipitation increases. The range varies from 0.09 to 0.19 for storage and 0.66 to 1.68 for release. However, the precipitation elasticity is not always linearly correlated with the percentage

of change in precipitation. For example, $\varepsilon_P(P,S)$ keeps increasing from a -30% to a 10% change in precipitation, but then remains constant from 10% to 30%. The increase in $\varepsilon_P(P,Q)$ indicates that an additional unit increase of precipitation will result in a larger increase of release. Eventually, the rise in inflow will cause the water level in the reservoir system to rise. However, because the optimal water level is defined by the CPS, reservoir managers need to release the excess water as soon as practical. This leads to limited growth of $\varepsilon_P(P,S)$ when $\Delta P/P$ increases from 10% to 30%. There is also a clear distinction among seasons, where winter-spring (DJF-MAM) tends to have larger values than summer-fall (JJA-SON). This can be explained by the higher evapotranspiration resulting from higher temperatures in the summer and fall seasons.

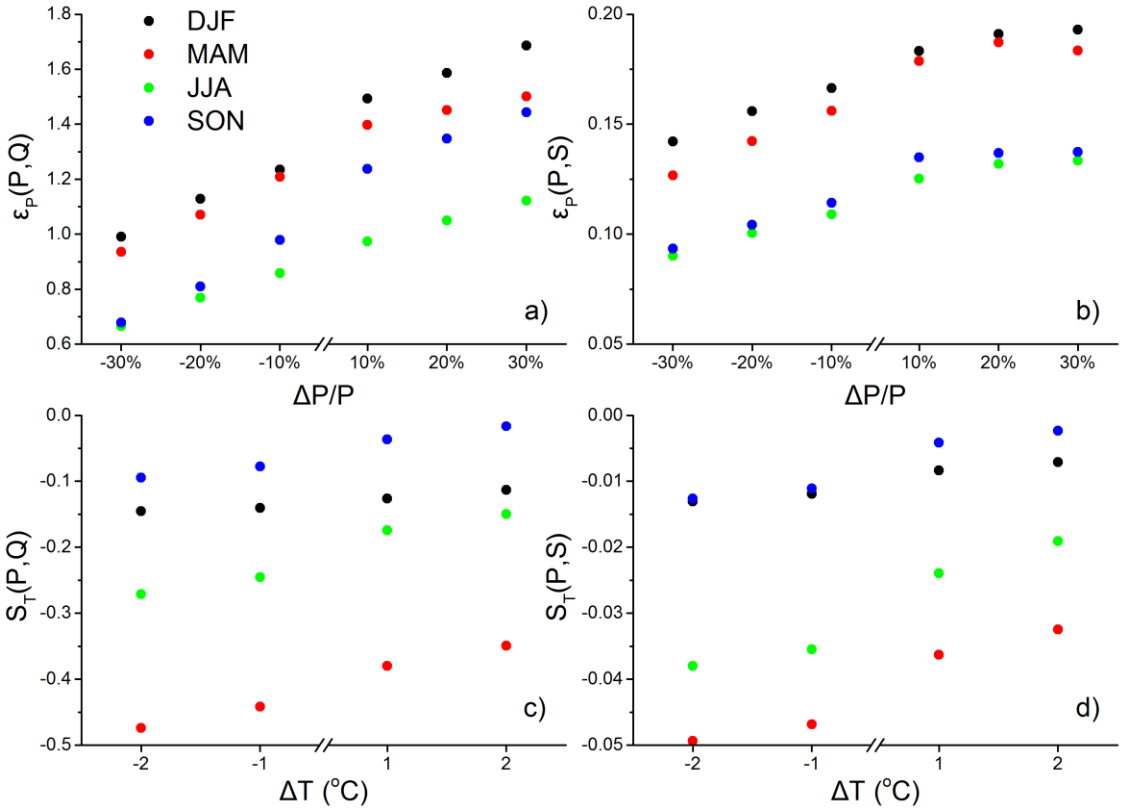

Figure 2.10 Precipitation elasticity and temperature sensitivity for storage and release, with a) precipitation elasticity of release, b) precipitation elasticity of storage, c) temperature sensitivity of release, and d) temperature sensitivity of storage. (Reprinted with permission from Zhao et al., 2016b)

The trend in temperature sensitivity is similar to that of precipitation elasticity, except that the values are all negative (Figure 2.10c, 10d). For the same amount of precipitation, higher temperature will lead to a larger evapotranspiration rate, which results in less runoff. The positive trend of the temperature sensitivity indicates that an additional unit increase of temperature will result in a smaller decrease of release. Regarding seasonality, temperature sensitivity behaves differently from precipitation elasticity. Compared to spring-summer (MAM-JJA), fall-winter (SON-DJF) has lower absolute $S_T(P,Q)$ and $S_T(P,S)$ values. This is because,

in Texas, fall-winter (the cold season) is more water limited, which results in a smaller increase in ET than during spring-summer.

2.5 Conclusion

Due to the spatial heterogeneity and temporal variation of hydrological variables, it is impossible to provide constantly reliable and riskless water supply from unimpounded river flow. To increase the reliability and water-use flexibility, numerous reservoirs have been constructed around the world. Under the impacts of overwhelming environmental changes, how to best manage our water resources in a sustainable manner is a growing concern. However, robust estimation of future water availability is still facing great challenges because of the difficulties involved with linking natural hydrological processes and reservoir operations. Therefore, in this study, a new reservoir module was incorporated into DHSVM to close this gap. The integrated modeling framework sets a base for improving the hyper-resolution representation of interdependent natural – human systems, and for supporting adaptation under non-stationary conditions. By conducting a case study using this integrated model, we have shown several outcomes:

- The model calibration and validation results (as shown in Figures 6 and 7) suggest that the integrated model is able to capture the reservoir release and storage variations at a sub-monthly level. By adding reservoirs into DHSVM, the downstream flow values can be simulated more accurately.
- Reservoirs play an important role in streamflow regulation, especially with regard to flood control practices. After being rerouted by Lake Whitney, the upstream peak flows can almost always be controlled to under the downstream channel capacity.

- Our results have shown that both storage and release values are sensitive to several parameters—but especially to conservation pool storage. For Lake Whitney, conservation pool storage (which is a parameter that both storage and release values are sensitive to) has been changed several times in the 1960s to meet water management needs.
- Precipitation elasticity and temperature sensitivity of release and storage have been quantified. The precipitation elasticity of both release and storage increases when precipitation increases, but the scale varies by season. The temperature sensitivity of release and storage also shows a positive trend (in both case), but the values are negative. These results can be beneficial for future flood and drought risk mitigation, which is important for a semi-arid climate watershed.

Even though the case study was carried out over USACE reservoirs, the integrated model is applicable for other reservoirs as most water management agencies use similar pool configurations. Model users can always tailor the settings to their own needs. For example, some reservoirs may not be used for flood control. This can be addressed by assigning a value of zero to the flood control pool volume in the module. If the reservoir has very limited information about the pool configuration, the corresponding parameter can also be obtained by calibration. This integrated model can also be coupled with optimization algorithms to improve the existing operation rules. Because the impoundment phase can be captured by the reservoir module, new reservoir design and operation rules can also be evaluated using our model. In addition, the capability of simulating hydropower generation can be beneficial for future energy management under the impact of global environmental changes.

While this module performs well in reservoir simulations, it does have some limitations. First of all, it is not a fully distributed reservoir module. Even though it can be located within a user-specified river segment, it cannot calculate the water interactions between the lake and its surrounding area in a distributed manner. To address this, we used an empirical monthly parameter ($MSRR$) to represent the process. In addition, this module was not designed to calculate daily hydropower water demand, which can be extremely complicated due to the highly variable hydropower demand. Instead, it only uses a monthly value to represent the overall release for hydropower. Our primary objective was to integrate a reservoir module that can provide accurate sub-monthly storage and release values. Therefore, we expect that the integrated model can provide a platform that will contribute to water availability estimation at the watershed scale by including natural-human system interactions. Furthermore, it can be used to investigate the effects of climate change on water release (and possible adaptation strategies, such as changes in operation rules, or by including a new reservoir) in terms of reservoir management practices.

CHAPTER III

A MODELING FRAMEWORK FOR EVALUATING SURFACE WATER SUPPLY SYSTEM UNDER NON-STATIONARITY[†]

3.1. Introduction

Resilient water supply systems are critical for urban socio-economic development. To be classified as resilient, a water supply system should not respond precipitously to a major 'surprise' during its economic life (Fiering, 1982). Currently, most of the existing water infrastructures were designed with the assumption of stationarity—a belief that historical statistics can be applied to future decision making (Matthews et al., 2011; Koutsoyiannis & Montanari, 2015). However, this assumption is challenged by ongoing global environmental changes, such as climate change, population growth, and land use land cover (LULC) change (Milly et al., 2008; Gao & Bryan, 2017). Subsequently, the sustainability of our water resources management systems is at unprecedented risk (Dovers & Handmer, 1992; Hirsch, 2011).

To manage a water supply system sustainably, the key is to balance water availability with water demand. Yet both availability and demand are susceptible to non-stationarity. On the availability side, there are multiple non-stationary factors such as climate change, flow regulation, LULC change, and increasing groundwater withdrawals (Kundzewicz et al., 2008; Zhang et al., 2015; McDonald et al., 2014; Barlow & Leake, 2012). Among these, climate change induced precipitation alteration is expected to result in the largest impact on water

---

[†] *Reprinted from Journal of Hydrology, Volume 563, Gang Zhao, Huilin Gao, Shih-Chieh Kao, Nathalie Voisin, Bibi S. Naz, "A modeling framework for evaluating the drought resilience of a surface water supply system under non-stationarity", Pages 22-32, Copyright (2018), with permission from Elsevier*

availability (Milly et al., 2005; Schewe et al., 2014). In the past several decades, both observations and model simulations have shown increasing aridity trends across the globe due to the changing climate (Dai, 2013). Moreover, with enhanced evapotranspiration loss due to increasing global temperatures, droughts are likely to be more severe with longer duration (Parry, 2007). On the demand side, both the net growth and migration of population challenge the stationarity assumption. Global freshwater consumption has increased nearly six-fold from 1900 to 1995 as a result of population growth (Shiklomanov, 1999). Specifically, regional water demand has surged due to urbanization (population redistribution) for many regions in the world. How to best provide sufficient water for the world's growing cities has become the most difficult and urgent problem for water management (House-Peters & Chang, 2011). Results from McDonald et al. (2011) suggest that there were 150 million people in city areas suffering from perennial water shortage in the year 2000. This number will increase to 1 billion by 2050 due to population growth.

However, evaluating future water supply resilience in a non-stationary fashion is critically difficult, primarily due to three challenges. The first challenge is that the current modeling tools are inadequate to represent the dynamic feedback between hydrologic variabilities and water management decisions. Currently, natural hydrological processes and water management activities are modeled in a separate or not-fully-integrated manner (Muttiah & Wurbs, 2002; Portland Water Bureau, 2002; O'Hara & Georgakakos, 2008; Matonse et al., 2013). Despite in-depth thoughts and processes existing in both types of models (i.e., natural rainfall-runoff versus operational reservoir management models), the connections were usually loosely made through a few selected surface water controlling points. This simplification would inevitably lead to inaccurate simulation of water availability and demand, as well as their

dynamic two-way interactions (Zhao et al., 2016b). A few models—such as the Hydrological Simulation Program-Fortran (HSPF; Bicknell et al., 2001) model and the Soil and Water Assessment Tool (SWAT; Arnold et al., 2012)—are capable of addressing processes on both sides. However, such models are usually lumped/semi-lumped and are insufficient to represent dynamic features such as enhanced open water evaporation through reservoirs. Therefore, full integration of the spatially distributed hydrological processes with water management activities should be prioritized for model development and employment.

The second challenge is that droughts are intrinsically difficult to predict—especially in the long-term future (given the large uncertainties). Considering its low probability and our limited observational records, future drought scenarios that fully rely on historical observations (Frick et al., 1990; Bekele & Knapp, 2010) may underestimate the severity and trend of future droughts in the context of notable thermodynamical and dynamical global changes (Emori & Brown, 2005; Seager et al., 2010). Even for the historical period, there are still disagreements about the trends of global drought (Dai, 2013; Sheffield et al., 2012). In order to evaluate water supply resilience more reliably, there is a need to utilize ensemble-based future drought projections to support our decision making.

The third challenge is that both availability and demand estimates involve large uncertainties, which add another layer of complexity to the water supply resilience evaluation. Yet uncertainty analysis is important for policy makers who make important decisions under an environment of risk. Thus, quantification of uncertainties associated with non-stationarities is critical for water resilience evaluation.

To our knowledge, there have been very few studies that focus on water supply resilience under multi-year droughts using fully distributed hydrological models dynamically coupled with water management systems (Amarasinghe et al., 2016; Watts et al., 2012; Collet et al., 2015). Most of these studies mainly tested the system resilience based on historical or artificially designed droughts—and not on the expected future droughts derived from state-of-the-art climate models. Therefore, in this study we used a novel modeling framework which integrates hydrological processes and water management decisions (Zhao et al., 2016b) to overcome these limitations and dynamically evaluated water supply resilience under the impacts of two most significant sources of non-stationarities—potential multi-year droughts, and the growing demand from an increasing population. We specifically want to answer three scientific questions:

1) How do sources of non-stationarities from both availability, especially under multi-year droughts, and demand influence the resilience of a water supply system?
2) How do uncertainties associated with these sources of non-stationarities compare, and which side (i.e., availability or demand) is dominant?
3) What are the possible mitigation strategies to improve water supply resilience?

In this dissertation, we use a case study to demonstrate a holistic approach for evaluating the future water resilience of large cities under an environment of non-stationarity by bridging the gap between hydrological modeling, water management practices, climate change studies, and population/demographic projections. In Section 2.2, the selected study area, the City of Dallas, is introduced. The detailed methodology is explained in Section 2.3. In Section 2.4, the model calibration/validation results are first demonstrated, and then the future water supply and demand are compared and analyzed under various drought scenarios (with the goal of answering

the aforementioned scientific questions). Section 2.5 discusses the conclusions and the general applicability of this approach.

3.2. Study area

The City of Dallas in Texas (Figure 3.1) was selected as our pilot study area to demonstrate the modeling framework, which is applicable to any surface water dominated urban water supply system. Dallas is the ninth largest city in the U.S. in terms of population size. From 1950 to 2010, Dallas has experienced very fast urbanization, both inside of the city boundaries and in the surrounding suburbs. Within the city alone, the population has increased from 0.43 million to 1.20 million during this time period. With this rapid urbanization process, the capability of existing water systems to handle increasing future demand becomes a main concern for water resources planners in the area.

Because of the limited groundwater resources, the water supply of Dallas fully depends on surface water, which is highly variable seasonally and inter-annually. During the severe 1950s statewide drought, Dallas' municipal water supply was fully depleted. The city's major water source, Lake Dallas, only had a capacity of 2.39×10^8 m^3. This was quickly depleted once the drought started, and the city had to purchase salty water from the distant Red River to survive. Because of the severe water stress induced by this drought, policy makers launched extensive reservoir construction projects to reduce future drought impacts on the city (Figure 3.1). In the Trinity River Basin, four lakes were gradually constructed—Grapevine Lake (impounded in 1952), Lavon Lake (1953), Lake Ray Hubbard (1969), and Ray Roberts Lake (1987). Lake Dallas was also expanded to 5.38×10^8 m^3 and renamed as Lewisville Lake (1955). In addition,

the City of Dallas contracted with the Sabine River Authority for additional water supply from Lake Tawakoni (1960) and Lake Fork (1980). In 2010, these seven multi-purpose reservoirs were capable of providing about 1.89×10^6 m^3/d for Dallas. Dallas Water Utilities (DWU) is responsible for the municipal water supply for the city, and for 27 wholesale customer cities. The total population served by DWU from the connected reservoirs was 2.40 million in 2010, with a total water demand of 1.63×10^6 m^3/d (Texas Commission on Environmental Quality, 2017).

Even though the combined capacity of these seven reservoirs is sufficient to satisfy Dallas water demand at 1.63×10^6 m^3/d, the real-time reservoir storage varies considerably due to climate variability and other factors. How this water supply system will respond in a non-stationary environment is an unsolved question for the policy makers. Climate change, and the associated increase in severity and frequency of extreme events that affect future water availability, are increasing this challenge (Venkataraman et al., 2016). Meanwhile, the city will also be stressed by increasing water demand from population growth, which will be exacerbated by decreasing water availability due to more frequent drought conditions. Therefore, to better support policy making for the sustainable development of the City of Dallas, it is essential to quantify the resilience of the water supply system in the context of demographic growth and future potential droughts.

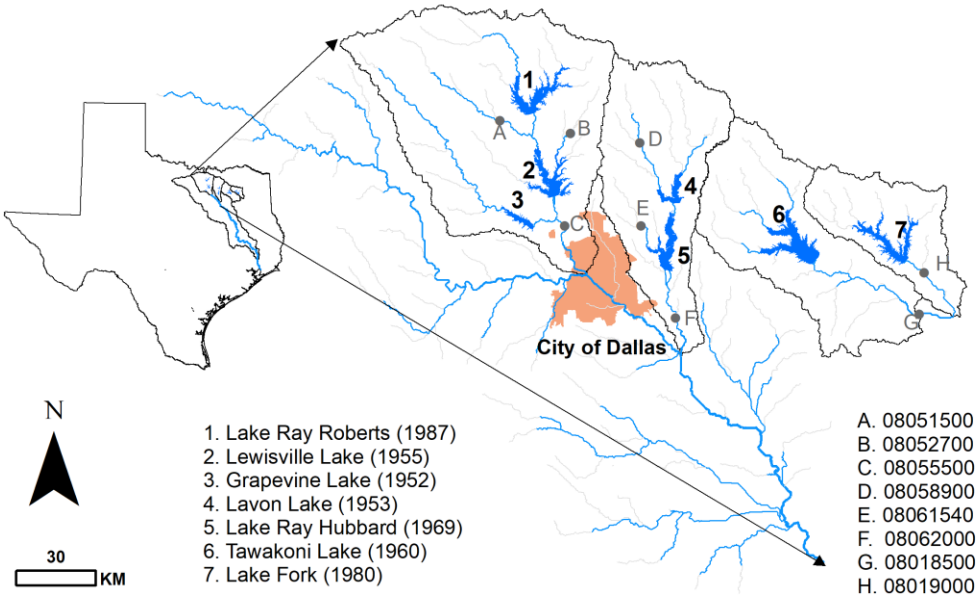

Figure 3.1 Simulated watersheds which provide inflows to the Dallas water source reservoirs. Both the reservoirs and USGS streamflow gauges used for model calibration and validation are indicated. (Reprinted with permission from Zhao et al., 2018)

3.3. Methodology

3.3.1 Drought quantification under future climate conditions

In a changing climate, drought projections that only use historical data are no longer appropriate for representing the non-stationary system. In the past decades, general circulation models (GCMs) have been substantially improved with regard to both model algorithms and spatiotemporal resolutions (IPCC, 2013). Even though these physically based models provide quite different projections for the future, they offer a range of possible conditions by simulating the evolution of the physical processes. Therefore, they are widely used for drought evaluation under a non-stationary climate (Ghosh & Mujumdar, 2007; Touma et al., 2015).

There are several drought indexes that are commonly used for quantification of different drought types (e.g., atmospheric, hydrological, and agricultural). In this study, we employed the widely used Palmer Drought Severity Index (PDSI; Palmer 1965) to quantify meteorological drought. As it uses the Available Water Content (AWC) of the soil to calculate other basic hydrologic terms (such as potential evapotranspiration (PET), potential runoff, soil recharge, and soil loss), it is capable of accurately capturing the drought characteristics impacting the surface water-based supply system of Dallas. For the PET calculation, currently there are several algorithms available (Thornthwaite [1948], Hamon [1960], Priestley & Taylor [1972], Penman-Monteith [Monteith, 1965], and others). Among these approaches, the Penman-Monteith approach is considered the most accurate because it uses precipitation, radiative forcing, wind speed, and humidity data to estimate PET (instead of only using temperature, for example, such as the Thornthwaite's method). The PDSI generated from Penman-Monteith PET calculations (PDSI-PM) has shown to be a more accurate representation of historical droughts than the more commonly used PDSI from Thornthwaite's PET method (Sheffield et al., 2012). Thus, in this study, we employed PDSI-PM to better represent the drought processes. From this perspective, PDSI-PM is more physically based and thus more appropriate in this case study than other indexes (such as the standardized precipitation index and the aridity index) (Dai, 2011).

Statistically downscaled meteorological forcings were adopted from the Downscaled Coupled Model Intercomparison Project Phase 5 (CMIP5) Climate and Hydrology Projections (Reclamation, 2013). However, not all GCMs from CMIP5 are suitable for application on any given target watershed (Chiew et al., 2009). By comparing the cumulative probabilities between the GCM-based PDSI-PM and the observation-based PDSI-PM during the historical period (1950–1999), 8 models (out of 19) were selected to provide future drought scenarios given their

abilities to better represent the historical drought patterns. Representative Concentration Pathway (RCP) 8.5 was selected as an example to demonstrate the drought quantification framework. Compared with other RCPs, RCP 8.5 offers a larger uncertainty range for testing the water supply resilience.

Drought quantification was conducted in two steps. First, PDSI-PM time series were calculated for each of the 8 GCMs. In order to choose the drought events of interest from the time series, a threshold (under which droughts are defined) was applied. In the original study conducted by Palmer (1965), -0.50 was used as a threshold based on a case study in central Iowa and Kansas. However, this value was rather arbitrarily selected and was not identified based on physical meaning (Alley 1984). Thus, a location specific PDSI-PM threshold is more appropriate for quantifying the beginning and ending of droughts (Burke et al. 2006; Ryu et al. 2014; Svoboda et al. 2015). In this study, we used the 20th percentile of historical PDSI-PM values as the threshold. Second, the most severe droughts were selected based on the cumulative PDSI-PM deficit for two future periods (Figure 3.2 and Table 3.1). Period 1 is from 2000 to 2049, and Period 2 is from 2050 to 2099. We used the most severe droughts because they can better test the resilience of the water supply system, and therefore provide the worst possible situation (that can, in turn, help to adjust current policy).

Both Figure 3.2 and Table 3.1 suggested significant non-stationarity in future water availability (introduced by prolonged droughts). From Period 1 to Period 2, the average drought duration has increased from 23 months to 36 months. Similarly, the drought severity, which is the cumulative PDSI-PM deficit, has increased from 36.5 to 84.1. Specifically, the most severe drought in Period 2 lasts for 61 months, resulting in a severity of 181.3.

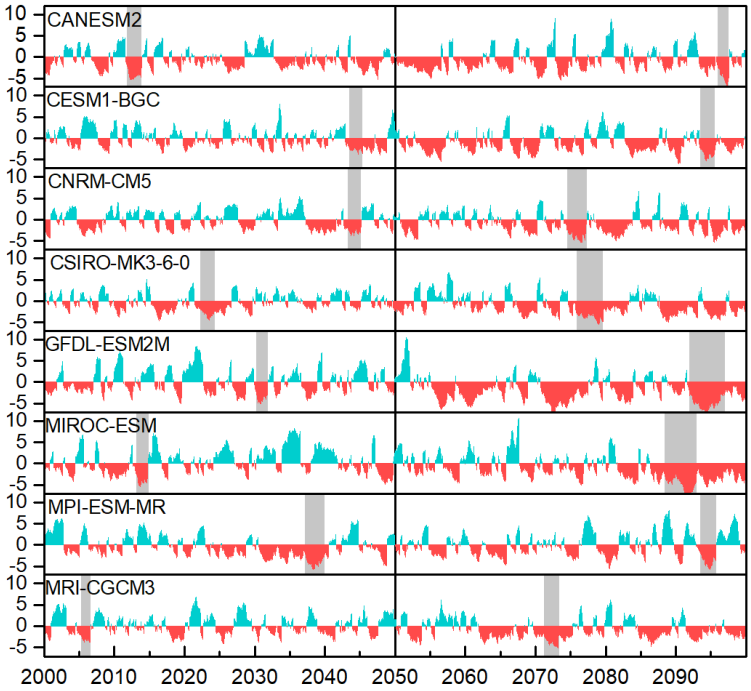

Figure 3.2 PDSI-PM time series from 8 GCMs in the RCP8.5 scenario. Grey shaded areas represent the most severe droughts based on a threshold of -1.924 (i.e., the 20th percentile of historical PDSI-PM) for Period 1 and Period 2. (Reprinted with permission from Zhao et al., 2018)

Table 3.1 List of the most severe droughts in the historical record and projected by GCMs. The 1950s drought was used as a baseline (Reprinted with permission from Zhao et al., 2018)

	GCM	Start date	End date	Average P (mm/month)	Average T (°C)	Length (months)	PDSI-PM Deficit
1950–1999	Observation	3/1/1954	11/30/1956	58.4	19.7	33	39.1
2000–2049	CANESM2	12/1/2011	11/30/2013	47.8	20.2	24	58.1
	CESM1-BGC	7/1/2043	5/31/2045	65.1	20.5	23	15.8
	CNRM-CM5	5/1/2043	2/28/2045	65.4	20.8	22	21.7
	CSIRO-MK3-6-0	4/1/2022	5/31/2024	58.3	19.9	26	26.4
	GFDL-ESM2M	4/1/2030	11/30/2031	53.8	22.0	20	38.3
	MIROC-ESM	2/1/2013	10/31/2014	51.4	21.0	21	43.2
	MPI-ESM-MR	3/1/2037	12/31/2039	51.8	21.6	34	70.6
	MRI-CGCM3	4/1/2005	7/31/2006	63.1	20.5	16	18.3
2050–2099	CANESM2	1/1/2096	7/31/2097	46.4	25.6	19	48.3
	CESM1-BGC	7/1/2093	7/31/2095	62.5	23.7	25	46.0
	CNRM-CM5	7/1/2074	3/31/2077	58.1	22.1	33	61.9
	CSIRO-MK3-6-0	11/1/2075	8/31/2079	55.4	23.1	46	77.9
	GFDL-ESM2M	12/1/2091	12/31/2096	52.9	22.3	61	181.3
	MIROC-ESM	6/1/2088	12/31/2092	59.5	24.9	55	159.3
	MPI-ESM-MR	7/1/2093	9/30/2095	56.7	25.2	27	52.6
	MRI-CGCM3	4/1/2071	5/31/2073	68.4	21.1	26	45.4

3.3.2 Water demand under growing population

Water demand is the total amount of water used by consumers. To ensure the regular operations of a society, the water demand should be satisfied regardless of the external circumstances (e.g. flood or drought). However, there are a number of factors that can influence water demand, especially with respect to population growth and changes in water use per capita per day (WUPCD). Some other influential factors include economic activities, LULC change, water price, water leakage, water recycling, and others.

Since water demand is affected by many factors (each with associated uncertainties), its future projection is usually limited. For example, many climate studies use fixed values for these parameters and provide multiple (or even single) scenarios for the water demand (Wu et al., 2015; Ranatunga et al., 2014; Laghari et al., 2012). Furthermore, there are no quantified uncertainties associated with the demand scenarios. This dramatically restricts the application of these studies in the policy making process.

Historically, the city planners have been managing the water supply reservoirs as a system. Therefore, we made future projections based on the total water use from these 7 reservoirs (instead of making an individual projection for each one of them). Using the 2007-2011 water use data as the initial condition, a Monte-Carlo simulation was utilized to estimate future water demand in order to obtain the most likely demand values with their associated confidence intervals. It is assumed that the future water demand is primarily affected by population and WUPCD. For population, we defined an increase rate, r_N, which follows a normal distribution – an approach used in many studies (Hone, 1999; Nam & Reilly, 2013). The average population increase rate (r_N,) is set to 1.32%/yr for the City of Dallas according to the Dallas City Council (2014). With respect to WUPCD, there is a decreasing trend due to technology improvement and policy intervention over the past 30 years (Texas Water Development Board [TWDB], 2016). In 2011, the average WUPCD for Dallas was about 745 liters, which has reduced by 235 liters since 2000. However, compared with other US cities – such as New York City, which currently has a WUPCD of 450 liters – there is a large potential to further reduce the Dallas water demand per capita. Thus, TWDB projected a continuous reduction of WUPCD for Dallas. The average decrease rate is 0.45%/yr (TWDB, 2016). The decreasing rate of WUPCD, r_U, is also assumed to follow a normal distribution to account for

possible uncertainties (Billings & Jones, 2011). The parameters of these two normal distributions were estimated according to the Dallas City Council (2014). Other factors such as water supply leakage and rainfall harvest – which are considered to be water conservation practices (see Section 2.4.3) –are not represented in Equation 3.1.

$$WD = N_0 \cdot (1 + r_N)^t \times U_0 \cdot (1 - r_U)^t \tag{3.1}$$

$$r_N = d_{norm}(\mu_N, \sigma_N, a_{N,min}, b_{N,max}) \tag{3.2}$$

$$r_U = d_{norm}(\mu_U, \sigma_U, a_{U,min}, b_{U,max}) \tag{3.3}$$

where WD is total water demand, N_0 is the initial population, r_N is the population growth rate, U_0 is the initial WUPCD, and r_U is the WUPCD decrease rate. Both r_N and r_U follow normal distributions (Equations 3.2-3.3), where μ, σ, a, and b are the mean, standard deviation, lower boundary, and upper boundary for the normal distribution. Both r_N and r_U are assumed to be statistically independent. A total of 10000 samples were generated through Monte-Carlo simulation to support the analysis.

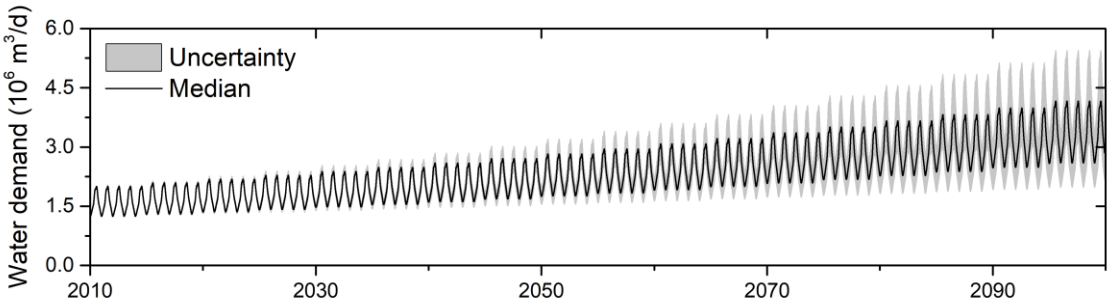

Figure 3.3 Water demand projections from 2010 to 2099. The solid line shows the median value, and the shaded area shows the uncertainty (1st and 99th percentiles from Monte-Carlo simulations). (Reprinted with permission from Zhao et al., 2018)

After computing the probability distribution of WD, the 1st, 50th, and 99th percentiles were selected to represent the best, median, and worst future water demand scenarios. Due to the randomness feature of the Monte Carlo simulation, the minimum and maximum values from the samples are usually sensitive to the sample size. Thus, the 1st and 99th percentiles are more suitable (and additionally, they can represent most of the uncertainty range of the simulation). The 1st percentile value represents we have a 99% confidence level that future water demand will be higher than this value. For convenient illustration, the 1st, 50th, and 99th percentiles are referred as the minimum, median, and maximum hereafter. Once the total water demand data for the entire City of Dallas for a future year is determined, it is distributed to the 7 reservoirs proportionally based on the historical water use pattern. Seasonal variation is prescribed based on the 5-year historical data from 2007 to 2011. Figure 3.3 shows the continuous increase of total water demand (i.e., non-stationarity in water demand). The median water demand increases from 1.63×10^6 m^3/d in 2010 to 3.35×10^6 m^3/d in 2095. Along with the magnitude, the uncertainty range (the difference between minimum and maximum) is also increasing. In 2020, the uncertainty range is 1.32×10^5 m^3/d, which increases to 1.84×10^6 m^3/d in 2095.

3.3.3 Hydrological and water management simulations

As explained in the Introduction, a thorough understanding about the interplay between natural and managed water systems is critically lacking. This is because there are few distributed models that fully integrate natural hydrological processes and systematic water management practices. To close this knowledge gap, a newly developed model was employed in this study. The Distributed Hydrology Soil Vegetation Model with reservoirs (DHSVM-Res; Zhao et al., 2016b) is a physically-based fully-distributed model that has explicit reservoir operation functions incorporated (Figure 3.4). Built upon the high spatial-temporal resolution DHSVM

(Wigmosta et al., 1994), the model is suitable for investigating hydrologic regimes over heterogeneous domains under extreme events and/or a changing environment.

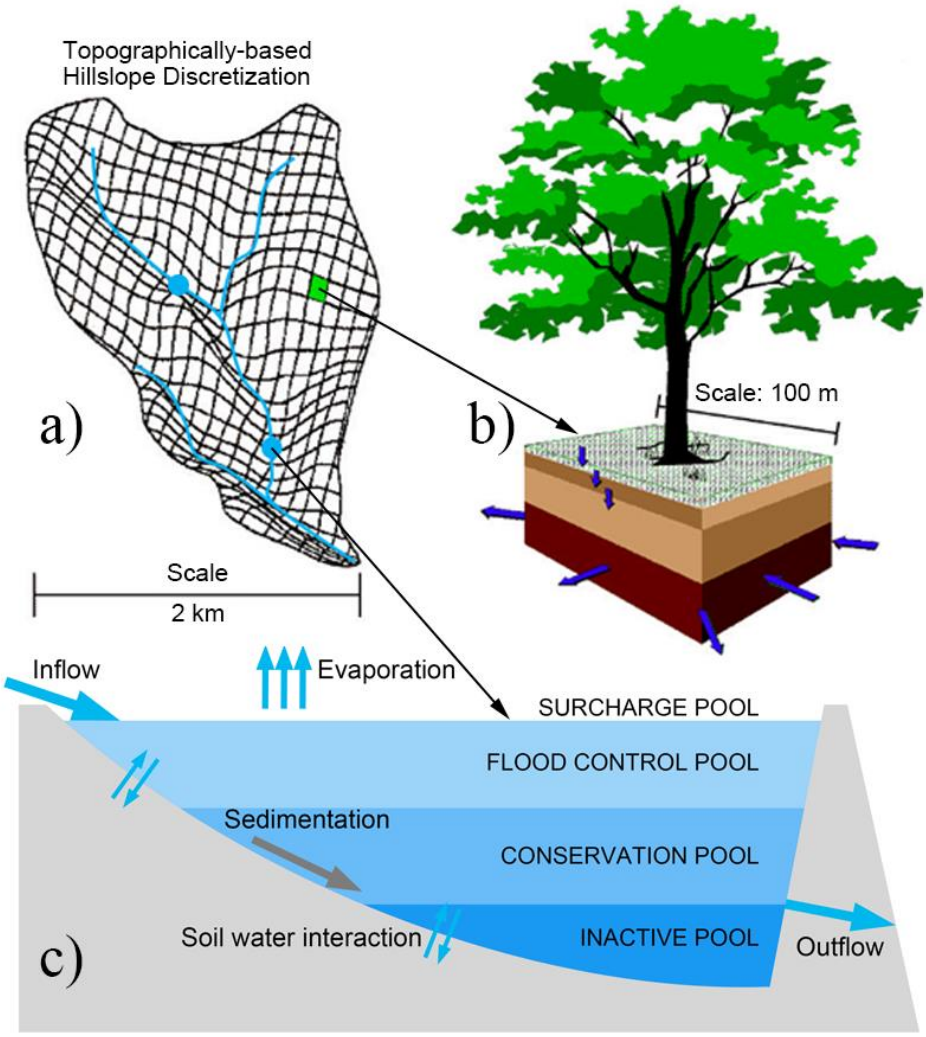

Figure 3.4 Conceptual representation of DHSVM-Res which includes: (a) topographically based basin discretization in original DHSVM; (b) water movement for each grid cell; and (c) the integrated, multi-purpose reservoir with a flood control pool, a conservation pool, and an inactive pool. (Reprinted with permission from Zhao et al., 2018)

Specifically, DHSVM-Res has two features which are essential for studying integrated natural and managed water systems under conditions of non-stationarity. First, it explicitly represents the effects of urban land cover on hydrological processes using fractional impervious area and detention storage (Cuo et al., 2008). Second, the reservoir module is capable of simulating the management of a water system (e.g., multi-reservoirs) using either real or optimized operation rules (Zhao et al., 2016b). In-channel water withdrawals, reservoir storage withdrawals, reservoir water release, and return flows (e.g., flow from wastewater treatment plants) can be all simulated at their real-world locations within the model. In this study, we used historical monthly water use observations from TWDB and prescribed reservoir operation rules from the U.S. Army Corps of Engineers (for the water management simulations). Because most wastewater treatment plants for Dallas are located downstream of the simulated watersheds (Figure 3.1), return flow is not included in this study.

The hydrological and water management simulations involved three steps. First, the DHSVM-Res model was calibrated and validated using historical observations, including streamflow station data and reservoir storage data from multiple locations. We simulated each of the 4 subbasins (Figure 3.1) at a 200-meter resolution and a 3-hour time step. To focus on the non-stationarities of availability and demand, a fixed LULC map (i.e., National Land Cover Database 2006) was used. Because the urban growth is mostly located in the downstream regions of the study area (Figure 3.1), impacts of LULC change on reservoir storage and supply reliability are very limited. The next step involved scenario simulations. The meteorological data during the selected drought events (Section 2.3.1) were used to drive DHSVM-Res. For each drought event, the reservoir release was calculated based on the projected water demand data. For example, the most severe drought projected for Period 1 by MPI-ESM-MR lasts from March

2037 to December 2039. Thus, the predicted water demand for this time period (Section 2.3.2) was used for the DHSVM-Res simulation associated with this drought event. In this study, the 1950s drought (from March 1954 to November 1956) was used as a baseline drought event. Because all reservoirs in the Dallas region were constructed after the 1950s drought, there was no corresponding water use data for this drought. Thus, we used three designed water demand scenarios (i.e. 2010, 2050, and 2090 water demand data) to take into account the uncertainty due to population and WUPCD changes. Outputs from Period 1 (2000–2049) and Period 2 (2050–2099) were compared with the baseline (1950s drought) to assess the long-term trend. Finally, several mitigation strategies to promote water supply resilience were tested using DHSVM-Res to identify the optimal solution for mitigating drought impact.

3.4. Results and discussions

3.4.1 DHSVM-Res calibration and validation

The model was calibrated from 2005 to 2011, and validated from 1980 to 2004 (Figure 3.5). To best represent the subbasin hydrological processes and reduce the risk of overfitting, we chose to calibrate and validate for multiple streamflow monitoring locations. Based on data availability and watershed characteristics, 8 USGS gages were selected. The coefficient of determination (R^2) and the Nash-Sutcliff model efficiency (NSE) were used as the calibration criteria. Overall, the simulated outputs (including reservoir water elevation and streamflow) are in good agreement with the observed ones. For reservoir water elevation, the R^2 value ranges from 0.60 to 0.95 and the NSE ranges from 0.46 to 0.95. The low NSE for Ray Hubbard might be caused by the incomplete water use data. It is worth noting that the model can also capture the reservoir impoundment activities in an accurate manner, which can be useful for evaluating new

reservoir operations. For streamflow simulations, the R^2 ranges from 0.70 to 0.85 and the NSE ranges from 0.43 to 0.84. These good levels of agreement benefit from the hyper-resolution and the explicit water management system simulations of DHSVM-Res.

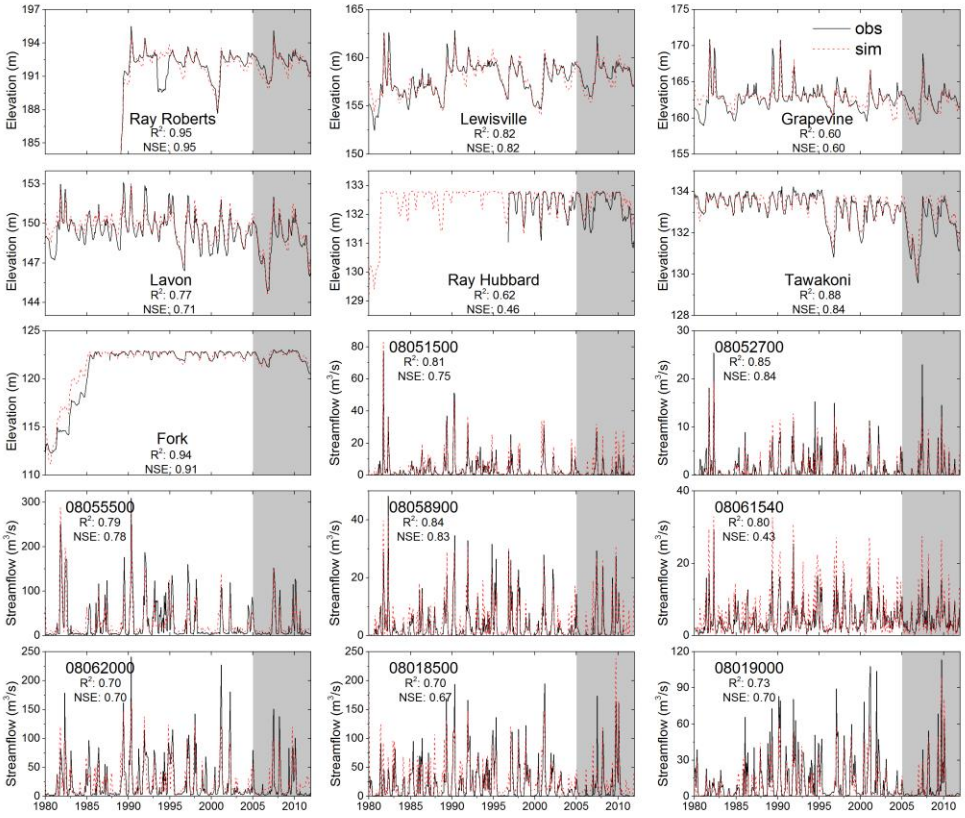

Figure 3.5 Model calibration and validation results (on a monthly scale) over 7 reservoirs and 8 streamflow gauge locations. (Reprinted with permission from Zhao et al., 2018)

3.4.2 Impacts of non-stationary water availability and demand on system supply resilience

Both reduced availability from multi-year drought events and increasing demand from population growth will significantly affect the water supply resilience. As discussed in detail in Sections 2.3.1 and 2.3.2, the hydrological model was used to simulate the water availability

under future drought events extracted from a GCM ensemble, while Monte Carlo simulations were adopted to calculate the growing demand from population growth and WUPCD changes. To quantify the water supply resilience in Dallas, we employed two metrics: the relative storage and the water supply reliability. Because city planners manage the 7 reservoirs as a system to meet the water needs of the Dallas area, we evaluated these metrics for the system (rather than individual reservoirs). Thus, the relative storage is defined as the total storage divided by the total conservation storage over the 7 reservoirs in the study domain. Similarly, the water supply reliability is defined as the total water supply divided by the total water demand for each month. The overall supply reliability for a projected drought event is calculated by simply averaging the monthly values. Both metrics were shown as percentage values. To facilitate the analysis, we focused on the temporal evolution of the droughts with the assumption that the reservoir storage initial state is at the top of the conservation pool for every reservoir at the beginning of each drought event.

Figure 3.6a shows the relative storage from the ensemble of droughts during Period 1 and Period 2, as well as the relative storage from the 1950s drought under 2010, 2050, and 2090 demands. For these simulations, the corresponding median values of the projected water demand were used. Clearly, the average drought duration in Period 2 (36.25 months) is significantly longer than that in Period 1 (21.75 months). Due to the larger severity and longer duration, the average relative storage during a drought drops from 69.7% to 53.6% (16.1% difference) from Period 1 to Period 2.

Figure 3.6b shows water supply reliability from the ensemble of droughts during the two periods. During Period 1, the reservoirs can still provide a sufficient amount of water to the city under severe drought. Water supply reliability for most droughts can maintain a level of 100%.

Yet with respect to Period 2, the water supply reliability decreases dramatically due to both longer drought durations and larger water demand. During the first year of the drought, all of these 7 reservoirs can still maintain 100% supply reliability. However, the reliability value drops to 26% after 50 months, which indicates that these potential long-term droughts will cause devastating economic and ecological consequences. Comparing Period 1 with Period 2, the average water supply reliability during a drought drops from 95.9% to 81.7% (14.2% difference). There is also a significant difference in the first decision point (i.e., the first time water reliability drops under 100%) between Period 1 and Period 2. The median value for these 8 models decreases from 24 months to 14 months from Period 1 to Period 2. This decrease is mainly caused by water demand increase. For the 1950s drought, the first decision point decreases from 29 months to 20 months to 13 months, as the water demand changes from the 2010 water demand to the 2050 demand to the 2090 demand. Typically, supply reliability is assessed under a worst case scenario associated with a return period, or under a large sample of events. In this study, we mainly focused on the most severe droughts (which are the worst scenarios that water managers are typically concerned with). Therefore, the reliability values are relatively low.

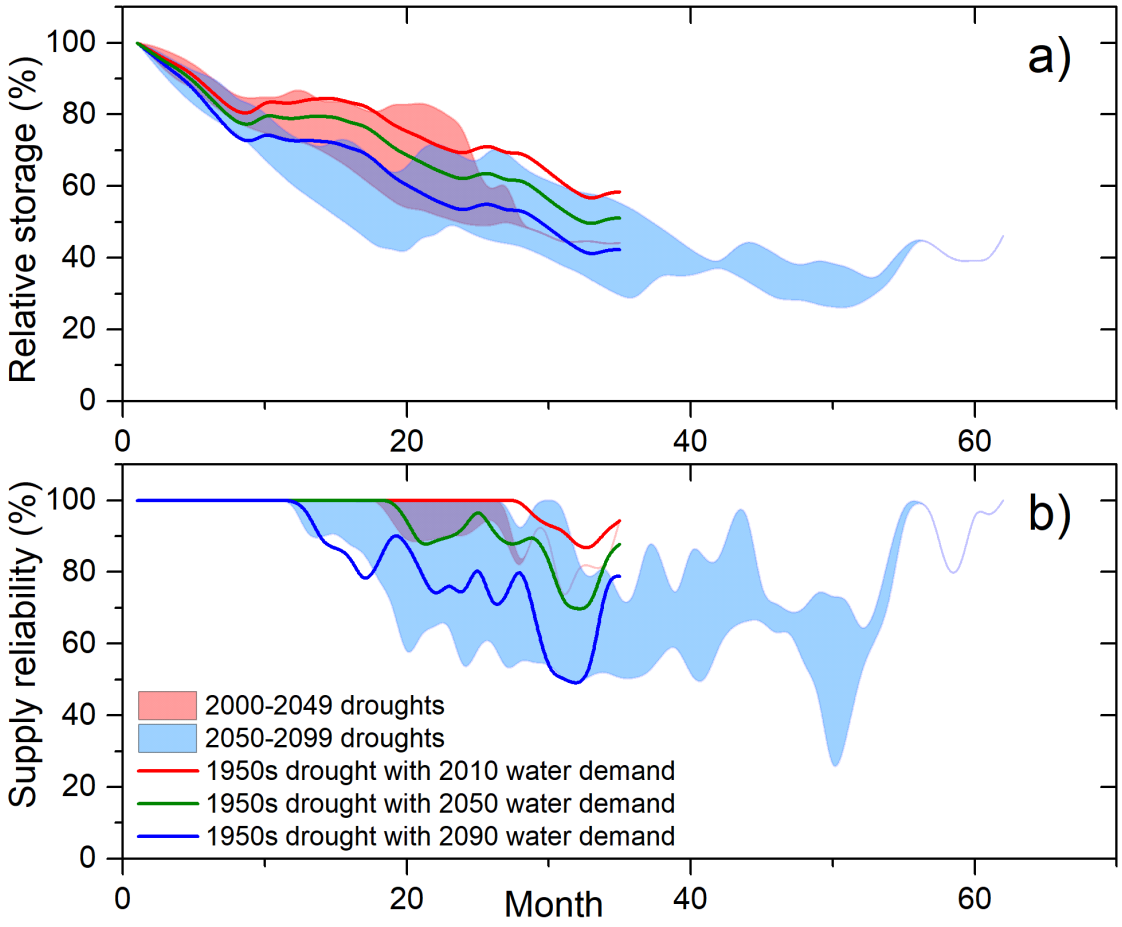

Figure 3.6 Responses of (a) relative storage and (b) water supply reliability to the CMIP5 drought events (with the corresponding water demand) and the 1950s drought (with the 2010, 2050, and 2090 water demand). Storage and water supply are the summation of 7 reservoirs. (Reprinted with permission from Zhao et al., 2018)

3.4.3 Uncertainties associated with the non-stationary water availability and demand

Both sides of the non-stationarities – water availability and demand – involve considerable uncertainties. For the availability side, uncertainties can be attributed to climate models, greenhouse gas emission scenarios, downscaling methods, and hydrological models. Among these, uncertainties associated with GCM structures are generally the largest (Kay et al., 2009; Prudhomme & Davies, 2009a; Prudhomme & Davies, 2009b; Bennett et al., 2012). By

choosing 8 GCM models, the uncertainties from different GCM structures can be represented in this study. On average, this uncertainty can result in a 13.3% variation of relative storage (Figure 3.6a), and an 18.7% variation of supply reliability (Figure 3.6b), for Period 2.

With respect to the demand side, primary sources of uncertainties include population growth rate and WUPCD change rate (Billings & Jones, 2011). The uncertainties from population growth and WUPCD changes can be represented using results from the Monte Carlo simulation (Figure 3.3). Using the projected minimum/median/maximum water demands in DHSVM-Res, the seasonality of relative storage and supply reliability was generated (Figure 3.7). Figure 3.7 shows how these water demand uncertainties – represented by the minimum/median/maximum demand values (as shown in Figure 3.3) – propagate to the DHSVM-Res simulated relative storage and supply reliability under the ensemble of drought events. For storage, clear seasonality can be observed, with September having the lowest value. This is mainly caused by high summer water consumption beginning in June. In addition, the high evaporation rate in the summer months also exacerbates the reservoir storage depletion. This lowest storage level also leads to the lowest supply reliability in the same month (Figure 3.7b).

Compared to Period 1, Period 2 shows a much larger uncertainty range for both relative storage and water supply reliability. For example, the storage uncertainty range for September in Period 2 is 9% (from 54% to 63%) while it is 2% (72% to 74%) in Period 1. Similar to the results in Figure 3.6, supply reliability in Period 1 is always close to 100%, with the exception of August and September. Because the demand uncertainty during Period 1 is small, it has little effect on the storage and supply reliability. However, in Period 2, demand uncertainty will have a

significant impact. The resultant uncertainty range of supply reliability in September for Period 2 is 19% (71% to 90%).

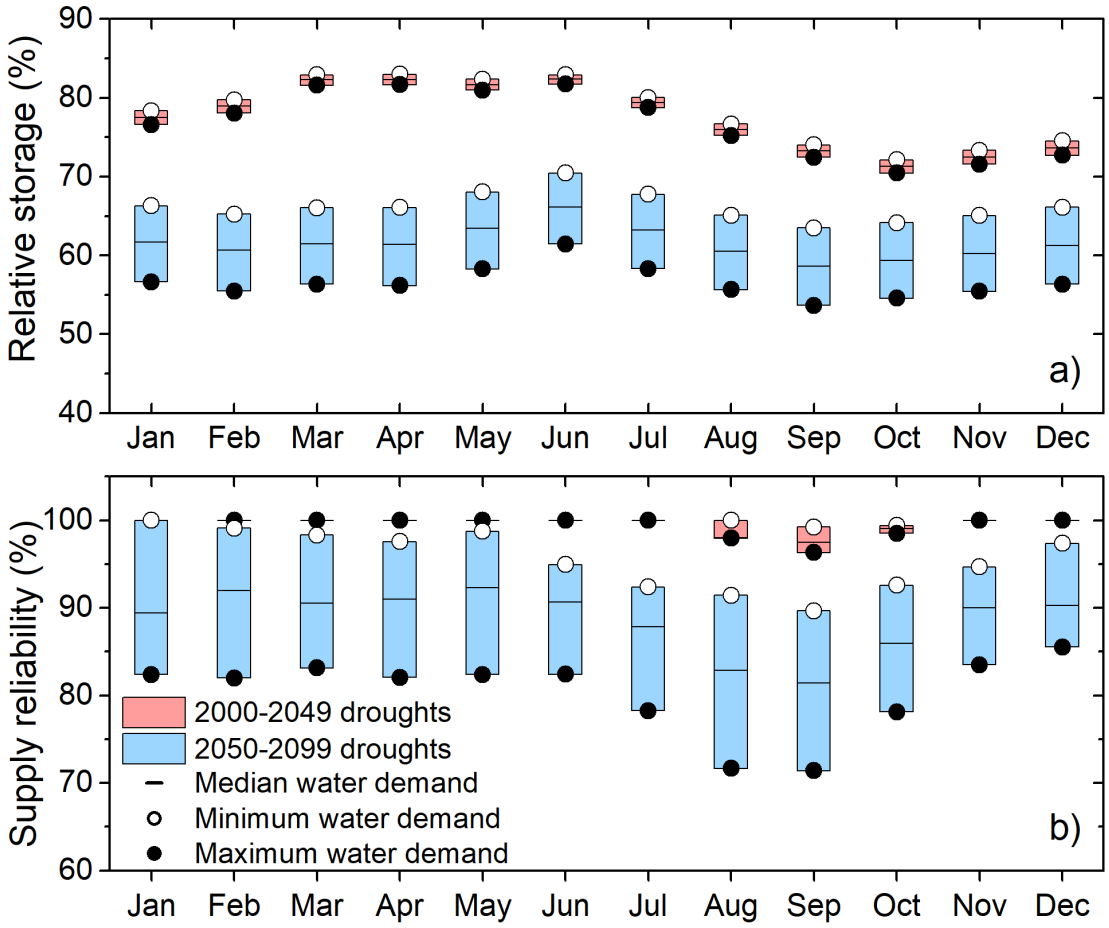

Figure 3.7 Impacts of different water demand scenarios on (a) relative storage and (b) water supply reliability for each month. The water demand scenarios have minimum, median, and maximum values as indicated in Figure 3.3. (Reprinted with permission from Zhao et al., 2018)

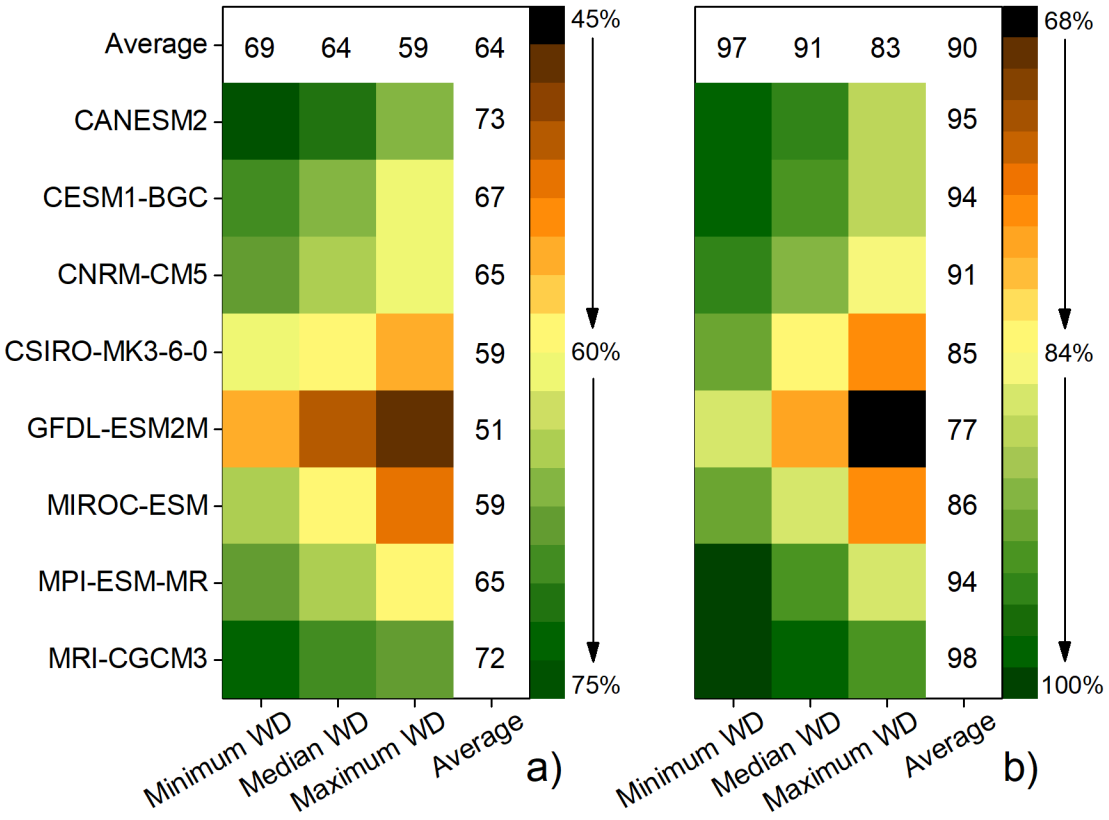

Figure 3.8 a) Relative storage and b) supply reliability for each GCM and each water demand scenario for Period 2 (2050-2099). Each colored grid represents the average value during the drought projected by the selected GCM under a given water demand scenario. Each value to the right is the average of its corresponding row, while each value on the top is the average of the corresponding column. (Reprinted with permission from Zhao et al., 2018)

As discussed above, both availability and water demand have notable uncertainties. Thus, it is essential to identify which of these parts plays a more dominant role with regard to water supply resilience. We compared the water resilience level (in terms of relative storage and reliability) driven by each GCM and water demand scenario (Figure 3.8). For relative storage, the uncertainty range associated with GCMs is from 51% to 73%, while that from the increasing water demand is from 59% to 69%. Water supply reliability is in the 77% to 98% uncertainty range with GCMs, and the water demand uncertainty range is from 83% to 97%. In general,

water availability non-stationarity shows a slightly larger uncertainty range. It is worth noting that these range values were calculated from an ensemble mean (averaged either from the 8 GCMs, or from the 3 demand scenarios). Because the study site for this research is the City of Dallas—one of the fastest growing large cities in the U.S.—the uncertainty range results from water demand non-stationarity are considerably significant. However, the GCM-based uncertainty is larger.

3.4.4 Mitigation strategy evaluations

In order to improve the water supply reliability, DWU has proposed several mitigation strategies such as additional conservation, integrating a new water source, and water use redistribution. In this study, the efficiency of these mitigation strategies was tested using DHSVM-Res:

(1) **Additional conservation**. Additional conservation mainly includes improving water use technology and reducing leakage and outdoor water use. The estimated saving percentage of total water use is 7% (TWDB, 2016). These additional conservation practices are proposed on top of the traditional conservation measures, especially during drought events. The traditional and long-term conservation measures (e.g., public awareness, policy intervention) were incorporated into the WUPCD projections (r_U in Equation 3.1), which tempers down the overall demand increase due to population growth.

(2) **Integrating a new water source**. Lake Palestine is a reservoir located in the nearby Neches River Basin, and is proposed to supply water to Dallas in the future. Palestine is estimated to be able to provide 3.86×10^5 m^3/d for DWU. However, the long distance to Dallas requires intensive construction of pipelines for water transfer.

(3) **Water use redistribution**. The current water use distribution among these reservoirs is based on the travel distance to the city, instead of the water availability (conservation storage) for each reservoir. For example, Lake Tawakoni has the largest conservation storage (which accounts for 23.8% of the total storage from the 7 reservoirs), yet it only contributes 10.9% of the total water supply. Redistributing the water use among these reservoirs based on reservoir storage can significantly improve the water supply reliability.

(4) **Combination strategy**. A combination of aforementioned 3 strategies was also tested. We compared the efficiency of these strategies over the longest potential future drought projected from GFDL-ESM2M during Period 2 (i.e., the most extreme drought) with the business-as-usual scenario (i.e., no mitigation strategies). Figure 3.9 shows that reservoir storage is continuously depleted during the drought for all of the strategies. The strategy by redistributing the water use shows the lowest relative storage. Consequently, even though more water can be supplied in the beginning, reliability will drop significantly around Month 50. Both additional conservation and new water source strategies show a slight increase of supply reliability. When all of these three strategies are combined, supply reliability shows the most improvement. The average supply reliability during the drought for business-as-usual is 77.8%, while it is 81.0%, 81.8%, 87.3%, and 93.7% for strategy 1 through strategy 4. These relative low reliability values are mainly caused by the chosen GCM (i.e., GFDL-ESM2M), which projects the worst drought in the future in this example demonstration. A non-parametric Kolmogorov-Smirnov Test was carried out to test whether the supply reliability is significantly improved using these strategies (as compared with the baseline run). P values for the tests (Figure 3.9b) show that both redistribution and combined strategies can significantly improve the supply reliability. However, the redistribution strategy shows no improvement for the extreme condition

(and has even worse supply reliability around Month 50). Therefore, compared with the individual strategies, the combined strategy is the most appropriate option to efficiently increase the water supply reliability.

There are two limitations worth noting in the strategy evaluations. First, we tested these strategies only based on hydrologic factors without considering economic factors, although we acknowledge that hydrologic evaluation needs to be complemented with economic analysis before supporting decision making. For example, an economic evaluation would allow for the design of a step-wise curtailment of the water supply as the drought intensifies in order to improve the water supply reliability in the long term and inform cost-benefit evaluation for additional infrastructure or contracts. Second, we used uniform mitigation strategies in a drought event. However, water managers might use adaptive management (changing strategies based on the strategy performance) in real world situations – which will improve supply reliability (Gao et al., 2016).

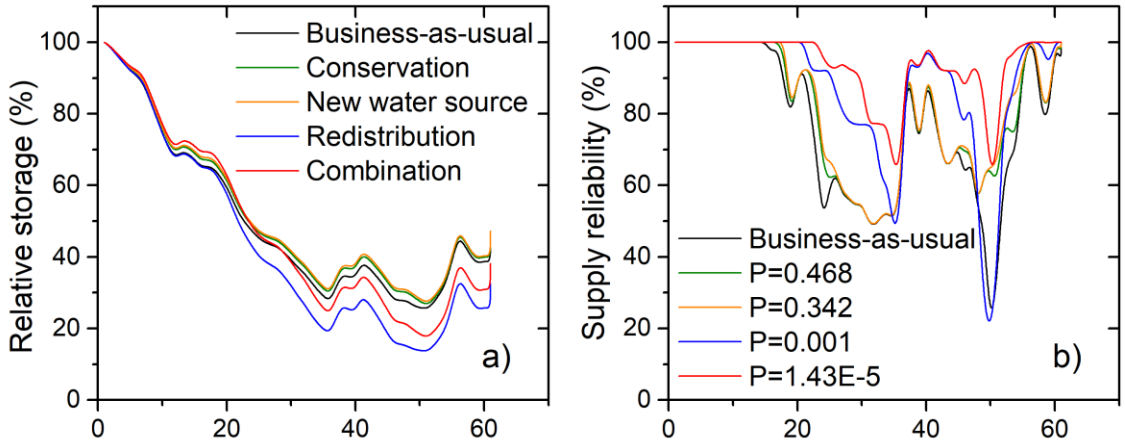

Figure 3.9 Mitigation strategy evaluations by showing (a) relative storage and (b) supply reliability (using the longest potential future drought from GFDL-ESM2M as an example). (Reprinted with permission from Zhao et al., 2018)

The representativeness of the results from this study is limited by several assumptions. First, we assumed that the initial reservoir level is at the top of the conservation pool at the onset of the drought. Although this makes the analysis straight forward, it tends to underestimate water stress. Another assumption is the simplified representation of the urban water demand (Equation 3.1) based on population growth and WUPCD changes. However, other factors, such as economic development, drought specific increase in landscape water demand, water conservation and efficiency measures, can significantly affect our estimates (although population growth and WUPCD have the largest impact). Finally, Dallas fully depends on surface water, and therefore the groundwater contribution (less than 3% of total water supply; TWDB, 2016) was not considered in this study. However, techniques such as the managed aquifer recharge (MAR) method can help to store water in the underlying Trinity Aquifer system (Gao et al., 2014). Similar to the function of surface water reservoirs, the aquifer could help improving the supply reliability for Dallas in the future. In addition, groundwater should be incorporated in other study areas where it plays a significant part in the water supply system.

3.5. Conclusion

The resilience of water supply systems is affected by water availability and water demand, both of which are characterized with non-stationarity. In this study, by applying DHSVM-Res (which integrates detailed hydrology with water management operations) under selected multi-year drought scenarios in the City of Dallas, we quantified how the combined non-stationarity and uncertainties in multi-year drought severities and water demand growth will impact the future water supply resilience. Reduced availability is induced by the future droughts

derived from GCM projections, and growing demand is calculated using Monte Carlo simulation by taking into account the population growth and WUPCD change uncertainties.

Using reservoir relative storage and water supply reliability as resilience metrics, the conclusions of this study are:

1). Both non-stationarities in water availability (associated with drought changes) and demand (associated with demand growth) have significant impacts on the water supply resilience. Droughts in Period 2 (2050-2099) are much more severe (with longer duration) than those in Period 1 (2000-2049). Consequently, water supply becomes less reliable in Period 2. With no curtailments or changes in operations, supply reliability could drop to 26% after a 4-year drought. The first decision point (at which reliability drops under 100%) decreases from 24 months to 14 months from Period 1 to Period 2.

2). Both uncertainties associated with availability and demand non-stationarity are large, and their combination affects the projected future water resilience estimates. For water availability, the primarily source of uncertainties is GCM structure. In this study, it was found that the GCM model ensemble (which contains the 8 best performing models for drought simulation in the region) results in an average of 22% uncertainty range in relative storage and an average of 21% uncertainty range in supply reliability when taking Period 2 as an example. For water demand, the uncertainties are from population growth and WUPCD reduction, and result in a 10% range in relative storage and 14% in supply reliability. Over the second period, both uncertainties are of the same order of magnitude, which should further motivate water supply resources adequacy studies to explicitly consider both as none clearly dominates potential decision making.

3). None of the tested individual water management strategies (i.e., additional conservation, integrating a new water source, and water use redistribution) alone would be sufficient to significantly improve the water supply resilience for the City of Dallas under combined uncertainties in multi-year drought induced water availability decrease and population-growth induced water demand increase. A combination of these adaptation strategies is more appropriate for more robust long-term water supply resilience. With the feedback to water availability represented, this fully integrated framework can help inform economic analysis to select the best mitigation strategy.

This study demonstrates an end-to-end approach for evaluating water supply resilience under multiple sources of non-stationarity in an urbanized watershed. It bridges the gap between climate projections, demographic projections, high resolution hydrological modeling, water management operations, and best management practices. The current framework allows for representing water availability and associated uncertainties in space and time in a consistent manner (instead of deriving synthetic uncorrelated flow at each reservoir). The simulation results can be beneficial for the city managers to improve the water supply resilience, especially under extreme conditions.

CHAPTER IV

ESTIMATING RESERVOIR EVAPORATION LOSSES FOR THE UNITED STATES

4.1. Introduction

With the fast growing population, it was projected that 5.3 billion people will live under water stress and water scarcity globally by 2030 (Organisation for Economic Co-operation and Development, 2008). Most of the affected population relies on surface water—especially the water impounded by reservoirs, which can be easily accessed and managed (United Nations Environment Programme, 2013). In addition to supplying water for agricultural, municipal, and industrial uses, reservoirs can also be used for flood control and hydropower generation. From 1950 to 2007, the volume of global accumulative water impounded by reservoirs rose from about 1,000 km^3 to 11,000 km^3, reducing the global sea level rise by 30 mm (Chao et al., 2008). According to the Global Reservoir and Dam Database (GRanD; Lehner et al., 2011), the United States is the country with the largest number of reservoirs. These reservoirs are capable of storing 1300 km^3 of water, which is almost equivalent to the region's annual mean runoff (Graf, 1999).

Globally there are about 16.7 million reservoirs that have a surface area of 100 m^2 or greater (Lehner et al., 2011). These reservoirs have increased the global terrestrial water surface area by about 305,000 km^2. With the large surface area introduced by these artificial impoundments, the evaporative loss is significant—especially in semi-arid and arid regions (Ali et al., 2008; Morton, 1979). For example, the annual evaporation from 200 major reservoirs in Texas, USA, equals to 20% of their active storage (Zhang et al., 2017). The long-term evaporation from Lake Tahoe, which is located in the arid western United States, accounts 40%-

60% for the total reservoir output (Friedrich et al., 2017). From a global perspective, Shiklomanov (1999) estimated a total of ~270 km^3/year of reservoir evaporation, which is larger than the combined domestic and industrial water use in the year of 2010 (~250 km^3). Therefore, to better support efficient water resources management, it is essential to incorporate accurate reservoir evaporation information into current reservoir operation rules.

Despite the critical need for reservoir evaporation information, until now there has been no continentally consistent and locally practical evaporation dataset that can be used in the policy making process at a regional scale. To precisely quantify the evaporation losses from a given reservoir, water surface area and evaporation rate data are needed. However, both high quality reservoir surface area and evaporation rate data can be difficult to gather.

Reservoir surface area cannot be measured directly. Instead, it is usually inferred from in-situ measurements, or estimated from remote sensing images. By applying in-situ measured reservoir elevation values to a known elevation-area relationship, a reservoir's area can be calculated. The elevation-area relationship is typically derived from bathymetry investigation (either before or after the reservoir is constructed) using sonar/laser and GIS technologies. However, this method is limited by its large expense and the changes of reservoir bathymetry due to sedimentation. Remote sensing has the advantage of estimating water surface area from satellite images at low cost (McFeeters, 1996; Sawaya et al., 2003; Gao, 2015). Even though there is a compromise between spatial and temporal resolution with remote sensing technologies, usually high quality images with acceptable time intervals can be obtained. Compared with other remote sensing data, Landsat has the advantages of long temporal coverage with a 16-day revisit time and high spatial resolution (30 m), which makes it suitable for water surface area change studies (Pekel et al., 2016; Donchyts et al., 2016; Khandelwal et al., 2017). However, a major

limitation of using Landsat images for continuous water area monitoring is the frequent contaminations from multiple sources, such as clouds, cloud shadows, terrain shadows, and the Scan Line Corrector (SLC) failure (for Landsat 7). As a result, direct water extraction from the contaminated images can lead to significant underestimation. To generate reliable water area estimates, most studies simply removed the contaminated images. For instance, Busker et al. (2018) removed all the images which are more than 5% contaminated to get the surface area time series for 135 global lakes. However, this has led to many missing values in the time series, especially for the regions that have frequent cloud coverage. To bridge this gap, Zhao and Gao (2018) developed an image enhancement algorithm to automatically repair the contaminated images and generate more continuous area time series for any of the Landsat detectable lakes/reservoirs. The algorithm was built upon the Joint Research Centre (JRC) Global Surface Water Dataset (GSWD; Pekel et al., 2016). Compared to the simple contaminated image removal method, the new algorithm can significantly improve the continuity of the water area time series (i.e., 81% improvement on a global scale).

The evaporation rate of open water has been studied for decades. A comprehensive review of evaporation rate estimation methods can be found in Friedrich et al. (2017). The pan evaporation method is employed by the National Weather Service (NWS) for estimating the point evaporation rate operationally. Although there are about 950 pan evaporation stations across the CONUS, only a very small portion are located close enough to dams to represent reservoir evaporation. Furthermore, lake evaporation estimation based on pan evaporation is subject to large errors due to multiple factors including microclimate difference with the reservoir and the pan, little consideration of heat storage, extra heat absorption from the pan's sides, water splashing, overflow due to intensive rainfall, freezing conditions, human errors, etc.

(McMahon et al., 2013; Friedrich et al., 2017). Thus, it is regarded as one of the least accurate evaporation estimation methods and is not suitable for precise water management practices (Tanny et al., 2008; Harwell, 2012; McJannet et al., 2017). In addition to the pan evaporation method, eddy covariance (EC), scintillometer, mass balance, Bowen ratio energy budget (BREB), and combination equation methods are frequently used. In general, EC is considered the most accurate approach—but it has been primarily used for evapotranspiration related research. Constrained by the expensive cost and the sensitivity to wind direction (relative to both sensor and reservoir location), very few lake evaporation data have been collected using this approach. By measuring the sensible heat flux, a scintillometer can estimate the latent heat flux if other energy terms are known, even though it has multiple limitations such as signal satuation (Moene et al., 2009). The mass balance and BREB methods are data intensive, and they can introduce considerable errors because of the complex interactions between the reservoir water and its surrounding environment (Friedrich et al., 2017).

Among the various approaches for estimating the evaporation rate on a large scale, the most practical one involves using a physically based combination equation such as the Penman equation (Penman, 1948). Some variants include PenPan (Rotstayn et al., 2006; for estimation of pan evaporation), Penman-Monteith (Monteith, 1965; commonly used for evapotranspiration estimation), and the Priestley-Taylor (Priestley and Taylor, 1972; derived from Penman-Monteith by removing the aerodynamic terms and is widely used for evapotranspiration estimation) equations. These physically based models are proven to be reliable for applications over shallow water reservoirs (typically less than 3 m in depth) where heat storage is insignificant (Abtew, 2001; Linacre, 1993; McMahon et al., 2013; Zhao et al., 2016b). However, open water—as defined by Penman (1948)—is the surface thin water layer that evaporation

solely depends on. Actual water bodies such as lakes and reservoirs have a considerable heat storage effect, causing combination equations to be biased with regard to evaporation rate estimation (Finch and Hall, 2001; McMahon et al., 2013). For instance, Lake Tahoe (California, US) has the highest air temperature in July, but the largest evaporation rate occurs in September (Tahoe Environmental Research Center, 2015). To address this issue, Edinger et al. (1968) introduced the equilibrium water temperature and de Bruin (1982) incorporated it into evaporation rate estimation. The equilibrium temperature concept has been used in several studies, and was proven to be appropriate for open-water evaporation estimation (Finch, 2001; Finch and Hall, 2001; Bogan et al., 2003; Caissie et al., 2005; McJannet et al., 2008; Mekonnen and Hoekstra, 2012). Although the derivations of the equilibrium temperature in these studies were all based on the energy balance of the water body, different studies have adopted different simplified energy terms. For instance, the most generic form of the equilibrium temperature was from Mohseni and Stefan (1999), which used a simplified latent heat flux formulation. Therefore, there is a lack of a generalized formulation of the equilibrium temperature to improve the open-water evaporation estimation using Penman equation.

Therefore, this study focuses on breaking the above key barriers in reservoir evaporation quantification to better support more precise water resources management at both local (individual reservoir) and regional (multiple reservoirs) scales. A total of 209 reservoirs (Figure 4.1), which account for 47.2% of the storage capacity in the CONUS, were chosen as our study sites. Specifically, our three objectives are to: (i) adopt continuous reservoir surface area time series generated from a Landsat reservoir water classification dataset free of image contamination; (ii) quantify heat storage changes in the Penman equation to better simulate the monthly reservoir evaporation rate; (iii) generate the long-term monthly evaporation amount

dataset for the 209 reservoirs and analyze the long-term trends of reservoir evaporation. Even though this study focuses on reservoirs in the CONUS, the retrieval algorithms and the data analyzing approaches are transferable to other regions or to a global scale. These objectives provide the structural sub-headings used the following Methods, Results and Discussions sections.

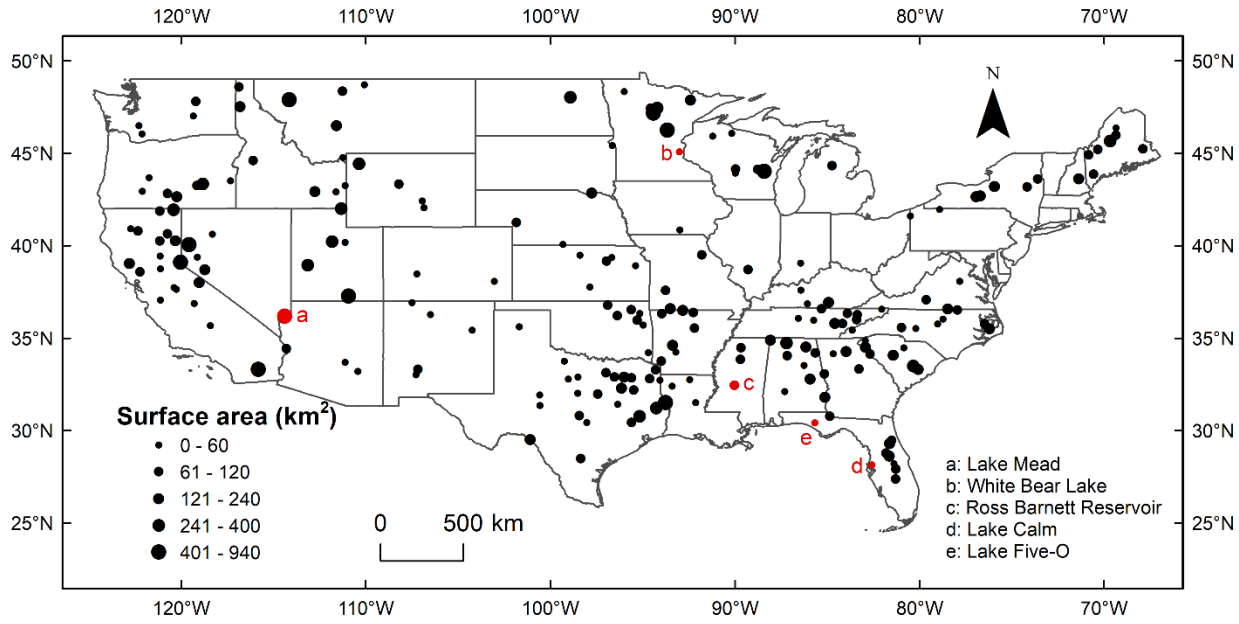

Figure 4.1 The 209 major reservoirs over the CONUS selected in this study. The five reservoirs with EC or BREB evaporation rates were shown in red. Among these reservoirs, 205 of them are major reservoirs with a storage capacity larger than 0.5 km3, and the remaining 4 are smaller reservoirs (but with in situ evaporation rate data available, which is used for validation purposes).

4.2.1 Estimation of reservoir surface area

In this study, we used the image enhancement algorithm from Zhao and Gao (2018) to extract the water surface area time series for the 209 CONUS reservoirs. There are three types of data employed to generate the area time series for the 209 reservoirs.

1. Reservoir polygon shapefiles. Reservoir polygon shapefiles were collected from the HydroLakes dataset (Messager et al., 2016). Derived from multiple data sources, this global geographic dataset contains information about most of the world's lakes/reservoirs—including their geographic extent (polygon shapefiles), location, elevation, capacity, depth, and other features. For each of the 209 reservoir, a 1 km buffer was applied to generate the reservoir masks, such that the computational costs can be reduced.
2. Monthly raw water coverage maps. Appling the expert system classification method to 3 million Landsat images, Pekel et al. (2016) generated the GSWD, which includes the global water areas for each month from March 1984 to October 2015. However, because GSWD removed all the contaminated pixels (i.e., snow, ice, cloud, shadow, and SLC failure) for qualify control purpose, direct extraction of water area can result in significant underestimation. Thus, the image enhancement algorithm from Zhao and Gao (2018) was employed in this study to automatically repair the contaminated images.
3. Global water occurrence image. GSWD provides the global water occurrence image by stacking all the monthly water coverage maps together and then calculating the probability for each pixel that is covered by water for the 32 years. This occurrence

image contains similar information as a bathymetry map contains that can be used to enhance the contaminated monthly images.

4.2.2 Estimation of reservoir evaporation rate

4.2.2.1 Data for calculating evaporation rate

The meteorological data used for calculating the evaporation rate include air temperature, vapor pressure deficit, wind speed, and surface shortwave radiation. These are the four primary meteorological variables governing the evaporation process (McVicar et al., 2012). To consider the uncertainties from the inputs, these variables were adopted from three long-term datasets: 1) TerraClimate (1/24 degree spatial resolution; Abatzoglou et al., 2018); 2) North American Land Data Assimilation System phase 2 (NLDAS-2) forcings (1/8 degree; Xia et al., 2012); and 3) Global Land Data Assimilation System Version 2 and Version 2.1 (GLDAS-2 and GLDAS-2.1; 1/4 degree; Rodell et al., 2004).

The global high resolution TerraClimate data have combined the downscaled Climate Research Unit time series data version 4.0 (CRU Ts4.0) and the Japanese 55-year Reanalysis (JRA-55) data using WorldClim. In particular, TerraClimate inherited the solar radiation and wind speed from JRA-55 while air temperature and vapor pressure were inherited from CRU Ts4.0.

Primarily based on the North American Regional Reanalysis (NARR) dataset, NLDAS-2 combined multiple data sources including ground and satellite data to generate the meteorological dataset with a high temporal resolution (3-hourly). The monthly data were calculated by simply averaging the 3-hourly values. Validations against in-situ observations suggest that the NLDAS retrospective forcing data are of high quality (Luo et al., 2003; Xia et al., 2012).

GLDAS-2 and GLDAS-2.1 data extend the periods from 1948 to 2010 and from 2000 to present, respectively. GLDAS-2 was generated primarily from the Princeton global meteorological dataset (Sheffield et al., 2006), while and GLDAS-2.1 was driven by a set of land surface models and observation data (Rui and Beaudoing, 2011). To cover the entire period of this study (i.e., 1984 to 2015), we used both the GLDAS-2 (from 1984 to 1999) and GLDAS-2.1 (from 2000 to 2015).

For each of the reservoirs, the forcing data time series were generated by averaging the overlapping cells from the gridded forcing data with the reservoir shapefiles. Instead of calculating evaporation rate for each cell, this approach can reduce the uncertainty of gridded forcing data and facilitate the usage of universal fetch for all the cells.

4.2.2.2 Algorithm for evaporation rate

With both energy budget and mass transfer terms included, combination equations can provide precise reservoir evaporation estimation. In 1948, Penman derived the first combination equation for open water evaporation estimation (Equation 4.1).

$$E = \frac{s(R_n - \Delta U) + \gamma f(u)(e_s - e_a)}{\lambda_v(s + \gamma)} \quad (4.1)$$

where E is the open water evaporation rate (mm·d^{-1}); s is the slope of the saturation vapor pressure curve (kPa·°C^{-1}); R_n is the net radiation (MJ·m^{-2}·d^{-1}); ΔU is the heat storage changes of the water body (MJ·m^{-2}·d^{-1}); $f(u)$ is the wind function (MJ·m^{-2}·d^{-1}·kPa^{-1}); e_s is the saturated vapor pressure (kPa); e_a is the air vapor pressure (kPa); λ_v is the latent heat of vaporization (MJ·kg^{-1}); and γ is the psychrometric constant (kPa·°C^{-1}). The Penman equation and its variants (e.g., Penman-Monteith equation) have been widely employed for potential evapotranspiration as

well as for open water evaporation estimations (McJannet et al., 2008; Tanny et al., 2008; McMahon et al., 2013).

However, there are two key factors need to be considered when applying the Penman equation on open water evaporation estimation. The first one is associated with the meteorological data that are used to drive the Penman equation. Ideally, the meteorological data should be directly collected on top of the water surface. However, due to the difficulties in over-water measurement, most studies employed the land-based meteorological data as a substitute (Winter et al., 1995; dos Reis and Dias, 1998; McJannet et al., 2012). Direct use of land-based meteorological data in the Penman equation is likely to result in biased estimation, given the meteorological differences between land and water areas (Weisman and Brutsaert, 1973). Specifically, when air moves from land across the water body (i.e., increase of fetch), its humidity gradually increases due to the evaporation processes on the water surface. This will lead to decreasing evaporation fluxes in the downwind direction.

To solve this problem, McJannet et al. (2012) developed a generally applicable wind function that facilitate open-water evaporation rate calculation using standard land-based meteorology. This wind function considers the fact that air becomes saturated when moving from land to water and was derived by combining 19 published wind functions for multiple types of water bodies with various sizes and climate conditions (Equation 4.2).

$$f(u_2) = \lambda_v(2.33 + 1.65u_2)L^{-0.1} \quad (4.2)$$

where $f(u_2)$ is the wind function ($MJ \cdot m^{-2} \cdot d^{-1} \cdot kPa^{-1}$); u_2 is the wind speed at the height of 2 m ($m \cdot s^{-1}$); L is the fetch length of the water body (m).

The fetch length was calculated for each reservoir and each month (Figure 4.2). With a given wind direction (monthly dominant wind direction derived from NLDAS), the width is

defined as the distance between the two reservoir-tangent lines that are parallel to the wind direction. Then fetch length was calculated by dividing the total area with the width.

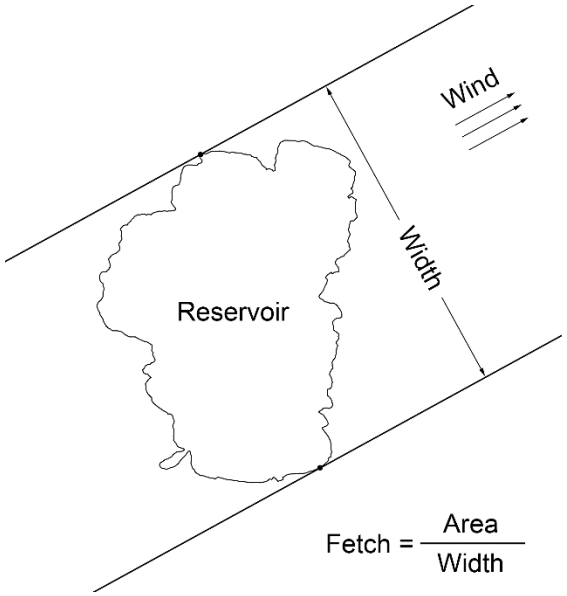

Figure 4.2 Calculation of the reservoir fetch for a given wind direction.

The second key factor to be considered when applying Penman equation to open water evaporation is the heat storage quantification (i.e., ΔU in Equation 4.1). For instance, lakes tend to store heat in the spring/summer and release heat in the fall/winter. Without considering this heat storage effect, the evaporation rate would be overestimated in the former and underestimated in the latter.

To represent the heat storage effect when calculating the evaporation rate, an approach using "equilibrium temperature" was adopted. The equilibrium temperature is defined as the water temperature at which there is no heat exchange between air and water (Edinger et al., 1968). If the water is under constant radiative forcing for a long enough time, the water will

reach a steady state with the water temperature equal to the equilibrium temperature. In reality, the actual water temperature tends to approach the equilibrium temperature gradually. The lag time, which is defined as τ, is dependent on the water body depth. Built upon previous studies (Edinger et al., 1968; de Bruin,1982; Mohseni and Stefan, 1999; McMahon et al., 2013), we have derived a more general and accurate equation for calculating the equilibrium temperature described as follows.

The calculation of equilibrium temperature is based on the energy balance equation (Equation 4.3)

$$(1-\alpha)K^{\downarrow} + L^{\downarrow} - L^{\uparrow} - \lambda_v E - H = 0 \quad (4.3)$$

where α is the water surface albedo; $K^{\downarrow}$is the downward shortwave radiation (MJ·m^{-2}·d^{-1}); $L^{\downarrow}$ is the downward longwave radiation (MJ·m^{-2}·d^{-1}); $L^{\uparrow}$ is the upward longwave radiation (MJ·m^{-2}·d^{-1}); $\lambda_v E$ is the latent head flux (MJ·m^{-2}·d^{-1}); and H is the sensible head flux (MJ·m^{-2}·d^{-1}). When the water temperature at the surface is within -30 °C to 50 °C, $L^{\downarrow}$ and $L^{\uparrow}$ can be approximated using Equations 4.4 and 4.5 (Mohseni and Stefan, 1999). Because the water body is at equilibrium state, the outgoing longwave radiation is calculated with T_e.

$$L^{\downarrow} = \varepsilon_a \sigma (T_a + 273.15)^4 \approx \varepsilon_a (kT_a + b) \quad (4.4)$$

$$L^{\uparrow} = \varepsilon_w \sigma (T_e + 273.15)^4 \approx \varepsilon_w (kT_e + b) \quad (4.5)$$

where ε_a is the emissivity of air (Satterlund, 1979); ε_w is the emissivity of water (0.97 after Mohseni and Stefan, 1999); σ is the Stefan-Boltzman constant (4.9×10^{-9} MJ·m^{-2}·K^{-4}·d^{-1}); T_a is air temperature (°C) and T_e is equilibrium temperature (°C); and k and b are constants of 0.46 MJ·m^{-2}·d^{-1}·°C^{-1} and 28.38 MJ·m^{-2}·d^{-1}, respectively.

Latent and sensible heats are calculated after Equations 4.6 and 4.7. Same as Equation 4.5, T_e is used in the sensible heat calculation (Equation 4.7).

$$\lambda_v E = \frac{sR_n + \gamma f(u)(e_s - e_a)}{s + \gamma} = \frac{s[(1-\alpha)K^{\downarrow} + L^{\downarrow} - L^{\uparrow}] + \gamma f(u)(e_s - e_a)}{s + \gamma} \quad (4.6)$$

$$H = \gamma f(u)(T_e - T_a) \quad (4.7)$$

After plugging Equations 4.4, 4.5, 4.6 and 4.7 into Equation 4.3 (and some rearrangement), an equation for the equilibrium temperature (Equation 4.8) can be derived.

$$T_e = \frac{[k\varepsilon_a + f(u) \cdot (s + \gamma)] \cdot T_a + (1-\alpha)K^{\downarrow} - b(\varepsilon_w - \varepsilon_a) - f(u)(e_s - e_a)}{k\varepsilon_w + f(u) \cdot (s + \gamma)} \quad (4.8)$$

Then the actual water column temperature can be estimated after de Bruin (1982) (Equations 4.9 and 4.10).

$$T_w = T_e + (T_{w0} - T_e) \cdot e^{-\Delta t/\tau} \quad (4.9)$$

$$\tau = \frac{\rho_w c_w \bar{h}}{4\sigma(T_{wb} + 273.15)^3 + f(u)(s_{wb} + \gamma)} \quad (4.10)$$

where T_w is the water column temperature at current time step (°C); T_{w0} is the water column temperature at previous time step (°C); Δt is the time step (set as one month in this study); τ is the lag time (d); ρ_w is the water density (kg·m^{-3}); c_w is the specific heat of water (MJ·kg^{-1}·°C^{-1}); $\bar{h}$ is the average water depth (m); T_{wb} is the wet-bulb temperature (°C); and s_{wb} is the slope of the saturation vapor pressure curve at T_{wb} (kPa·°C $^{-1}$).

Time step for calculating equilibrium temperature varies in previous studies (Finch and Hall, 2001; McVicar et al., 2007). Finch and Hall (2001) compared the impacts of different time steps (5, 10, and 30 days) on evaporation rate estimation and found that 30 days can still generate acceptable results. To be consistent with TerraClimate dataset and the surface area values, we used a month as the Δt here. The reservoir depth data were collected from Messager et al.

(2016). If the lake depth is greater than 20 m, a constant value of 20 m was used. This is because the incoming radiation only affects the epilimnion layer, which is usually less than 20 m (Patalas, 1984). More complex reservoir stratification was not considered in this study.

Heat storage change can subsequently be calculated after McMahon et al. (2013) by Equation 4.11, which is then implemented into the Penman equation (Equation 4.1) for an improved estimation of evaporation rate.

$$\Delta U = \rho_w c_w \bar{h} \frac{T_w - T_{w0}}{\Delta t} \tag{4.11}$$

In addition to improving the heat storage estimation, using the actual water temperature can also better represent the outgoing longwave radiation in the net radiation (R_n) term (Equation 4.12) and the saturated vapor pressure (Equation 4.13, adopted from Bolton, 1980) (by replacing the original air temperature with calculated water temperature).

$$R_n = (1 - \alpha)K^{\downarrow} + L^{\downarrow} - \varepsilon_w \sigma (T_w + 273.15)^4 \tag{4.12}$$

$$e_s = 6.112 \cdot e^{\frac{17.67 \cdot T_w}{T_w + 243.5}} \tag{4.13}$$

4.2.3 Evaporation losses from the reservoirs

For each reservoir, the monthly evaporation amounts were calculated as the product of monthly surface area and monthly evaporation rate. Compared with the evaporation rate, evaporation losses from a specific reservoir are more important with regard to water management practices, as they directly affect water availability.

Using the evaporation data developed above, we introduce the reservoir evaporative losses index (RELI) for quantifying the role of evaporation in reservoir storage losses. The water storage losses of a reservoir include human water use, evaporation, and leakage to groundwater. For any given reservoir, the water mass balance can be represented by Equation 4.14.

$$S_t - S_{t-1} = P + Q_{in} - Q_{out} - EA - WU - L \quad (4.14)$$

where S is the reservoir storage; t is the time step; P is precipitation; Q_{in} and Q_{out} are the inflow and outflow of the reservoir; EA is the evaporation amount; WU is the water use of the reservoir that is directly pumped from the reservoir; and L is the water leakage to groundwater.

By moving the water loss components to one side and the directly measurable terms to the other side, Equation 4.14 can be rearranged into Equation 4.15.

$$EA + WU + L = P + [Q_{in} - Q_{out}] - [S_t - S_{t-1}] \quad (4.15)$$

This way, the RELI can be calculated (Equation 3.16) to quantify the partitioning of evaporation in the total water losses of a given reservoir.

$$RELI = \frac{EA}{EP + WU + L} = \frac{EA}{P + [Q_{in} - Q_{out}] - [S_t - S_{t-1}]} \quad (4.16)$$

4.3. Results

4.3.1 Reservoir surface area

4.3.1.1 Validation of reservoir surface area

Detailed validations of the original GSWD and the enhancement algorithm can be found in Pekel et al. (2016) and Zhao and Gao (2018), respectively. In addition, two reservoirs are used as examples here to demonstrate the robustness of the surface area results over individual reservoirs. The Amistad Reservoir is located between USA and Mexico and it has a surface area of about 150 km^2. Lake Mead is located in between the states of Nevada and Arizona, USA and has a surface area of about 600 km^2. The remotely sensed surface area time series were compared with observed elevation/storage data (Figure 4.3a and Figure 4.4a). For Amistad

Reservoir, the coefficient of determination (R^2) between the remotely sensed area and the observed elevation was improved from 0.38 to 0.98 after the enhancement. For Lake Mead, the R^2 between the remotely sensed area and the observed storage was improved from 0.32 to 0.99. Since the remotely sensed area and gauge observations are completely independent of each other, these results suggest that the area estimations can accurately capture the seasonal and inter-annual variations. For each of the two reservoirs, we selected a high-water-level case (Figures 3.3b-3.3c, and Figures 3.4b-3.4c) and a low-water-level case (Figures 3.3d-3.3e, and Figures 3.4d-3.4e) to show the performance of the contamination correction.

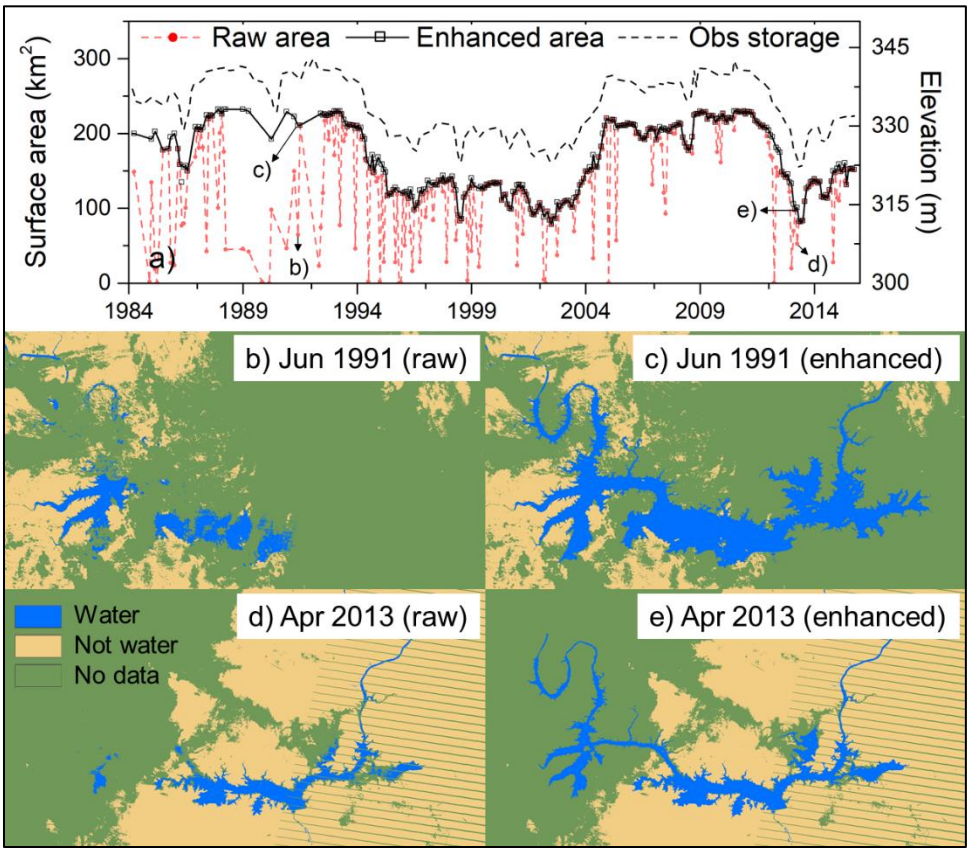

Figure 4.3 Water surface area estimation for the Amistad Reservoir in USA/Mexico. a) Time series of reservoir surface area and gauge observed elevation from March 1984 to October 2015.

b) GSWD classification result for June 1991; c) enhanced water area for June 1991; d) GSWD classification result for April 2013; and e) enhanced water area for April 2013.

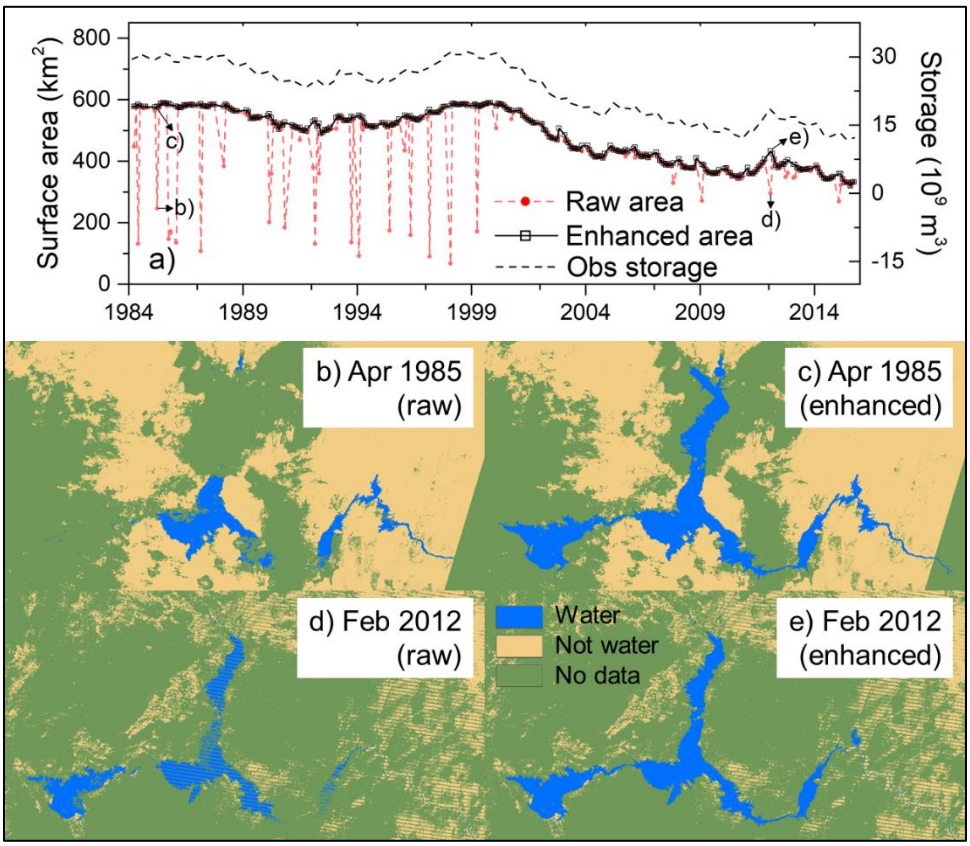

Figure 4.4 Water surface extraction for Lake Mead in Nevada/Arizona. a) Time series of reservoir surface area and gauge observed elevation from March 1984 to October 2015. b) GSWD classification result for April 1985; c) enhanced water area for April 1985; d) GSWD classification result for February 2012; and e) enhanced water area for February 2012.

4.3.1.2 Magnitude and trends of the surface area

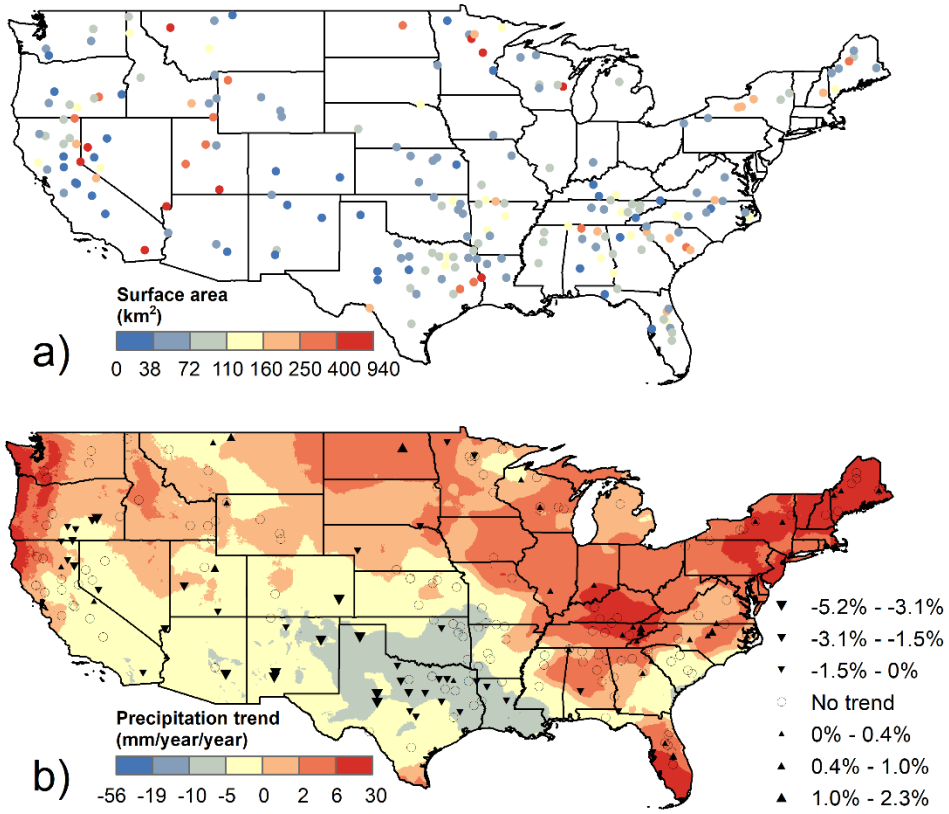

Figure 4.5 a) Long-term average (from 1985 to 2014) surface area for the 209 reservoirs and b) their trends detected by linear regression and Mann-Kendall test. The trends are shown in percentage and were calculated by dividing the area losses per year with the long-term average areas. The precipitation trend in b) was based on TerraClimate from 1985 to 2014.

The areas of the reservoirs show large spatial heterogeneity ranging from 0.1 km^2 (Lake Five-O) to 940 km^2 (Salton Sea) (Figure 4.5a). Because the surface area data from GSWD is from Mar 1984 to Oct 2015, we selected the complete years from 1985 to 2014 to conduct all the trend analysis. From 1985 to 2014, 133 reservoirs show insignificant trends, 43 reservoirs show

negative trends, and 33 reservoirs show positive trends. The reservoirs with increasing surface area are mostly located in the eastern US while the reservoir with decreasing surface area located in the central and western US. Specifically, the negative trends generally have larger values than the positive trends. For example, the E.V. Spence reservoir in Texas drops 5.2% of its area per year.

The long-term trend of surface area are generally correlated with precipitation trend (Figure 4.5b). Specifically, the three central states (i.e., Texas, Oklahoma, and Louisiana) have the largest decreasing trend of precipitation. As a result, the surface area of most reservoirs in the region have been decreasing. In the eastern US such as Tennessee and North Carolina, increasing precipitation leads to slightly increased surface area. In addition to the precipitation trend, local water management can also affect the changes of surface area. For instance, there are no significant trends for 11 reservoirs in Texas.

4.3.2 Reservoir evaporation rate

4.3.2.1 Validation using EC and BREB methods

As mentioned in Section 1, EC is considered the most reliable approach for measuring evaporation/evapotranspiration fluxes (Rimmer et al., 2009). It estimates the fluxes of heat, water vapor, and carbon dioxide by directly detecting the variation of eddies at a high frequency. Errors of EC open water evaporation usually attribute to the location of measurements, which requires homogeneous fetch. BREB is another widely used evaporation estimation approach that are considered to be reliable, but less accurate than EC because each energy flux component can introduce errors (Rosenberry et al., 2007). BREB are typically applied to the small water bodies due to the difficulties in quantifying heat storage of the large ones (Friedrich et al., 2017).

Through literature review, 3 reservoirs that have EC measurements and 2 reservoirs with BREB data were used as the validation sites (Figure 4.6). The reservoir information and their error statistics were summaries in Table 4.1. These five lakes are located in different states with various climatic conditions. In addition, they have a wide range of depths and fetch lengths. Thus, the validation results are deemed representative.

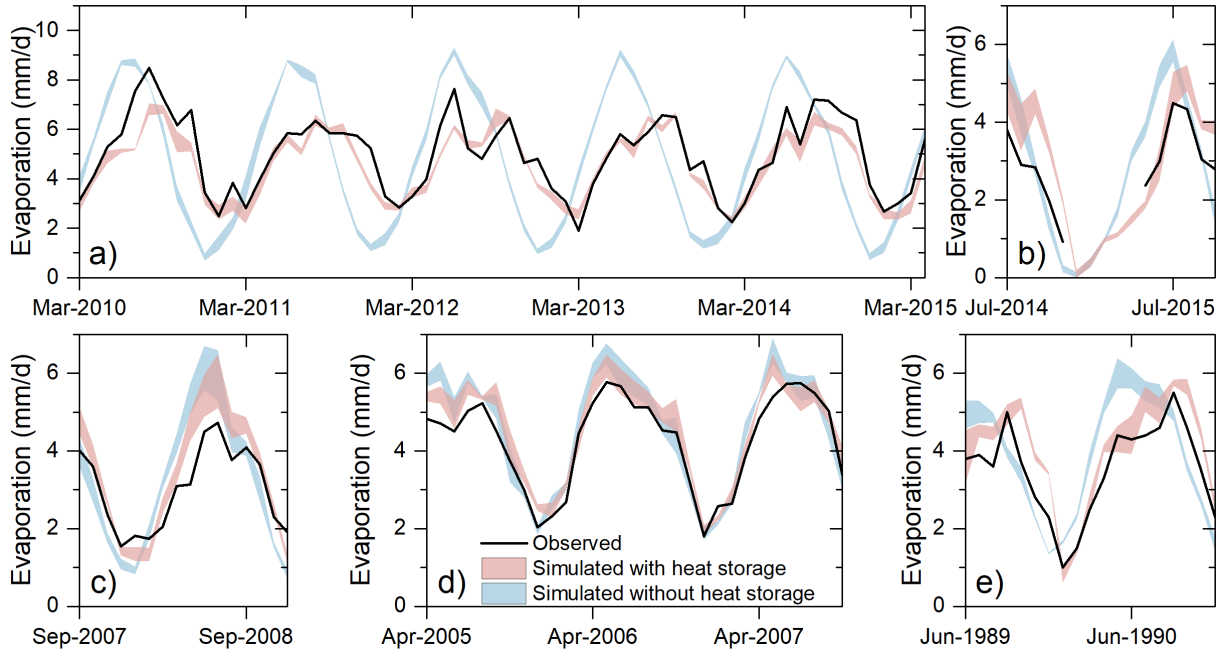

Figure 4.6 Comparisons of evaporation rate between modeled and observed for a) Lake Mead (Nevada/Arizona) from Mar 2010 to Dec 2011 with EC measurement; b) White Bear Lake (Minnesota) from Jul 2014 to Oct 2015 with EC measurement; c) Ross Barnett Reservoir (Mississippi) from Sep 2007 to Dec 2008 with EC measurement; d) Lake Calm (Florida) from Apr 2005 to Oct 2007 with BREB estimates; e) Lake Five-O (Florida) from Jun 1989 to Dec 1990 with BREB estimates. Shading area represents the estimation uncertainty from different input forcing datasets (i.e., TerraClimate, NLDAS, and GLDAS).

For Lake Mead (Figure 4.6a), there are clear time lags and magnitude differences between the observed and modeled evaporation when heat storage is not considered. By incorporating the heat storage term in the calculation, the R^2 is improved from 0.28 to 0.85.

White Bear Lake is the only lake in these five lakes that has a decreased R^2 and a slightly better root mean square error (RMSE) after adding heat storage. This is attributed to an overestimation in 2014, since the R^2 in 2015 alone is improved from 0.34 to 0.68. Ross Barnett Reservoir (Figure 4.6c) is a relatively shallow reservoir, which leads to slight time lags. The overestimation in 2008 is caused by the large solar radiation in the summer months. The time lags are barely seen for Lake Calm (Figure 4.6d), which is a 3-m deep lake in Florida. As a result of the shallow depth, the R^2 is only improved from 0.91 to 0.94. However, another deeper lake in Florida (Lake Five-O; Figure 4.6e) shows clear improvement after considering heat storage.

Table 4.1 Comparisons between modeled and observed evaporation rate results. The R2 values and RMSE were calculated based on the average evaporation rate from the three input datasets.

Lake	States (latitude)	Average fetch length (km)	Depth (m)	Observation method (duration in months)	R^2 (with/without heat storage)	RMSE (with/without heat storage)	Reference
Lake Mead	Nevada/Arizona (36.13º N)	9.76	> 20	EC (62)	0.85/0.28	0.7/2.2	Moreo, 2015
White Bear Lake	Minnesota (45.06º N)	2.53	8.3	EC (16)	0.64/0.69	0.9/1.0	Xiao et al., 2018
Ross Barnett Reservoir	Mississippi (32.45º N)	6.26	6	EC (16)	0.93/0.73	0.5/0.9	Liu et al., 2009 Liu et al., 2012
Lake Calm	Florida (28.13º N)	0.38	3	BREB (31)	0.94/0.91	0.3/0.5	Swancar, 2015
Lake Five-O	Florida (30.42º N)	0.27	9.5	BREB (19)	0.86/0.56	0.7/1.1	Sacks et al., 1994

4.3.2.2 Comparison with pan evaporation

Pan evaporation has been widely used for monitoring reservoir evaporation operationally (Tanny et al., 2008). Because of the errors introduced by multiple factors, intensive quality control processes need be implemented on the raw data to provide reliable information for further applications. Additionally, to reduce the impacts of the side heat absorption and the heat storage effect, a "pan coefficient" (i.e., the ratio of lake evaporation over pan evaporation) is usually applied to the pan observation to approximate reservoir evaporation. Despite of its many limitations, pan evaporation measurement provide a source for large scale validation.
Based on the observed pan evaporation across Texas and the pan coefficients from NWS Technical Report 33 (TR-33), the Texas Water Development Board (TWDB) created the monthly lake evaporation rates for 92 quadrangles that cover the entire Texas. The calculated evaporation rates of the 26 Texas reservoirs were compared with the TWDB pan evaporation data (Figure 4.7a). The R^2 and relative bias (in the parenthesis) values between pan evaporation and the simulated results of the three forcing datasets 0.66 (-5.0%), 0.69 (4.1%), and 0.63 (-9.6%) for TerraClimate, NLDAS, and GLDAS, respectively. These discrepancies can be attributed to the uncertainties from pan evaporation data, evaporation algorithm, and forcings errors.

Another pan evaporation dataset employed for validation in this study is the widely used TR-33 lake evaporation, which applied spatially variable pan coefficients to the long-term pan evaporation observations from 1956 to 1970 in the CONUS. For each lake, we extracted the average pan evaporation rate and then compared the value with the modeled average value from 1985 to 2014 (Figure 4.7b). The R^2 and relative bias (in the parenthesis) values between pan

evaporation and the simulated results of the three forcing datasets are 0.87 (-2.3%), 0.81 (7.1%), and 0.85 (-7.7%) for TerraClimate, NLDAS, and GLDAS, respectively.

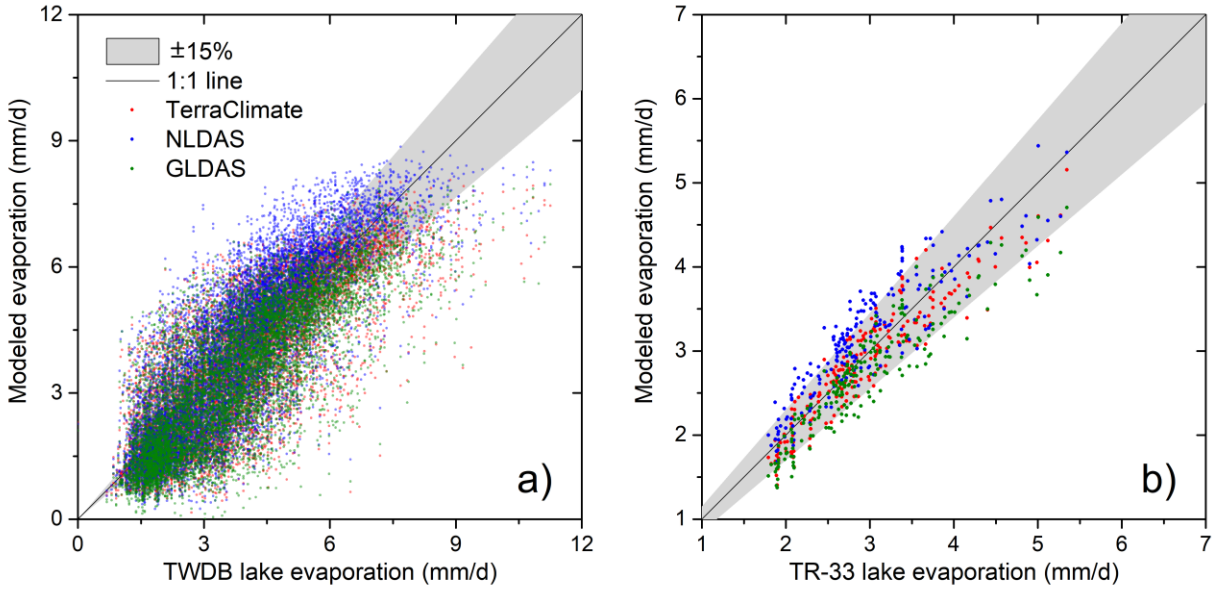

Figure 4.7 Comparison between a) modeled monthly evaporation rates and TWDB scaled pan evaporation; and b) modeled long-term average evaporation rates and TR-33 scaled pan evaporation.

4.3.2.3 Magnitude and trends of the evaporation rate

The long-term average evaporation rates are show in Figure 4.8a. Reservoirs that are located in southern CONUS have significantly larger values than other regions due to the stronger radiation. For instance, the average evaporation rate for the 26 reservoirs in Texas is 3.73 (3.50-4.01) mm/d (with the uncertainty range quoted after the average value thereafter), while the average rate for the 8 reservoirs in Minnesota is only 2.03 (1.87-2.28) mm/d. With respect to the long-term trends of evaporation rate (Figure 4.8b), most reservoirs show significant increasing trends (136 out of 209). The rest 73 reservoirs have no significant trends

(according to Mann-Kendall test) and most of them are located in the Pacific west. The increasing evaporation rate is primarily caused by the increasing shortwave radiation. The R^2 value for the 209 reservoirs between evaporation rate trends with shortwave radiation trends is 0.37. In particular, the central US shows significant brightening trend and this leads to increasing evaporation rate for the reservoirs in the region. The R^2 values are 0.19, 0.14, and 0.25 between evaporation rate trends with trends of air temperature, vapor pressure deficit and wind speed, respectively.

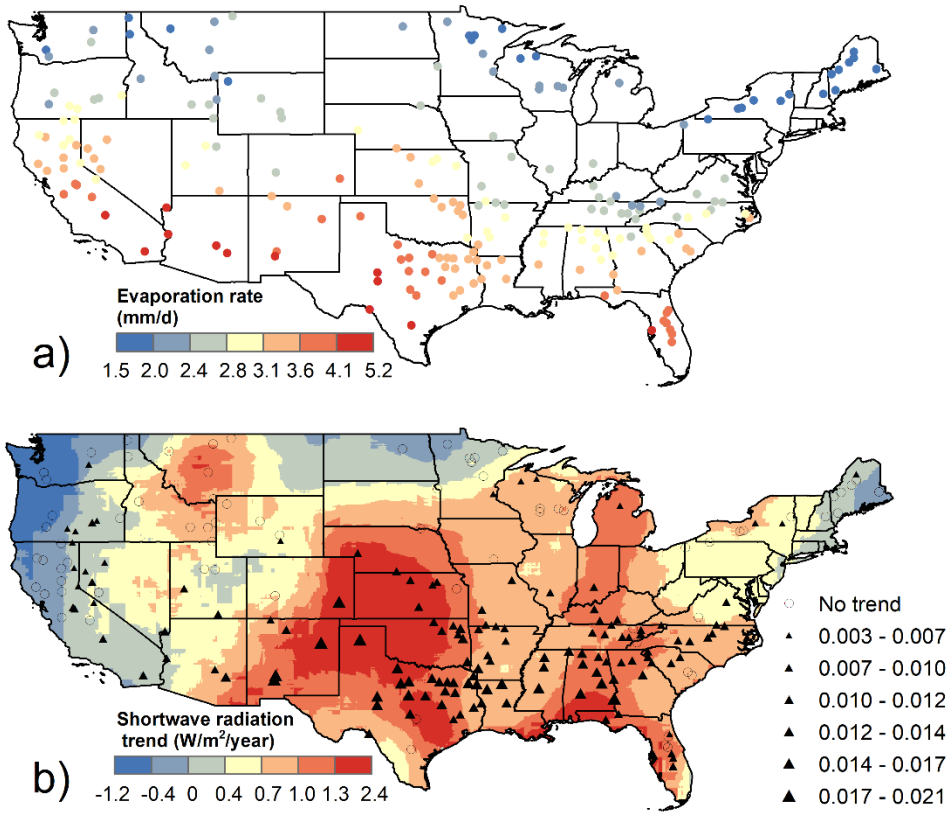

Figure 4.8 a) Long-term average evaporation rates and b) long-term trends of evaporation rate detected by linear regression. The base map for b) is shortwave radiation trend from 1985 to 2014 derived from the average of TerraClimate, NLDAS, and GLDAS.

4.3.3 Evaporation losses from the reservoirs

4.3.3.1 Magnitude and trends of evaporation losses

The amount of evaporation loss for each reservoir were estimated by multiplying the reservoir surface area with the evaporation rate (Figure 4.9). For reservoirs located in the same geographical region with the same (or similar) climate, the evaporation amount is primarily determined by the surface area (Figure 4.9a as compared with Figure 4.5a). However, the evaporation amount trends can be can be affected by both surface area and evaporation rate trends. For the reservoirs with significant surface area changes, the evaporation amount generally has the same trends (e.g., the reservoirs in the southwestern US). For the reservoirs with no significant surface area changes, the evaporation amount trends are generally dominated by the evaporation rate trends (e.g., the reservoirs in the southeastern US). The numbers of reservoirs with no trend, positive, and negative trends of evaporation amount are 92, 91, and 26, respectively.

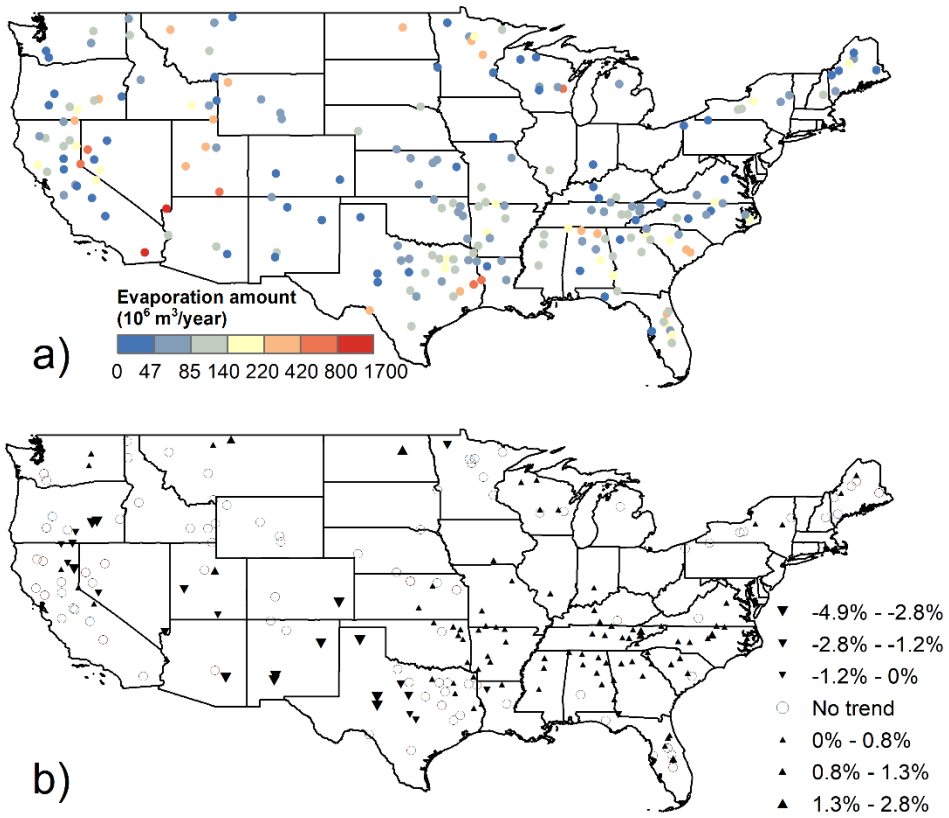

Figure 4.9 a) Long-term average evaporation amount and b) their trends detected by linear regression and Mann-Kendall test. The trends are shown in percentage and were calculated by dividing the annual evaporation trends by the long-term average evaporation amounts.

4.3.3.2 Long term trends for the CONUS

The average evaporation amount is 25.33 (23.64-27.51) $\times 10^9$ m^3 per year from 1985 to 2014, which is equivalent to 70.0% (65.1-75.7%) of the surface water used for public supply in the United States in 2010 (36.34×10^9 m^3 according to Maupin et al., 2014). Because the total surface area of these 209 reservoirs only accounts for ~27% of all the water bodies in the CONUS, the total evaporation amount can be much larger.

From an annual perspective, the average evaporation rate, total surface area, and total evaporation amount of these 209 reservoirs have shown non-stationary characteristics (Figure 4.10 and Table 4.2). The average evaporation rate has a significant increasing trend of about 0.008 (0.005-0.011) mm/d/year (p=0.00). This trend is mainly caused by an increased shortwave radiation of 0.245 W/m^2/year from 1985 to 2014. These trends of shortwave radiation are consistent with the findings from Long et al (2009) and Gan et al (2014), which suggest there is a global brightening trend in the recent decades. Although there is a clear long-term negative trend, the surface area inter-annual fluctuations are also notable. This pattern is consistent with the wet-dry conditions in the CONUS, including the severe 1988-89 North American drought (Heim Jr, 2002) and the most powerful El Nino in 1997-1998 (Changnon, 2000). Specifically, in recent years, areas of several large reservoirs (Lake Mead, Lake Powell, Goose Lake, and Sevier Lake) have plunged due to depletion. Although the total evaporation amount follows the area pattern in general, there is no significant long-term trend reported by Mann-Kendall test. This is caused by the joint effect of increasing evaporation rate and decreasing surface area.

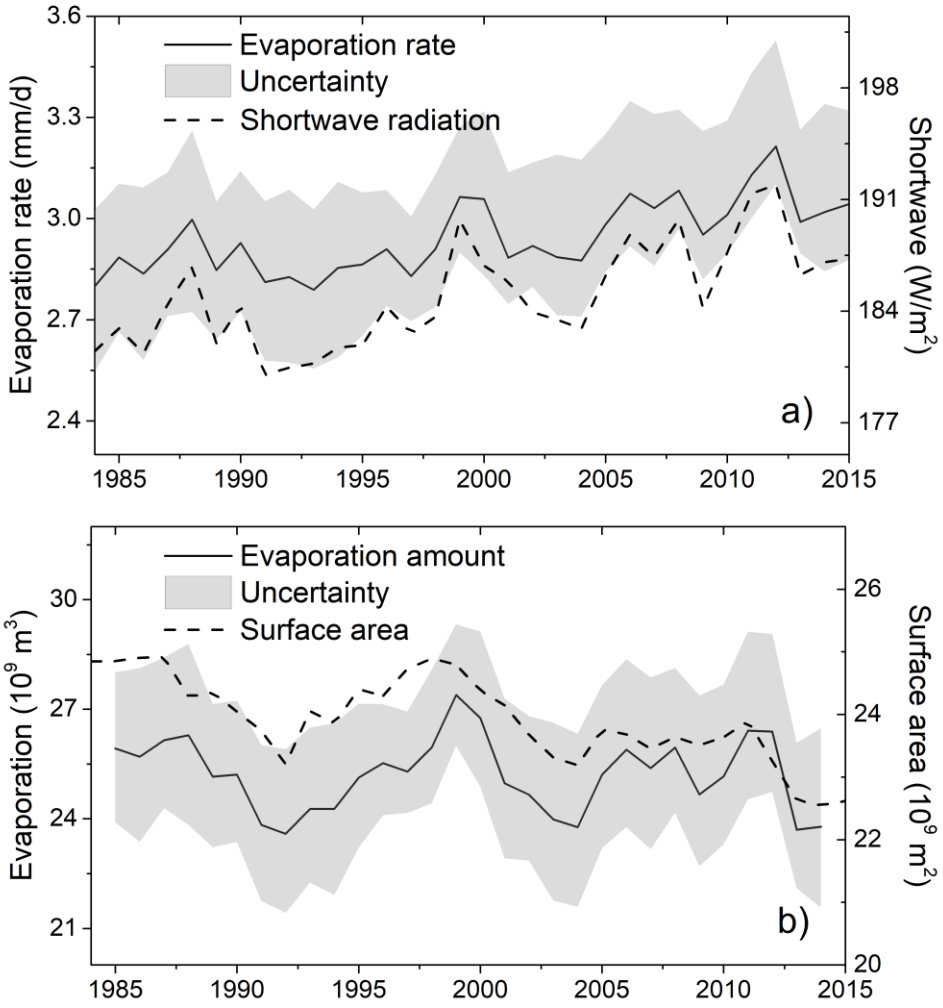

Figure 4.10 Annual average values of a) evaporation rate and shortwave radiation, b) surface area and annual evaporation (for the 209 reservoirs). Solid black line shows the average evaporation rates calculated by TerraClimate, NLDAS and GLDAS and shaded areas represent the uncertainties.

Table 4.2 Mann-Kendall trend test for the forcing data, evaporation rate, surface area, and evaporation amount. First value and second value in each cell represent the trend and p-value for the variable. The 'no trend' is marked when the p-value is larger than 0.05 (95% as the confidence interval)

	TerraClimate	NLDAS	GLDAS	Average
Shortwave radiation (W/m^2/year)	0.168/0.01	0.272/0.00	0.295/0.00	0.245/0.00
Air temperature (ºC/year)	0.019/0.04	0.022/0.03	no trend/0.32	no trend/0.10
Vapor pressure deficit (kPa/year)	no trend/0.08	0.005/0.00	0.004/0.00	0.003/0.00
Wind speed (m/s/year)	no trend/0.23	0.011/0.00	no trend/0.07	0.003/0.03
Evaporation rate (mm/d/year)	0.005/0.00	0.011/0.00	0.008/0.00	0.008/0.00
Surface area (10^9 m^2/year)	-0.052/0.00			
Evaporation amount (10^9 m^3/year/year)	no trend/0.10	no trend/0.80	no trend/0.80	no trend/0.59

4.3.4 Evaporation in total water losses

Four reservoirs were selected to evaluate the role evaporation plays in the total water losses (Figure 4.11). They are Lake Mead in Nevada/Arizona, E.V. Spence Reservoir, Sam Rayburn Reservoir, and Wright Patman Lake in Texas. The inflow, outflow, and storage data were collected from United States Geological Survey (USGS; https://waterdata.usgs.gov/nwis) (for Lake Mead) and United States Army Corps of Engineers (USACE; http://www.swf-wc.usace.army.mil/cgi-bin/rcshtml.pl) (for the three Texas reservoirs). The precipitation data were collected from the TerraClimate dataset.

Lake Mead—the largest reservoir in the CONUS by capacity—is critical to the regional socio-economic development (Christensen et al., 2004). Thus, the recent depletion of lake storage

has raised great concern for the water managers in the Southwest (Barnett and Pierce, 2008). The average RELI value for Lake Mead from 1990 to 2014 is 65% (61%-67%). This suggests that most of the storage losses of Lake Mead are through evaporation, while the rest is attributed to the combination of direct water use (WU) (by the Las Vegas Valley) and groundwater leakage (L). The WU only accounts for the direct pumpage from the reservoir and it does not include the downstream water use.

USACE provides the computed inflow (by incorporate all sources of inflows) and the observed outflow data for 29 reservoirs in Texas. Following Equation 4.16, the average RELI values for E.V. Spence Reservoir, Sam Rayburn Reservoir, and Wright Patman Lake are 61% (57%-63%), 46% (42%-51%), and 35% (32%-38%), respectively. The shrink of E.V. Spence Reservoir also leads to reduced evaporation amount and storage changes for the reservoir. For Sam Rayburn Reservoir and Wright Patman Lake, both evaporation amount and storage changes are relatively stable.

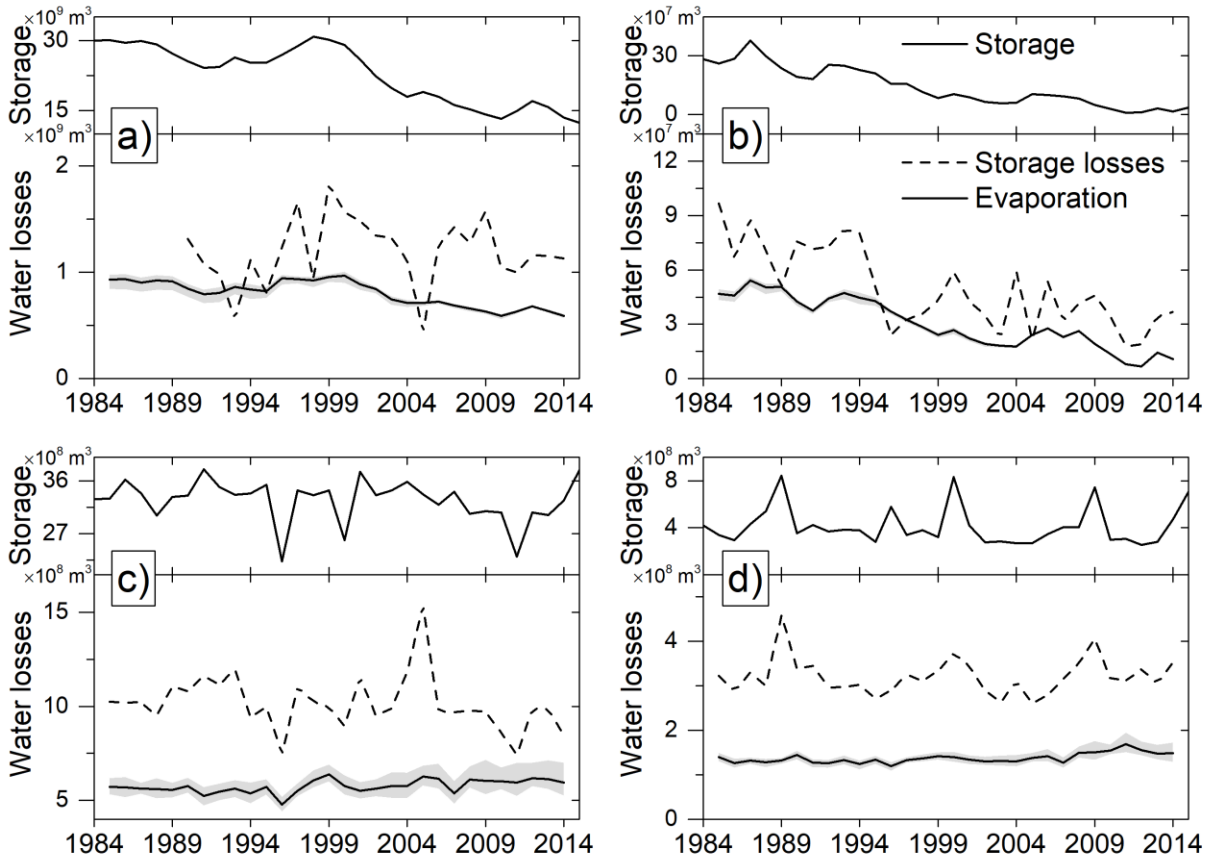

Figure 4.11 Annual time series of the reservoir storage, storage losses (the denominator in Equation 4.16), and evaporation amount (the numerator in Equation 4.16) for a) Lake Mead in Nevada/Arizona; b) Lake E.V. Spence in Texas; c) Sam Rayburn Reservoir in Texas; and d) Wright Patman Lake in Texas.

4.4. Discussion

4.4.1 Reservoir surface area

The generated long term reservoir evaporation dataset directly benefit from the high quality surface area estimations. Satellite images captured by VIS/NIR sensors usually suffer from multi-source contaminations including clouds, cloud shadows, and terrain shadows. For Landsat 7, the collected images also suffered from gaps due to the SLC failure. As a result, direct

extraction of water area from the satellite images can lead to notable underestimations. Comparing with the raw water classification results from Pekel et al. (2016), the image enhancement algorithm from Zhao and Gao (2018) can significantly improve the continuity of the reservoir area time series. Most of the contaminated classification results can be corrected to get the full water coverage. For example, there are 98 area values that were corrected for Amistad Reservoir (Figure 4.3) – leading to the improved R^2 between surface areas with observed storage.

The reservoir area variations and changes are driven by a number of factors. Because reservoirs accumulate all the water from upstream, the changes of area/storage are generally connected with the regional climate changes. As suggested by other studies (Prein et al., 2016; Barnett and Pierce, 2008), the southwestern region of US have been experiencing reduced precipitation for the last three decades. Consequently, the surface areas of the reservoirs in this region have significant decreasing trends. Specifically, several very large reservoirs such as Lake Mead and Lake Powell are located in this region. This lead to the overall decreasing reservoir surface area of the US (Table 4.2). It is also worth noting that the increasing water use can be another important factor that contributes to the decreasing reservoir surface area, especially in the drought event. For example, with the population growth, the surface water withdraw for public supply in Texas increased from 5.4×10^6 m^3 in 1985 to 1.26×10^7 m^3 in 2010 (https://water.usgs.gov/watuse), which exacerbated the reservoir depletion in the 2010-2013 very severe drought (Scanlon et al., 2013).

4.4.2 Reservoir evaporation rate

Compared to the reservoir surface area, estimation of evaporation rate has much larger uncertainties. The errors generally attribute to several major sources. The first is the meteorological forcing data. Even though TerraClimate, NLDAS, and GLDAS are all based on well-tested dataset/models, the usage of different data sources still leads to different meteorological forcing data output. For example, the long-term mean shortwave radiation for these 209 reservoir is 180.5 W/m^2 for TerraClimate, but 192.5 W/m^2 for NLDAS and 182.9 W/m^2 for GLDAS. Compounding with the uncertainties from other meteorological variables, evaporation rates from TerraClimate and GLDAS turn out to be lower than that from NLDAS. The second potential source of errors is the formulations of Penman equation including the wind function and the difference between skin and bulk water temperature (i.e., water column temperature). Based on the wind functions from 19 previous studies, McJannet et al. (2012) developed the generalized wind function with the fetch effect. As discussed in McJannet et al. (2012), the uncertainties of the wind function include the uncertainties from curve-fitting process, measurement errors, upwind roughness, stability conditions, and extrapolation of wind functions. Thus, the evaporation rate estimation using this generalized wind function still has large uncertainty although the usage of combination equation can reduce it to a certain extent (McJannet et al., 2012).

The skin layer of a water body is typically defined as the upper 10-500 μm layer of water (Donlon et al., 2002). Due the joint effects of outgoing longwave radiation and sensible/latent heat flux, the water temperature of the skin layer is lower than the water beneath – which is commonly known as skin effect (Fairall et al., 1996). However, the magnitude of skin effect is highly dependent on the depth where the bulk temperature is measured. For example, Murray et

al. (2000) reported daytime skin effect of +0.05 ± 0.51 K and nighttime skin effect of −0.20±0.46K of the ocean based on the 1m deep bulk temperature measurement. Donlon et al. (2002) found that skin effect with bulk temperature measurement at 0.1m is negative while that at 0.3m is positive. In Equation 4.12 and 4.13, the water temperature should be represented by the skin temperature. However, bulk temperature was used instead for simplicity with the assumption that there is no significant difference between skin and bulk water temperature. This assumption has been adopted several studies, even though its reliability is conditioned upon the depths of different reservoirs (McJannet et al., 2008; Finch et al., 2001).

Validation results against observed (EC and BREB) evaporation rates suggest that evaporation rate estimations can be notably improved for the relatively deep reservoirs (e.g., Lake Mead, White Bear Lake, and Lake Five-O) by incorporating the heat storage term in Penman equation. Specifically, the heat storage effects delay the timing for peak evaporation rate and reduce the seasonal variation. This phenomenon is more significant as the depth of the reservoir increases. Despite of the inaccuracy of pan evaporation, it is the only source that can be used for validation at a large scale. Comparison between modeled and pan evaporation rates shows large discrepancies, especially for the monthly evaporation rates. Results from all the three forcing datasets show similar R^2 values (Figure 4.7a). In addition, as discussed above, the NLDAS generally has larger values than TerraClimate and then than GLDAS. The R^2 between long-term average values of modeled and pan evaporation for all the 209 reservoirs show improved agreement.

From this study we have found a significant increasing trend of evaporation rate (0.008 mm/d/year). This seemingly contradicts the declining pan evaporation (so-called “evaporation paradox”) reported in Brutsaert and Parlange (1998). Nonetheless, several studies have

concluded that pan evaporation trend can be inversely correlated with the actual evaporation (Brutsaert, 2006; Lawrimore and Peterson, 2000; Golubev et al., 2001), which are in agreement with our results. Even though the relative humidity and wind speed can be critical for evaporation rate estimation, the solar radiation is the primary driving force for evaporation processes and thus the variable that the evaporation is most sensitive to (Brutsaert, 2006; Wild, 2012). However, because our study period coincides with the global brightening period, the trend of evaporation rate cannot be linearly extrapolated to the future (Wild, 2016).

Increase of air temperature can enhance the evaporation process by increasing the Bowen ratio, with less sensible heat but more latent heat (Wang et al., 2018). Our results also show the linkage between evaporation rate changes and air temperature trends. With respect to the wind speed, none of the three reanalysis based forcing datasets has revealed a significant stilling trends across the entire CONUS, a phenomenon suggested by other studies (McVicar et al., 2012; Vautard et al., 2010). This is because the reanalysis used the rawinsonde data, which is upper-air measurement instead of earth surface observations. In addition, the global stilling is still unexplained and can be caused by increased ground roughness (possibly does not apply on open water surface), global circulation, and even possibly the worn bearing of anemometer (Azorin-Molina et al., 2018).

4.4.3 Evaporation losses from the reservoirs

For the entire CONUS, the increasing trend of evaporation rate are counterbalanced by the decreasing trend of surface area and this leads to insignificant trend for the evaporation amount in the CONUS. For individual reservoirs, the trend for evaporation amount is primarily dominated by surface area changes. For instance, the reservoirs in southwestern US generally show decreasing trends for both surface area and evaporation amount while the reservoirs in the

eastern US show increasing trends. When there is no significant trend of surface area, the trend in evaporation rate can also propagate to the trend of evaporation amount. For example, the reservoirs in the central US (i.e., Kansas, Missouri, Oklahoma, and Arkansas) generally have increasing trends for both evaporation rate and evaporation amount. As a result, the insignificant trend of total evaporation amount consists of the decreasing trend in the southwestern US and the increasing trend in the eastern US. The decreasing trends of reservoir evaporation amount in the south and western US are caused by the decreasing surface area and originally region climate changes and local water use. The increasing trends of reservoir evaporation amount in the eastern US are caused by the increasing evaporation rates and originally the increasing solar radiation (global brightening).

4.4.4 Potential applications and algorithm caveats

Due to the challenges of estimating reservoir area and evaporation rate, there have been very few studies reporting the large scale reservoir evaporation. Most studies focused on single reservoir or catchment scale such that the wind function can be calibrated (Gianniou and Antonopoulos, 2007; Valiantzas, 2006; Linacre, 1993). On a large scale, evaporation rate is generally reported separately without considering the surface area changes (Alvarez et al., 2008; Mekonnen et al., 2015). By considering the heat storage term and adopting a generalized wind function, this study has improved the Penman equation for estimating the evaporation rate more accurately. Furthermore, the surface area data were extracted from a remotely sensed dataset for which an enhancement algorithm was applied to repair image contaminations. Subsequently, monthly time series of evaporation for 209 reservoir in the CONUS over a long-term were generated.

This evaporation dataset can help decision makers better manage water use for different purposes. First, the evaporation dataset from this study can help better allocate water rights. For example, in the State of Texas, water rights are allocated to each water user for legal extraction of surface water. Yet evaporation from reservoirs is not accurately incorporated into the current water rights allocation system. As a result, water resources can be excessively exploited or not sufficiently used. Second, in addition to evaporation, another major source of reservoir water loss is leakage to groundwater—which is extremely difficult to quantify due to the complex physical processes involved. Yet by employing the evaporation amount from this dataset in the reservoir water balance equation, reservoir leakage can be derived. The results can potentially improve the water management efficiency for both surface water and groundwater. Third, it can be used for quantifying the blue water footprint for hydropower. By constructing the reservoir, the latent heat flux was replaced from the original evapotranspiration to open water evaporation, which might be significantly larger, especially in the western US (Mekonnen and Hoekstra, 2012). As a result, the value of the hydropower benefit is reduced. Therefore, quantification of the blue water footprint is important for future energy policies. Last, this data product potentially can be used for improving reservoir operation rules under a changing climate.

Although the algorithms in this study have been developed to address many constraints of previous studies, there are still several limitations that are worth noting. First, because there are barely any observations over lakes, the evaporation rate errors associated with the forcing data (e.g., wind speed, shortwave/longwave radiation) are difficult to quantify. The uncertainties from the forcing data were analyzed via the usage of three reanalysis datasets. Second, due to the large scale nature of this study, reservoir bathymetry and stratification were not considered when the water temperature was calculated. Third, the energy fluxes other than the radiation such as the

inflow heat, outflow heat, and ground heat fluxes are not included. For some reservoirs, the outlet is located at the bottom of the dam and thus the temperature of released water is different with the inflow water, creating net energy fluxes to the reservoir.

4.5. Conclusion

This study presents a novel algorithm framework for reservoir evaporation quantification. By applying the algorithm to 209 reservoirs in the CONUS, a first-of-its-kind continentally consistent and locally practical evaporation data product was generated, providing significant benefits to the water resources management, hydrology, and remote sensing communities. The major conclusions are drawn as follows:

1. For the 209 reservoirs in the CONUS, long term average evaporation was found to be 25.33 (23.64-27.51) $\times 10^9$ m^3 per year from 1985 to 2014. This amount is equivalent to 70.0% (65.1-75.7%) of the surface water used for public supply in the United States in 2010.
2. Due to the increasing trend of shortwave radiation, the evaporation rate has been elevated accordingly. The long-term trend of reservoir surface area are largely connected with regional climate and local water management practices.
3. The evaporation amount trend for individual reservoirs can be affected by both surface area trend (mostly in the southwestern US) and evaporation rate trend (mostly in the eastern US). For all the 209 reservoirs, the decreasing trend of surface area have balanced off the increasing trend of evaporation, leading to insignificant trend of total evaporation amount.

CHAPTER V

CONCLUSION

Despite delivering multiple benefits to human society, reservoirs have also altered the natural hydrologic cycle extensively. With the increasing number of reservoirs that have been plugged into the world's river systems, comprehensive simulations of the impacts of reservoirs are needed. However, due to a number of constraints, such simulations—which are important for sustainable water resources management—have not been fully understood in previous studies. This dissertation demonstrates three frameworks (in Chapter II, III, and IV) towards simulating the interactions between hydrological processes and flow regulation, investigates future water resilience under climate change and urbanization, and quantifies reservoir evaporation loss.

Through the first study (Chapter II), a multi-purpose reservoir module with predefined complex operational rules was integrated into the DHSVM model. Conditional operating rules, which are designed to reduce flood risk and enhance water supply reliability, were adopted in this module. The performance of the integrated model was tested over the upper Brazos River Basin in Texas, where Lake Whitney and Aquilla Lake are located. The integrated DHSVM model was calibrated and validated using observed reservoir inflow, outflow, and storage data. The error statistics were summarized for both reservoirs on a daily, weekly, and monthly basis. Using the weekly reservoir storage for Lake Whitney as an example, the coefficient of determination (R^2) was 0.85 and the Nash-Sutcliff Efficiency (NSE) was 0.75. These results suggest that this reservoir module holds promise for use in sub-monthly hydrological simulations. The DHSVM-Res model provides a platform to support adaptive water resources

management under the impacts of evolving anthropogenic activities and substantial environmental changes.

Built upon the integrated modeling framework, the second study (Chapter III) evaluated how future potential droughts and population growth will affect the water supply reliability for the Dallas metropolitan region. Future potential droughts were chosen from the global circulation model outputs and the future water demand was generated using Monte Carlo simulations (to incorporate the uncertainties). Compared with the first half of the 21st century (2000–2049), reservoir storage and water supply reliability during the second half century (2050–2099) are projected to decline by 16.1% and 14.2%, respectively. While both future multi-year droughts and population growth will lower water supply resilience, the uncertainty associated with future climate projection is larger than that associated with urbanization. To reduce the drought risks, a combination of mitigation strategies (e.g., additional conservation, integrating new water sources, and water use redistribution) was found to be the most efficient approach and can significantly improve water supply reliability (by as much as 15.9%).

The third modeling framework (Chapter IV) utilized a state-of-the-art water mapping technology and evaporation rate calculation method to quantify the monthly evaporation amount for 209 major reservoirs in the contiguous United States. Reservoir surface areas were extracted and enhanced from the Global Surface Water Dataset (GSWD) from Mar 1984 to Oct 2015. The evaporation rate was modeled using the Penman equation with the lake heat storage effect considered. Validation results using Eddy Covariance measurement and Bowen Ratio Energy Budget estimations suggest that this approach can significantly improve the accuracy of the simulated monthly reservoir evaporation rate. The evaporation losses were subsequently estimated as the product of the surface area and the evaporation rate. This dissertation presents a

first of its kind, comprehensively validated, locally practical, and continentally consistent reservoir evaporation dataset. The results suggest that the long term averaged annual evaporation from these 209 reservoirs is 25.33×10^9 m^3, which is equivalent to 70.0% of the annual public water supply of the United States (in 2010). An increasing trend of the evaporation rate (0.008 mm/d/year) and a decreasing trend of the total surface area (-0.052×10^9 m^2/year) were both detected during the study period. As a result, the total evaporation shows an insignificant trend, yet with significant spatial heterogeneity. This new reservoir evaporation dataset can help facilitate more efficient water management practices.

REFERENCES

Abatzoglou, J. T., Dobrowski, S. Z., Parks, S. A., & Hegewisch, K. C. (2018). TerraClimate, a high-resolution global dataset of monthly climate and climatic water balance from 1958–2015. Scientific Data, 5, 170191.

Abtew, W. (2001). Evaporation estimation for Lake Okeechobee in south Florida. Journal of Irrigation and Drainage Engineering, 127(3), 140-147.

Ali, S., Ghosh, N. C., & Singh, R. (2008). Evaluating best evaporation estimate model for water surface evaporation in semi-arid region, India. Hydrological Processes, 22(8), 1093-1106.

Alley, W. M. (1984). The Palmer Drought Severity Index: Limitations and Assumptions. Journal of Climate and Applied Meteorology, 23(7), 1100-1109.

Alvarez, V. M., González-Real, M., Baille, A., Valero, J. M., & Elvira, B. G. (2008). Regional assessment of evaporation from agricultural irrigation reservoirs in a semiarid climate. Agricultural Water Management, 95(9), 1056-1066.

Amarasinghe, P., Liu, A., Egodawatta, P., Barnes, P., McGree, J., & Goonetilleke, A. (2016). Quantitative assessment of resilience of a water supply system under rainfall reduction due to climate change. Journal of Hydrology, 540, 1043-1052.

Arnold, J. G., & Fohrer, N. (2005). SWAT2000: current capabilities and research opportunities in applied watershed modelling. Hydrological Processes, 19(3), 563-572.

Arnold, J. G., Moriasi, D. N., Gassman, P. W., Abbaspour, K. C., White, M. J., Srinivasan, R., . . . Van Liew, M. W. (2012). SWAT: Model use, calibration, and validation. Transactions of the ASABE, 55(4), 1491-1508.

Azorin-Molina, C., Asin, J., McVicar, T. R., Minola, L., Lopez-Moreno, J. I., Vicente-Serrano, S. M., & Chen, D. (2018). Evaluating anemometer drift: A statistical approach to correct biases in wind speed measurement. Atmospheric Research, 203, 175-188.

Bader, D., Collins, W., Jacob, R., Jones, P., Rasch, P., Taylor, M., . . . Williams, D. (2014). Accelerated climate modeling for energy (ACME) project strategy and initial implementation plan, available at http://climatemodeling.science.energy.gov/.

Barlow, P. M., & Leake, S. A. (2012), Streamflow depletion by wells--Understanding and managing the effects of groundwater pumping on streamflow, Report 2330-5703, US Geological Survey.

Barnett, T. P., & Pierce, D. W. (2008). When will Lake Mead go dry? Water Resources Research, 44(3).

Battin, J., Wiley, M. W., Ruckelshaus, M. H., Palmer, R. N., Korb, E., Bartz, K. K., & Imaki, H. (2007). Projected impacts of climate change on salmon habitat restoration. Proceedings of the National Academy of Sciences, 104(16), 6720-6725.

Bekele, E. G., & Knapp, H. V. (2010). Watershed modeling to assessing impacts of potential climate change on water supply availability. Water Resources Management, 24(13), 3299-3320.

Bennett, K. E., Werner, A. T., & Schnorbus, M. (2012). Uncertainties in hydrologic and climate change impact analyses in headwater basins of British Columbia. Journal of Climate, 25(17), 5711-5730.

Bicknell, B. R., Imhoff, J. C., Kittle Jr, J. L., Jobes, T. H., Donigian Jr, A. S., & Johanson, R. (2001). Hydrological simulation program–fortran: HSPF, version 12 user's manual. AQUA TERRA Consultants, Mountain View, California.

Biemans, H., Haddeland, I., Kabat, P., Ludwig, F., Hutjes, R. W. A., Heinke, J., . . . Gerten, D. (2011). Impact of reservoirs on river discharge and irrigation water supply during the 20th century. Water Resources Research, 47(3).

Billings, R. B., & Jones, C. V. (2011), Forecasting urban water demand, American Water Works Association.

Bogan, T., Mohseni, O., & Stefan, H. G. (2003). Stream temperature-equilibrium temperature relationship. Water Resources Research, 39(9).

Bolton, D. (1980). The computation of equivalent potential temperature. Monthly Weather Review, 108(7), 1046-1053.

Brune, G. M. (1953). Trap efficiency of reservoirs. Eos, Transactions American Geophysical Union, 34(3), 407-418.

Brutsaert, W., & Parlange, M. (1998). Hydrologic cycle explains the evaporation paradox. Nature, 396(6706), 30.

Brutsaert, W. (2006). Indications of increasing land surface evaporation during the second half of the 20th century. Geophysical Research Letters, 33(20).

Burke, E. J., Brown, S. J., & Christidis, N. (2006). Modeling the recent evolution of global drought and projections for the twenty-first century with the Hadley Centre climate model. Journal of Hydrometeorology, 7(5), 1113-1125.

Busker, T., de Roo, A., Gelati, E., Schwatke, C., Adamovic, M., Bisselink, B., ... & Cottam, A. A global lake and reservoir volume analysis using a surface water dataset and satellite altimetry. Hydrology and Earth System Sciences Discussions, 2018, 1-32.

Caissie, D., Satish, M. G., & El-Jabi, N. (2005). Predicting river water temperatures using the equilibrium temperature concept with application on Miramichi River catchments (New Brunswick, Canada). Hydrological Processes, 19(11), 2137-2159.

Changnon, S. A. (2000), El Niño 1997-1998: the climate event of the century, Oxford University Press.

Chao, B. F., Wu, Y., & Li, Y. (2008). Impact of artificial reservoir water impoundment on global sea level. Science, 320(5873), 212-214.

Chiew, F., Teng, J., Vaze, J., & Kirono, D. (2009). Influence of global climate model selection on runoff impact assessment. Journal of Hydrology, 379(1), 172-180.

Christensen, N., Wood, A., Voisin, N., Lettenmaier, D., & Palmer, R. (2004). The effects of climate change on the hydrology and water resources of the Colorado River Basin. Climatic Change, 62(1-3), 337-363.

Collet, L., Ruelland, D., Estupina, V. B., Dezetter, A., & Servat, E. (2015). Water supply sustainability and adaptation strategies under anthropogenic and climatic changes of a meso-scale Mediterranean catchment. Science of the Total Environment, 536, 589-602.

Conway, D. (1996). The impacts of climate variability and future climate change in the Nile Basin on water resources in Egypt. International Journal of Water Resources Development, 12(3), 277-296.

Cressman, G. P. (1959). An operational objective analysis system. Monthly Weather Review, 87(10), 367-374.

Croley, T. E., & He, C. (2005). Distributed-parameter large basin runoff model. I: Model development. Journal of Hydrologic Engineering, 10(3), 173-181.

Cuo, L., Lettenmaier, D. P., Mattheussen, B. V., Storck, P., & Wiley, M. (2008). Hydrologic prediction for urban watersheds with the Distributed Hydrology–Soil–Vegetation Model. Hydrological Processes, 22(21), 4205-4213.

Cuo, L., Lettenmaier, D. P., Alberti, M., & Richey, J. E. (2009). Effects of a century of land cover and climate change on the hydrology of the Puget Sound basin. Hydrological Processes, 23(6), 907-933.

Dai, A. (2011). Characteristics and trends in various forms of the Palmer Drought Severity Index during 1900–2008. Journal of Geophysical Research: Atmospheres, 116(D12).

Dai, A. (2013). Increasing drought under global warming in observations and models. Nature Climate Change, 3(1), 52-58.

Dallas City Council (2014). Long range Water Supply plan update, available at: http://dallascityhall.com/government/Council%20Meeting%20Documents/2014/LongRangeWaterSupplyPlanUpdate_091714.pdf.

de Bruin, H. (1982). Temperature and energy balance of a water reservoir determined from standard weather data of a land station. Journal of Hydrology, 59(3-4), 261-274.

DHI (2003). MIKE SHE flow modules manual, Danish Hydraulic Institute, Denmark.

Donchyts, G., Baart, F., Winsemius, H., Gorelick, N., Kwadijk, J., & van de Giesen, N. (2016). Earth's surface water change over the past 30 years. Nature Climate Change, 6(9), 810-813.

Donlon, C. J., Minnett, P. J., Gentemann, C., Nightingale, T. J., Barton, I. J., Ward, B., & Murray, M. J. (2002). Toward improved validation of satellite sea surface skin temperature measurements for climate Research. Journal of Climate, 15(4), 353-369.

dos Reis, R. J., & Dias, N. L. s. (1998). Multi-season lake evaporation: energy-budget estimates and CRLE model assessment with limited meteorological observations. Journal of Hydrology, 208(3), 135-147.

Doten, C. O., Bowling, L. C., Lanini, J. S., Maurer, E. P., & Lettenmaier, D. P. (2006). A spatially distributed model for the dynamic prediction of sediment erosion and transport in mountainous forested watersheds. Water Resources Research, 42(4).

Dovers, S. R., & Handmer, J. W. (1992). Uncertainty, sustainability and change. Global Environmental Change, 2(4), 262-276.

Edinger, J. E., Duttweiler, D. W., & Geyer, J. C. (1968). The response of water temperatures to meteorological conditions. Water Resources Research, 4(5), 1137-1143.

Emori, S., & Brown, S. (2005). Dynamic and thermodynamic changes in mean and extreme precipitation under changed climate. Geophysical Research Letters, 32(17).

Fairall, C., Bradley, E. F., Godfrey, J., Wick, G., Edson, J. B., & Young, G. (1996). Cool-skin and warm-layer effects on sea surface temperature. Journal of Geophysical Research: Oceans, 101(C1), 1295-1308.

Fekete, B. M., Wisser, D., Kroeze, C., Mayorga, E., Bouwman, L., Wollheim, W. M., & Vörösmarty, C. (2010). Millennium ecosystem assessment scenario drivers (1970–2050): climate and hydrological alterations. Global Biogeochemical Cycles, 24(4).

Fiering, M. B. (1982). A screening model to quantify resilience. Water Resources Research, 18(1), 27-32.

Finch, J. W. (2001). A comparison between measured and modelled open water evaporation from a reservoir in south-east England. Hydrological Processes, 15(14), 2771-2778.

Finch, J., & Hall, R. (2001), Estimation of open water evaporation: A review of methods, Environment Agency.

Frick, D. M., Bode, D., & Salas, J. D. (1990). Effect of drought on urban water supplies. I: Drought analysis. Journal of Hydraulic Engineering, 116(6), 733-753.

Friedrich, K., Grossman, R. L., Huntington, J., Blanken, P. D., Lenters, J., Holman, K. D., . . . Kowalski, T. (2017). Reservoir evaporation in the western United States: Current science, challenges, and future needs. Bulletin of the American Meteorological Society, 99(1), 167-187.

Gallego-Elvira, B., Baille, A., Martín-Górriz, B., & Martínez-Álvarez, V. (2010). Energy balance and evaporation loss of an agricultural reservoir in a semi-arid climate (south-eastern Spain). Hydrological Processes, 24(6), 758-766.

Gan, C.-M., Pleim, J., Mathur, R., Hogrefe, C., Long, C. N., Xing, J., . . . Wei, C. (2014). Assessment of the effect of air pollution controls on trends in shortwave radiation over the United States from 1995 through 2010 from multiple observation networks. Atmospheric Chemistry and Physics, 14(3), 1701-1715.

Gao, L., Connor, J. D., & Dillon, P. (2014). The economics of groundwater replenishment for reliable urban water supply. Water, 6(6), 1662-1670.

Gao, H. (2015). Satellite remote sensing of large lakes and reservoirs: From elevation and area to storage. Wiley Interdisciplinary Reviews: Water, 2(2), 147-157.

Gao, L., Bryan, B. A., Nolan, M., Connor, J. D., Song, X., & Zhao, G. (2016). Robust global sensitivity analysis under deep uncertainty via scenario analysis. Environmental Modelling & Software, 76, 154-166.

Gao, L., & Bryan, B. A. (2017). Finding pathways to national-scale land-sector sustainability. Nature, 544(7649), 217.

Gesch, D., Oimoen, M., Greenlee, S., Nelson, C., Steuck, M., & Tyler, D. (2002). The national elevation dataset. Photogrammetric Engineering and Remote Sensing, 68(1), 5-32.

Ghosh, S., & Mujumdar, P. (2007). Nonparametric methods for modeling GCM and scenario uncertainty in drought assessment. Water Resources Research, 43(7).

Gianniou, S. K., & Antonopoulos, V. Z. (2007). Evaporation and energy budget in Lake Vegoritis, Greece. Journal of Hydrology, 345(3-4), 212-223.

Gökbulak, F., & Özhan, S. (2006). Water loss through evaporation from water surfaces of lakes and reservoirs in Turkey. Official Publication of the European Water Association, EWA.

Golubev, V. S., Lawrimore, J. H., Groisman, P. Y., Speranskaya, N. A., Zhuravin, S. A., Menne, M. J., . . . Malone, R. W. (2001). Evaporation changes over the contiguous United States and the former USSR: A reassessment. Geophysical Research Letters, 28(13), 2665-2668.

Graf, W. L. (1999). Dam nation: A geographic census of American dams and their large-scale hydrologic impacts. Water Resources Research, 35(4), 1305-1311.

Graf, W. L. (2006). Downstream hydrologic and geomorphic effects of large dams on American rivers. Geomorphology, 79(3), 336-360.

Gutierrez, F., & Dracup, J. (2001). An analysis of the feasibility of long-range streamflow forecasting for Colombia using El Nino–Southern Oscillation indicators. Journal of Hydrology, 246(1), 181-196.

Haddeland, I., Lettenmaier, D. P., & Skaugen, T. (2006). Effects of irrigation on the water and energy balances of the Colorado and Mekong river basins. Journal of Hydrology, 324(1–4), 210-223.

Hamlet, A. F., & Lettenmaier, D. P. (1999). Effects of climate change on hydrology and water resources in the Columbia River Basin. JAWRA Journal of the American Water Resources Association, 35(6), 1597-1623.

Hamon, W. R. (1960), Estimating potential evapotranspiration, Massachusetts Institute of Technology.

Hanasaki, N., Kanae, S., & Oki, T. (2006). A reservoir operation scheme for global river routing models. Journal of Hydrology, 327(1), 22-41.

Harwell, G. R. (2012), Estimation of evaporation from open water—A review of selected studies, summary of US Army Corps of Engineers data collection and methods, and evaluation of two methods for estimation of evaporation from five reservoirs in Texas, Report 2328-0328, US Geological Survey.

Heim Jr, R. R. (2002). A review of twentieth-century drought indices used in the United States. Bulletin of the American Meteorological Society, 83(8), 1149-1165.

Hirsch, R. M. (2011). A perspective on nonstationarity and water management. JAWRA Journal of the American Water Resources Association, 47(3), 436-446.

Homer, C., Dewitz, J., Fry, J., Coan, M., Hossain, N., Larson, C., . . . Wickham, J. (2007). Completion of the 2001 National Land Cover Database for the Conterminous United States. Photogrammetric Engineering and Remote Sensing, 73(4), 337.

Hone, J. (1999). On rate of increase (r): patterns of variation in Australian mammals and the implications for wildlife management. Journal of Applied Ecology, 36(5), 709-718.

House-Peters, L. A., & Chang, H. (2011). Urban water demand modeling: Review of concepts, methods, and organizing principles. Water Resources Research, 47(5).

Hsu, N.-S., & Wei, C.-C. (2007). A multipurpose reservoir real-time operation model for flood control during typhoon invasion. Journal of Hydrology, 336(3), 282-293.

Huang, C., Goward, S. N., Masek, J. G., Thomas, N., Zhu, Z., & Vogelmann, J. E. (2010). An automated approach for reconstructing recent forest disturbance history using dense Landsat time series stacks. Remote Sensing of Environment, 114(1), 183-198.

HydroLogics Inc (2007). User manual for OASIS with OCL, Columbia, MD.

IPCC, Stocker, T. F., Qin, D., Plattner, G.-K., Tignor, M., Allen, S. K., . . . Midgley, P. M. (2013). Climate change 2013: The physical science basis. Intergovernmental Panel on Climate Change, Working Group I Contribution to the IPCC Fifth Assessment Report (AR5) (Cambridge Univ Press, New York).

Jarvis, A., Reuter, H. I., Nelson, A., & Guevara, E. (2008). Hole-filled SRTM for the globe Version 4, available at the CGIAR-CSI SRTM 90m Database (http://srtm.csi.cgiar.org).

Kavvas, M., Chen, Z.-Q., Tan, L., Soong, S.-T., Terakawa, A., Yoshitani, J., & Fukami, K. (1998). A regional-scale land surface parameterization based on areally-averaged hydrological conservation equations. Hydrological Sciences Journal, 43(4), 611-631.

Kay, A., Davies, H., Bell, V., & Jones, R. (2009). Comparison of uncertainty sources for climate change impacts: flood frequency in England. Climatic Change, 92(1), 41-63.

Khandelwal, A., Mithal, V., & Kumar, V. (2015), Post classification label refinement using implicit ordering constraint among data instances, paper presented at Data Mining (ICDM), 2015 IEEE International Conference on, IEEE.

Khandelwal, A., Karpatne, A., Marlier, M. E., Kim, J., Lettenmaier, D. P., & Kumar, V. (2017). An approach for global monitoring of surface water extent variations in reservoirs using MODIS data. Remote Sensing of Environment, 202, 113-128.

Klein, I., Dietz, A., Gessner, U., Dech, S., & Kuenzer, C. (2015). Results of the Global WaterPack: A novel product to assess inland water body dynamics on a daily basis. Remote Sensing Letters, 6(1), 78-87.

Koutsoyiannis, D., & Montanari, A. (2015). Negligent killing of scientific concepts: the stationarity case. Hydrological Sciences Journal, 60(7-8), 1174-1183.

Kundzewicz, Z. W., Mata, L. J., Arnell, N. W., DÖLl, P., Jimenez, B., Miller, K., . . . Shiklomanov, I. (2008). The implications of projected climate change for freshwater resources and their management. Hydrological Sciences Journal, 53(1), 3-10.

Labadie, J., & Larson, R. (2007). MODSIM 8.1: River basin management decision Support system. User manual and documentation. Colorado State University, Fort Collins, 123.

Laghari, A., Vanham, D., & Rauch, W. (2012). The Indus basin in the framework of current and future water resources management. Hydrology and Earth System Sciences, 16(4), 1063.

Lawrimore, J. H., & Peterson, T. C. (2000). Pan evaporation trends in dry and humid regions of the United States. Journal of Hydrometeorology, 1(6), 543-546.

Lehner, B., Liermann, C. R., Revenga, C., Vörösmarty, C., Fekete, B., Crouzet, P., . . . Magome, J. (2011). High-resolution mapping of the world's reservoirs and dams for sustainable river-flow management. Frontiers in Ecology and the Environment, 9(9), 494-502.

Linacre, E. T. (1993). Data-sparse estimation of lake evaporation, using a simplified Penman equation. Agricultural and Forest Meteorology, 64(3), 237-256.

Liu, H., Zhang, Y., Liu, S., Jiang, H., Sheng, L., & Williams, Q. L. (2009). Eddy covariance measurements of surface energy budget and evaporation in a cool season over southern open water in Mississippi. Journal of Geophysical Research: Atmospheres, 114(D4).

Liu, H., Zhang, Q., & Dowler, G. (2012). Environmental controls on the surface energy budget over a large southern inland water in the United States: An analysis of one-year eddy covariance flux data. Journal of Hydrometeorology, 13(6), 1893-1910.

Liu, X., Tang, Q., Voisin, N., & Cui, H. (2016). Projected impacts of climate change on hydropower potential in China. Hydrology and Earth System Sciences Discussions, 2016, 1-30.

Livneh, B., Rosenberg, E. A., Lin, C., Nijssen, B., Mishra, V., Andreadis, K. M., . . . Lettenmaier, D. P. (2013). A long-term hydrologically based dataset of land surface fluxes and states for the conterminous United States: Update and extensions. Journal of Climate, 26(23), 9384-9392.

Livneh, B., Bohn, T. J., Pierce, D. W., Munoz-Arriola, F., Nijssen, B., Vose, R., . . . Brekke, L. (2015). A spatially comprehensive, hydrometeorological data set for Mexico, the U.S., and Southern Canada 1950–2013. Scientific Data, 2, 150042.

Long, C. N., Dutton, E. G., Augustine, J., Wiscombe, W., Wild, M., McFarlane, S. A., & Flynn, C. J. (2009). Significant decadal brightening of downwelling shortwave in the continental United States. Journal of Geophysical Research: Atmospheres, 114(D10).

Lund, J. R., & Ferreira, I. (1996). Operating rule optimization for Missouri River reservoir system. Journal of Water Resources Planning and Management-Asce, 122(4), 287-295.

Luo, L., Robock, A., Mitchell, K. E., Houser, P. R., Wood, E. F., Schaake, J. C., . . . Sheffield, J. (2003). Validation of the North American land data assimilation system (NLDAS) retrospective forcing over the southern Great Plains. Journal of Geophysical Research: Atmospheres, 108(D22).

Mahmood, K. (1987), Reservoir sedimentation: impact, extent, and mitigation. Technical paper, International Bank for Reconstruction and Development, Washington, DC (USA).

Mateo, C. M., Hanasaki, N., Komori, D., Tanaka, K., Kiguchi, M., Champathong, A., . . . Oki, T. (2014). Assessing the impacts of reservoir operation to floodplain inundation by combining hydrological, reservoir management, and hydrodynamic models. Water Resources Research, 50(9), 7245-7266.

Matonse, A. H., Pierson, D. C., Frei, A., Zion, M. S., Anandhi, A., Schneiderman, E., & Wright, B. (2013). Investigating the impact of climate change on New York City's primary water supply. Climatic Change, 116(3-4), 437-456.

Matthews, J. H., Wickel, B. A., & Freeman, S. (2011). Converging currents in climate-relevant conservation: water, infrastructure, and institutions. PLoS Biology, 9(9), e1001159.

Maupin, M. A., Kenny, J. F., Hutson, S. S., Lovelace, J. K., Barber, N. L., & Linsey, K. S. (2014), Estimated use of water in the United States in 2010, Report 2330-5703, US Geological Survey.

McDonald, R. I., Green, P., Balk, D., Fekete, B. M., Revenga, C., Todd, M., & Montgomery, M. (2011). Urban growth, climate change, and freshwater availability. Proceedings of the National Academy of Sciences, 108(15), 6312-6317.

McDonald, R. I., Weber, K., Padowski, J., Flörke, M., Schneider, C., Green, P. A., . . . Montgomery, M. (2014). Water on an urban planet: Urbanization and the reach of urban water infrastructure. Global Environmental Change, 27, 96-105.

McFeeters, S. K. (1996). The use of the Normalized Difference Water Index (NDWI) in the delineation of open water features. International Journal of Remote Sensing, 17(7), 1425-1432.

McJannet, D., Webster, I., Stenson, M., & Sherman, B. (2008). Estimating open water evaporation for the Murray Darling basin. Report for CSIRO, Australia.

McJannet, D. L., Webster, I. T., & Cook, F. J. (2012). An area-dependent wind function for estimating open water evaporation using land-based meteorological data. Environmental Modelling & Software, 31, 76-83.

McJannet, D., Hawdon, A., Van Niel, T., Boadle, D., Baker, B., Trefry, M., & Rea, I. (2017). Measurements of evaporation from a mine void lake and testing of modelling approaches. Journal of Hydrology, 555, 631-647.

McMahon, T., Peel, M., Lowe, L., Srikanthan, R., & McVicar, T. (2013). Estimating actual, potential, reference crop and pan evaporation using standard meteorological data: a pragmatic synthesis. Hydrology and Earth System Sciences, 17(4), 1331.

McVicar, T. R., Li, L., Van Niel, T. G., Zhang, L., Li, R., Yang, Q., . . . Liu, W. (2007). Developing a decision support tool for China's re-vegetation program: simulating regional impacts of afforestation on average annual streamflow in the Loess Plateau. Forest Ecology and Management, 251(1-2), 65-81.

McVicar, T. R., Roderick, M. L., Donohue, R. J., Li, L. T., Van Niel, T. G., Thomas, A., . . . Dinpashoh, Y. (2012). Global review and synthesis of trends in observed terrestrial near-surface wind speeds: Implications for evaporation. Journal of Hydrology, 416-417, 182-205.

Mekonnen, M., & Hoekstra, A. (2012). The blue water footprint of electricity from hydropower. Hydrology and Earth System Sciences, 16, 179-187.

Mekonnen, M. M., Gerbens-Leenes, P., & Hoekstra, A. Y. (2015). The consumptive water footprint of electricity and heat: a global assessment. Environmental Science: Water Research & Technology, 1(3), 285-297.

Messager, M. L., Lehner, B., Grill, G., Nedeva, I., & Schmitt, O. (2016). Estimating the volume and age of water stored in global lakes using a geo-statistical approach. Nature Communications, 7, 13603.

Milly, P. C., Dunne, K. A., & Vecchia, A. V. (2005). Global pattern of trends in streamflow and water availability in a changing climate. Nature, 438(7066), 347.

Milly, P. C., Betancourt, J., Falkenmark, M., Hirsch, R. M., Kundzewicz, Z. W., Lettenmaier, D. P., & Stouffer, R. J. (2008). Stationarity is dead: Whither water management? Science, 319(5863), 573-574.

Moene, A. F., Hartogensis, O. K., & Beyrich, F. (2009). Developments in scintillometry. Bulletin of the American Meteorological Society, 90(5), 694-698.

Mohseni, O., & Stefan, H. (1999). Stream temperature/air temperature relationship: a physical interpretation. Journal of Hydrology, 218(3), 128-141.

Monteith, J. L. (1965), Evaporation and environment, paper presented at Symp. Soc. Exp. Biol.

Moreo, M. T., & Swancar, A. (2013), Evaporation from Lake Mead, Nevada and Arizona, March 2010 through February 2012, Report 2328-0328, US Geological Survey.

Morton, F. (1979). Climatological estimates of lake evaporation. Water Resources Research, 15(1), 64-76.

Moy, W.-S., Cohon, J. L., & ReVelle, C. S. (1986). A programming model for analysis of the reliability, resilience, and vulnerability of a water supply reservoir. Water Resources Research, 22(4), 489-498.

Murray, M., Allen, M., Merchant, C., Harris, A., & Donlon, C. (2000). Direct observations of skin-bulk SST variability. Geophysical Research Letters, 27(8), 1171-1174.

Muttiah, R. S., & Wurbs, R. A. (2002). Modeling the impacts of climate change on water supply reliabilities. Water International, 27(3), 407-419.

Nam, K.-M., & Reilly, J. M. (2013). City size distribution as a function of socioeconomic conditions: an eclectic approach to downscaling global population. Urban Studies, 50(1), 208-225.

Nash, L. L., & Gleick, P. H. (1991). Sensitivity of streamflow in the Colorado Basin to climatic changes. Journal of Hydrology, 125(3–4), 221-241.

Naz, B. S., Frans, C. D., Clarke, G. K. C., Burns, P., & Lettenmaier, D. P. (2014). Modeling the effect of glacier recession on streamflow response using a coupled glacio-hydrological model. Hydrology and Earth System Sciences, 18(2), 787-802.

O'Hara, J. K., & Georgakakos, K. P. (2008). Quantifying the urban water supply impacts of climate change. Water Resources Management, 22(10), 1477-1497.

Oki, T., & Kanae, S. (2006). Global hydrological cycles and world water resources. Science, 313(5790), 1068-1072.

Organisation for Economic Co-operation and Development (2008), OECD Environmental Outlook to 2030, Organisation for Economic Co-operation and Development.

Palmer, W. C. (1965), Meteorological drought, US Department of Commerce, Weather Bureau Washington, DC.

Parry, M. L. (2007), Climate change 2007-impacts, adaptation and vulnerability: Working group II contribution to the fourth assessment report of the IPCC, Cambridge University Press.

Patalas, K. (1984). Mid-summer mixing depths of lakes of different latitudes. Verhandlung Internationale Vereinigung Limnologie, 22(1).

Pekel, J.-F., Cottam, A., Gorelick, N., & Belward, A. S. (2016). High-resolution mapping of global surface water and its long-term changes. Nature, 540(7633), 418-422.

Penman, H. L. (1948), Natural evaporation from open water, bare soil and grass, paper presented at Proceedings of the Royal Society of London A: Mathematical, Physical and Engineering Sciences, The Royal Society

Portland Water Bureau (2002). The impacts of climate change on Portland's water supply: an investigation of potential hydrologic and management impacts on the Bull Run system.

Prein, A. F., Holland, G. J., Rasmussen, R. M., Clark, M. P., & Tye, M. R. (2016). Running dry: The US Southwest's drift into a drier climate state. Geophysical Research Letters, 43(3), 1272-1279.

Priestley, C., & Taylor, R. (1972). On the assessment of surface heat flux and evaporation using large-scale parameters. Monthly Weather Review, 100(2), 81-92.

Prudhomme, C., & Davies, H. (2009a). Assessing uncertainties in climate change impact analyses on the river flow regimes in the UK. Part 1: baseline climate. Climatic Change, 93(1), 177-195.

Prudhomme, C., & Davies, H. (2009b). Assessing uncertainties in climate change impact analyses on the river flow regimes in the UK. Part 2: future climate. Climatic Change, 93(1), 197-222.

Ranatunga, T., Tong, S. T., Sun, Y., & Yang, Y. J. (2014). A total water management analysis of the Las Vegas Wash watershed, Nevada. Physical Geography, 35(3), 220-244.

Reclamation (2013). Downscaled CMIP3 and CMIP5 climate projections: release of downscaled CMIP5 climate projections, comparison with preceding information, and summary of user needs. U.S. Department of the Interior, Bureau of Reclamation, Technical Service Center,

Denver, Colorado, 116 p., available at: http://gdo-dcp.ucllnl.org/downscaled_cmip_projections/techmemo/downscaled_climate.pdf.

Reed, S., Koren, V., Smith, M., Zhang, Z., Moreda, F., Seo, D. J., & Participants, D. M. I. P. (2004). Overall distributed model intercomparison project results. Journal of Hydrology, 298(1-4), 27-60.

Rodell, M., Houser, P., Jambor, U., Gottschalck, J., Mitchell, K., Meng, C.-J., . . . Bosilovich, M. (2004). The global land data assimilation system. Bulletin of the American Meteorological Society, 85(3), 381-394.

Rosenberry, D. O., Winter, T. C., Buso, D. C., & Likens, G. E. (2007). Comparison of 15 evaporation methods applied to a small mountain lake in the northeastern USA. Journal of Hydrology, 340(3–4), 149-166.

Rotstayn, L. D., Roderick, M. L., & Farquhar, G. D. (2006). A simple pan-evaporation model for analysis of climate simulations: Evaluation over Australia. Geophysical Research Letters, 33(17).

Rui, H., & Beaudoing, H. (2011). Readme document for global land data assimilation system version 2 (GLDAS-2) products. GES DISC.

Ryu, J. H., Sohrabi, M., & Acharya, A. (2014). Toward mapping gridded drought indices to evaluate local drought in a rapidly changing global environment. Water Resources Management, 28(11), 3859-3869.

Sacks, L., Lee, T., & Radell, M. (1994). Comparison of energy-budget evaporation losses from two morphometrically different Florida seepage lakes. Journal of Hydrology, 156(1-4), 311-334.

Sankarasubramanian, A., Vogel, R. M., & Limbrunner, J. F. (2001). Climate elasticity of streamflow in the United States. Water Resources Research, 37(6), 1771-1781.

Satterlund, D. R. (1979). An improved equation for estimating long-wave radiation from the atmosphere. Water Resources Research, 15(6), 1649-1650.

Sawaya, K. E., Olmanson, L. G., Heinert, N. J., Brezonik, P. L., & Bauer, M. E. (2003). Extending satellite remote sensing to local scales: land and water resource monitoring using high-resolution imagery. Remote Sensing of Environment, 88(1), 144-156.

Scanlon, B. R., Duncan, I., & Reedy, R. C. (2013). Drought and the water–energy nexus in Texas. Environmental Research Letters, 8(4), 045033.

Schaake, J. C. (1990), From climate to flow, edited, pp. 177-206, John Wiley and Sons Inc., New York.

Schewe, J., Heinke, J., Gerten, D., Haddeland, I., Arnell, N. W., Clark, D. B., . . . Colón-González, F. J. (2014). Multimodel assessment of water scarcity under climate change. Proceedings of the National Academy of Sciences, 111(9), 3245-3250.

Seager, R., Harnik, N., Robinson, W. A., Kushnir, Y., Ting, M., Huang, H. P., & Velez, J. (2005). Mechanisms of ENSO-forcing of hemispherically symmetric precipitation variability. Quarterly Journal of the Royal Meteorological Society, 131(608), 1501-1527.

Seager, R., Naik, N., & Vecchi, G. A. (2010). Thermodynamic and dynamic mechanisms for large-scale changes in the hydrological cycle in response to global warming. Journal of Climate, 23(17), 4651-4668.

Sheffield, J., Goteti, G., & Wood, E. F. (2006). Development of a 50-year high-resolution global dataset of meteorological forcings for land surface modeling. Journal of Climate, 19(13), 3088-3111.

Sheffield, J., Wood, E. F., & Roderick, M. L. (2012). Little change in global drought over the past 60 years. Nature, 491(7424), 435-438.

Shiklomanov, I. A. (1999). World water resources and their use: a joint SHI/UNESCO product, available at: http://webworld.unesco.org/water/ihp/db/shiklomanov/index.shtml.

Shiklomanov, I. A. (2000). Appraisal and assessment of world water resources. Water International, 25(1), 11-32.

Smith, M. B., Seo, D. J., Koren, V. I., Reed, S. M., Zhang, Z., Duan, Q., ... & Cong, S. (2004). The distributed model intercomparison project (DMIP): motivation and experiment design. Journal of Hydrology, 298(1-4), 4-26.

Soil Survey Staff Natural Resources Conservation Service, United States Department of Agriculture. Web Soil Survey, available online at http://websoilsurvey.nrcs.usda.gov/.

Stocker, T., Qin, D., Plattner, G., Tignor, M., Allen, S., Boschung, J., . . . Midgley, B. (2013). Climate change 2013: the physical science basis. Contribution of working group I to the fifth assessment report of the intergovernmental panel on climate change.

Sun, N., Yearsley, J., Voisin, N., & Lettenmaier, D. P. (2015). A spatially distributed model for the assessment of land use impacts on stream temperature in small urban watersheds. Hydrological Processes, 29(10), 2331-2345.

Svoboda, M. D., Fuchs, B. A., Poulsen, C. C., & Nothwehr, J. R. (2015). The drought risk atlas: Enhancing decision support for drought risk management in the United States. Journal of Hydrology, 526, 274-286.

Swancar, A. (2015), Comparison of evaporation at two central Florida lakes, April 2005–November 2007, Report 2331-1258, US Geological Survey.

Tahoe Environmental Research Center (2015). Tahoe: State of the lake report, available at: http://terc.ucdavis.edu/stateofthelake/index.html.

Tanny, J., Cohen, S., Assouline, S., Lange, F., Grava, A., Berger, D., . . . Parlange, M. (2008). Evaporation from a small water reservoir: Direct measurements and estimates. Journal of Hydrology, 351(1), 218-229.

Texas Commission on Environmental Quality (2017). Water Rights and Water Use Datam available at: https://www.tceq.texas.gov/permitting/water_rights/permitting/water_rights/wrwud/, accessed on Dec 3, 2015.

Texas Water Development Board (2006). Volumetric survey of Lake Whitney, available at http://www.twdb.texas.gov/hydro_survey/whitney/2005-06/Whitney2005_FinalReport.pdf.

Texas Water Development Board (2009). Volumetric survey of Aquilla Lake, available at https://www.twdb.texas.gov/hydro_survey/aquilla/2008-03/AquillaLake2008_FinalReport.pdf.

Texas Water Development Board (2016). Population and Water Demand Projections, available at: https://www.twdb.texas.gov/waterplanning/rwp/planningdocu/2016/doc/current_docs/project_docs/20130430_Pop_Dmd_Projections.pdf, data available at: https://www.twdb.texas.gov/waterplanning/data/projections/.

Texas Water Development Board (2017). Water for Texas 2017, available at: https://www.twdb.texas.gov/mapping/doc/maps/WFT2017.pdf.

Thornthwaite, C. W. (1948). An approach toward a rational classification of climate. Geographical Review, 38(1), 55-94.

Touma, D., Ashfaq, M., Nayak, M. A., Kao, S.-C., & Diffenbaugh, N. S. (2015). A multi-model and multi-index evaluation of drought characteristics in the 21st century. Journal of Hydrology, 526, 196-207.

U.S. Bureau of Reclamation (1991). HYDROSS version 4.3 user's manual, Information Resources Division, Bureau of Reclamation, Billings, MT.

United Nations Environment Programme (2013), Global Environment Outlook 2000, Routledge.

Valiantzas, J. D. (2006). Simplified versions for the Penman evaporation equation using routine weather data. Journal of Hydrology, 331(3), 690-702.

VanRheenen, N., Wood, A., Palmer, R., & Lettenmaier, D. (2004). Potential implications of PCM climate change scenarios for Sacramento–San Joaquin River Basin hydrology and water resources. Climatic Change, 62(1-3), 257-281.

Vautard, R., Cattiaux, J., Yiou, P., Thépaut, J.-N., & Ciais, P. (2010). Northern Hemisphere atmospheric stilling partly attributed to an increase in surface roughness. Nature Geoscience, 3(11), 756.

Venkataraman, K., Tummuri, S., Medina, A., & Perry, J. (2016). 21st century drought outlook for major climate divisions of Texas based on CMIP5 multimodel ensemble: Implications for water resource management. Journal of Hydrology, 534, 300-316.

Vicente-Serrano, S. M., Pérez-Cabello, F., & Lasanta, T. (2008). Assessment of radiometric correction techniques in analyzing vegetation variability and change using time series of Landsat images. Remote Sensing of Environment, 112(10), 3916-3934.

Voisin, N., Li, H., Ward, D., Huang, M., Wigmosta, M., & Leung, L. (2013a). On an improved sub-regional water resources management representation for integration into earth system models. Hydrology and Earth System Sciences, 17(9), 3605-3622.

Voisin, N., Liu, L., Hejazi, M., Tesfa, T., Li, H., Huang, M., . . . Leung, L. R. (2013b). One-way coupling of an integrated assessment model and a water resources model: evaluation and implications of future changes over the US Midwest. Hydrology and Earth System Sciences, 17(11), 4555-4575.

Voisin, N., Hejazi, M., Leung, L. R., Liu, L., Huang, M., Li, H., & Tesfa, T. (2015). Representing groundwater use and return flow and their signatures on surface hydrology and water stress in integrated water models. PNNL-SA-109215, Pacific Northwest National Laboratory, Richland, WA.

Vörösmarty, C. J., Green, P., Salisbury, J., & Lammers, R. B. (2000). Global water resources: vulnerability from climate change and population growth. Science, 289(5477), 284-288.

Wang, W., Lee, X., Xiao, W., Liu, S., Schultz, N., Wang, Y., . . . Zhao, L. (2018). Global lake evaporation accelerated by changes in surface energy allocation in a warmer climate. Nature Geoscience, 11(6), 410-414.

Watts, G., von Christierson, B., Hannaford, J., & Lonsdale, K. (2012). Testing the resilience of water supply systems to long droughts. Journal of Hydrology, 414, 255-267.

Weisman, R. N., & Brutsaert, W. (1973). Evaporation and cooling of a lake under unstable atmospheric conditions. Water Resources Research, 9(5), 1242-1257.

Wigmosta, M. S., Vail, L. W., & Lettenmaier, D. P. (1994). A distributed hydrology-vegetation model for complex terrain. Water Resources Research, 30(6), 1665-1679.

Wild, M. (2012). Enlightening global dimming and brightening. Bulletin of the American Meteorological Society, 93(1), 27-37.

Wild, M. (2016). Decadal changes in radiative fluxes at land and ocean surfaces and their relevance for global warming. Wiley Interdisciplinary Reviews: Climate Change, 7(1), 91-107.

Winter, T., Rosenberry, D., & Sturrock, A. (1995). Evaluation of 11 equations for determining evaporation for a small lake in the north central United States. Water Resources Research, 31(4), 983-993.

Wood, E. F., Roundy, J. K., Troy, T. J., van Beek, L. P. H., Bierkens, M. F. P., Blyth, E., . . . Whitehead, P. (2011). Hyperresolution global land surface modeling: Meeting a grand challenge for monitoring Earth's terrestrial water. Water Resources Research, 47(5).

World Commission on Dams (2000). Dams and development: a new framework for decision making. Earthscan, London, UK.

Wu, F., Zhan, J., & Güneralp, İ. (2015). Present and future of urban water balance in the rapidly urbanizing Heihe River basin, northwest China. Ecological Modelling, 318, 254-264.

Wurbs, R. A. (1996), Modeling and analysis of reservoir system operations, Prentice Hall.

Wurbs, R. (2012), Water rights analysis package (WRAP) modeling system users manual, Texas Water Resources Institute.

Wurbs, R. A., & Ayala, R. A. (2014). Reservoir evaporation in Texas, USA. Journal of Hydrology, 510, 1-9.

Xia, Y., Mitchell, K., Ek, M., Sheffield, J., Cosgrove, B., Wood, E., . . . Meng, J. (2012). Continental-scale water and energy flux analysis and validation for the North American Land Data Assimilation System project phase 2 (NLDAS-2): 1. Intercomparison and application of model products. Journal of Geophysical Research: Atmospheres, 117(D3).

Xiao, K., Griffis, T. J., Baker, J. M., Bolstad, P. V., Erickson, M. D., Lee, X., . . . Nieber, J. L. (2018). Evaporation from a temperate closed-basin lake and its impact on present, past, and future water level. Journal of Hydrology, 561, 59-75.

Yang, G., Bowling, L. C., Cherkauer, K. A., & Pijanowski, B. C. (2011). The impact of urban development on hydrologic regime from catchment to basin scales. Landscape and Urban Planning, 103(2), 237-247.Rimmer, A., Samuels, R., & Lechinsky, Y. (2009). A comprehensive study across methods and time scales to estimate surface fluxes from Lake Kinneret, Israel. Journal of Hydrology, 379(1-2), 181-192.

Yates, D., Sieber, J., Purkey, D., & Huber-Lee, A. (2005). WEAP21—A demand-, priority-, and preference-driven water planning model: part 1: model characteristics. Water International, 30(4), 487-500.

Zagona, E. A., Fulp, T. J., Shane, R., Magee, T., & Goranflo, H. M. (2001). Riverware: A generalized tool for complex reservoir system modeling. JAWRA Journal of the American Water Resources Association, 37(4), 913-929.

Zhang, Q., Gu, X., Singh, V. P., Xiao, M., & Chen, X. (2015). Evaluation of flood frequency under non-stationarity resulting from climate indices and reservoir indices in the East River basin, China. Journal of Hydrology, 527, 565-575.

Zhang, H., Gorelick, S. M., Zimba, P. V., & Zhang, X. (2017). A remote sensing method for estimating regional reservoir area and evaporative loss. Journal of Hydrology, 555, 213-227.

Zhao, G., Gao, H., & Cuo, L. (2016a). Effects of Urbanization and Climate Change on Peak Flows over the San Antonio River Basin, Texas. Journal of Hydrometeorology, 17(9), 2371-2389.

Zhao, G., Gao, H., Naz, B. S., Kao, S.-C., & Voisin, N. (2016b). Integrating a reservoir regulation scheme into a spatially distributed hydrological model. Advances in Water Resources, 98, 16-31.

Zhao, G., & Gao, H. (2018). Automatic correction of contaminated images for assessment of reservoir surface area dynamics. Geophysical Research Letters, 45(12), 6092-6099.

Zhao, G., Gao, H., Kao, S.-C., Voisin, N., & Naz, B. S. (2018). A modeling framework for evaluating the drought resilience of a surface water supply system under non-stationarity. Journal of Hydrology, 563, 22-32

Zhou, T., Nijssen, B., Gao, H., & Lettenmaier, D. P. (2016). The contribution of reservoirs to global land surface water storage variations. Journal of Hydrometeorology, 17(1), 309-325.